

THERMOPHILICITY AND CATALYTIC EFFICIENCY IN DIHYDROFOLATE REDUCTASE

A thesis submitted to Cardiff University for the degree of Doctor of

Philosophy by

Jiannan Guo

Supervisor: Prof. Rudolf K. Allemann

2013

DECLARATION

This work has not previously been accepted in substance for any degree and is not being concurrently submitted in candidature for any degree.

Signed..... (Candidate)

Date.....

STATEMENT 1

This thesis is being submitted in partial fulfilment of the requirements for the degree of Doctor of Philosophy.

Signed..... (Candidate)

Date.....

STATEMENT 2

This thesis is the result of my own independent work/investigation, except where otherwise stated. Other sources are acknowledged by explicit references.

Signed..... (Candidate)

Date.....

STATEMENT 3

I hereby give consent for my thesis, if accepted, to be available for photocopying and for interlibrary loan, and for the title and summary to be made available to outside organisations.

Signed..... (Candidate)

Date.....

ABSTRACT

This thesis presents an investigation of the hydrogen transfer reactions between dihydrofolate (H_2F) and NADPH that are catalysed by the dihydrofolate reductase (DHFR) isolated from *Geobacillus stearothermophilus* (BsDHFR) as well as an artificial hybrid originating from the DHFRs from mesophilic *Escherichia coli* (EcDHFR) and hyperthermophilic *Thermotoga maritima* (TmDHFR). A broad spectrum of studies, focusing on the relationship between structure, thermostability and kinetics, showed that the catalytic behaviour of BsDHFR is generally similar to other monomeric DHFRs, including ones found in the mesophile *Escherichia coli* and the psychrophile *Moritella profunda*, but significantly different from the dimeric TmDHFR. The fact that all monomeric DHFRs display similar catalytic behaviour, regardless of their widely different optimal temperatures, suggests that thermostability does not directly relate to catalytic efficiency. The biophysical differences between monomeric DHFRs and TmDHFR are likely derived from the dimeric nature of the hyperthermophilic enzyme. An artificial dimeric variant of EcDHFR, Xet-3, was prepared by introducing residues at the dimer interface of TmDHFR. While thermostability of this variant is enhanced, it showed a great decrease in its steady-state and pre-steady-state rate constants. Given that the corresponding rate constants did not increase when the loops are released in the monomeric variant of TmDHFR, the lowered catalytic ability in Xet-3 is likely a consequence of geometric distortion of the active site and loss of loop flexibility that is catalytically important in EcDHFR. In contrast, the relatively poor activity of TmDHFR is not simply a consequence of reduced loop flexibility; the dimer interface of TmDHFR plays a rather complicated role in catalysis.

ACKNOWLEDGEMENTS

First and foremost I would like to thank my supervisor Professor Rudolf K. Allemann, who gave me the great opportunity to join in this exciting project. He was always patient when supervising me and showed continued confidence in me. I also thank Dr. Mahmoud Akhtar who was always ready to help me with my trivial things during my PhD. I would like to thank Professor Matthias Bochtler, Professor Gerald Richter and Dr. James Redman for their support during *viva* and report time. Their valuable advice greatly helped me and made my project better.

Thanks to all the people in the DHFR group. Especially thanks to Dr. Joel Loveridge for everything, teaching me and proofreading my paper. Thanks to Dr. Lai-Hock Tey and Dr. Louis Luk who also offered great help during my project, and to Enas Behiry, Will Dawson, Mark Beveridge, Stella Matthews and all other group members. I am very happy to have worked with you.

I would like to thank my family: Mam, Dad. Thank you for your love, belief and support always. And thanks to my friends: Uncle Paul, Levon, Apple, Andrew, his wife Yanling, Wahwah, Jingqi, Yang, Junjie, Yingyu, Yuncheng, Yi and Professor Blackburn, your presence makes my life in UK much more colourful. Most important, I would like to thank my girlfriend Ying Bi. You have always been ready to support me. I could not go further without you!

TABLE OF CONTENTS

1 INTRODUCTION: DIHYDROFOLATE REDUCTASE AND THERMOPHILES..	1
1.1 General introduction of extremophiles	2
1.2 Thermophiles	5
1.3 Survival mechanism.....	7
1.4 Biotechnological applications of thermophilic proteins	10
1.5 The effect of thermostability on catalysis	12
1.6 Dihydrofolate reductase (DHFR).....	13
1.7 Structure of DHFR from <i>Escherichia coli</i> (EcDHFR)	19
1.8 The kinetic cycle of EcDHFR.....	24
1.9 Loop and subdomain movements during the catalytic cycle	25
1.10 Principles of enzyme catalysis	27
1.10.1 Semi-classical transition state theory.....	27
1.10.2 Bell's tunnelling correction model.....	29
1.10.3 Development of Bell's tunnelling correction model.....	31
1.11 Protein dynamics in EcDHFR.....	32
1.12 Contribution of protein dynamics to catalysis in EcDHFR	35
1.13 Hyperthermophilic DHFR from <i>Thermotoga maritima</i> (TmDHFR)	38
1.14 Moderately thermophilic DHFR from <i>Geobacillus stearothermophilus</i> (BsDHFR).....	42
1.15 Investigations on the effect of catalysis due to thermal adaptation	45
2 MATERIALS AND METHODS	47
2.1 Materials	48
2.2 Media	48
2.2.1 Luria-Bertani (LB) medium.....	48
2.2.2 Luria-Bertani agar (1.5 % w/v).....	48
2.3 Solutions	49
2.3.1 Rubidium chloride solutions for preparation of ultra-competent cells	49

2.3.2 dNTPs	49
2.3.3 Ethidium bromide solution	49
2.3.4 TAE buffer stock (50x) for agarose gels	50
2.3.5 10% (w/v) sodium dodecyl sulfate (SDS)	50
2.3.6 Sodium dodecyl sulfate polyacrylamide gel electrophoresis (SDS PAGE) running buffer	50
2.3.6.1 Anode buffer	50
2.3.6.2 Cathode buffer	50
2.3.7 Protein loading dye	51
2.3.8 Protein staining buffer.....	51
2.3.9 Protein destaining buffer.....	51
2.3.10 Potassium phosphate stock solution	51
2.3.11 Protein dialysis buffer	51
2.3.12 Inclusion body dissolving buffer	51
2.3.13 Inclusion body refolding buffer	52
2.4 DNA manipulation.....	52
2.4.1 Purification of plasmid DNA.....	52
2.4.2 Quantification of oligonucleotides and plasmid DNA	52
2.4.3 DNA sequencing	53
2.4.3 Polymerase chain reaction (PCR) and site-directed mutagenesis.....	53
2.4.4 Restriction digestion of DNA and controls.....	59
2.4.5 DNA visualisation, isolation and purification.....	59
2.4.6 Cloning of BsDHFR gene into cloning vector pPCR-Script	60
2.4.7 Subcloning of BsDHFR gene into expression vector	61
2.4.8 EcDHFR/TmDHFR and BsDHFR/TmDHFR Hybrid construction	62
2.4.8.1 Construction method 1.....	62
2.4.8.2 Construction method 2.....	63
2.4.8.3 Construction method 3.....	64
2.4.9 Preparation of XL1 Blue, BL21(DE3) and BL21- CodonPlus(DE3)-RP cells	66

2.4.10 Transformation protocol and controls.....	66
2.5 BsDHFR and hybrid enzymes production and purification.....	67
2.5.1 Large scale expression	67
2.5.2 Protein identification: SDS-PAGE protocol	68
2.5.3 Protein purification	69
2.5.3.1 Inclusion body dissolving and refolding.....	69
2.5.3.2 Anion exchange chromatography	70
2.5.3.3 Cation exchange chromatography	70
2.5.3.4 Ni-Sepharose affinity chromatography.....	71
2.5.3.5 Size exclusion chromatography	71
2.5.4 Protein storage	72
2.5.5 Enzyme concentration determination	72
2.6 Cofactor preparation	73
2.6.1 Preparation of dihydrofolate	73
2.6.2 Preparation of NADPD.....	73
2.7 Enzyme kinetics.....	74
2.7.1 Buffers for kinetics	74
2.7.1.1 Potassium phosphate buffers.....	74
2.7.1.2 MTEN buffer	75
2.7.2 Steady-state kinetics via UV spectroscopy.....	75
2.7.3 Pre-steady-state kinetics	78
2.8 Circular Dichroism spectroscopy.....	80
2.8.1 Buffers for thermal denaturation experiments	81
2.8.2 Calculation of mean residue ellipticity (MRE).....	81
2.9 Errors and their propagation	82
2.9.1 Standard deviation and standard error of the mean	82
2.9.2 Propagation of errors	82
3 PREPARATION AND CHARACTERISATION OF WILD TYPE BsDHFR.....	83
3.1 Introduction.....	84
3.2 Results and Discussion	84

3.2.1 Expression of BsDHFR	84
3.2.2 Purification of BsDHFR	85
3.2.3 Sequence analysis of BsDHFR	87
3.2.4 Size exclusion chromatography analysis of BsDHFR	88
3.2.5 Circular dichroism analysis of BsDHFR	89
3.2.6 Thermal unfolding of BsDHFR	90
3.2.7 Environmental factors influencing the stability of BsDHFR.....	91
3.2.7.1 Effect of salts on BsDHFR thermostability and specific activity	91
3.2.7.2 Effect of substrate and cofactor binding on the thermostability of BsDHFR.....	93
3.2.8 Influence of temperature on the steady state kinetics of BsDHFR.....	94
3.2.9 Influence of pH on the steady state kinetics of BsDHFR	98
3.2.10 Influence of solvents on the steady state kinetics of BsDHFR.....	101
3.3 Summary and conclusions	104
4 EXPLORING THE HYDRIDE TRANSFER STEP OF BsDHFR	107
4.1 Introduction.....	108
4.2 Results and discussion	108
4.2.1 Temperature dependence of the hydride transfer of BsDHFR.....	108
4.2.2 pH dependence of the hydride transfer of BsDHFR.....	113
4.2.3 Influence of salt on the hydride transfer of BsDHFR.....	114
4.2.4 Influence of solvents on the hydride transfer of BsDHFR	117
4.3 Conclusions.....	121
5 ANALYSIS OF BsDHFR VARIANT PROTEINS.....	124
5.1 Introduction.....	125
5.2 Results and discussion	126
5.2.1 Circular dichroism analysis of BsDHFR variants.....	126
5.2.3 Steady-state kinetics of BsDHFR variants.....	127
5.2.4 Pre-steady-state kinetics of BsDHFR variants.....	130
5.2.5 Thermostability of BsDHFR variants	136

5.3 Conclusions.....	137
6 CREATION AND ANALYSIS OF HYBRID ENZYMES.....	139
6.1 Introduction.....	140
6.2 Results and discussion	141
6.2.1 Strategies of hybrid enzyme preparation	141
6.2.2 Preparation of worked hybrid enzyme Xet-3.....	141
6.2.3 Size exclusion chromatography analysis of Xet-3.....	145
6.2.4 Circular dichroism analysis and thermal unfolding of Xet-3	146
6.2.5 The steady-state kinetics of Xet-3.....	148
6.2.7 The pre-steady-state kinetics of Xet-3	150
6.3 Conclusions.....	159
7 GENERAL SUMMARY AND CONCLUSIONS	161
7.1 The thermoadaptation of BsDHFR	162
7.2 The contribution of protein dynamics to catalysis.....	163
7.3 The effect of thermophilicity on catalysis	165
7.4 The effect of dimerisation on catalysis	165
8 REFERENCES	167

LIST OF ABBREVIATIONS

A	adenosine
ABD	adenosine binding domain
Abs	absorbance
ADP	adenosine diphosphate
APS	ammonium persulfate
ATP	adenosine triphosphate
β -ME	β -mercaptoethanol
BsDHFR	dihydrofolate reductase from <i>Geobacillus stearothermophilus</i>
C	cytosine
c	concentration
CD	circular dichroism spectroscopy
CV	column volume
DEAE	diethylaminoethyl
dH ₂ O	deionised water
DHFR	dihydrofolate reductase
DNA	deoxyribose nucleic acid
dTMP	deoxythymidine monophosphate
dUMP	deoxyuridine monophosphate
E_a	activation energy
EcDHFR	dihydrofolate reductase from <i>Escherichia coli</i>
Fol	folate
FPLC	fast protein liquid chromatography
FRET	Förster (fluorescence) resonance energy transfer
G	guanine
H ₂ F	7,8-dihydrofolate
H ₄ F	5,6,7,8-tetrahydrofolate

List of Abbreviations

HPLC	high pressure (performance) liquid chromatography
IPTG	isopropyl- β -D-1-thiogalactopyranoside
KIE	kinetic isotope effect
K _i PO ₄	potassium phosphate
LB	Luria-Bertani growth media
LD	loop domain
MpDHFR	dihydrofolate reductase from <i>Moritella profunda</i>
MTEN	MES Tris ethanolamine sodium chloride
MTX	methotrexate
NADP ⁺	oxidised nicotinamide adenine dinucleotide phosphate
NADPD	deuterated reduced nicotinamide adenine dinucleotide phosphate
NADPH	reduced nicotinamide adenine dinucleotide phosphate
ND	N-terminal domain
pABA	p-aminobenzoate
RNA	ribose nucleic acid
RPM	revolutions per minute
SAM	S-adenosyl methionine
SDS-PAGE	sodium dodecyl sulfate - polyacrylamide gel electrophoresis
T	thymine
TEMED	N,N,N',N'-tetramethylenediamine
THF	tetrahydrofuran
T _M	melting temperature
TmDHFR	dihydrofolate reductase from <i>Thermotoga maritima</i>
Tris	tris(hydroxymethyl)aminomethane
TS	thymidylate synthase
U	uracil
UV/Vis	ultraviolet/visible spectroscopy

Through this work, amino acids are expressed as their triple or single letter code:

Amino Acid	3 letter code	1 letter code
Alanine	Ala	A
Arginine	Arg	R
Asparagine	Asn	N
Aspartic acid	Asp	D
Cysteine	Cys	C
Glutamic acid	Glu	E
Glutamine	Gln	Q
Glycine	Gly	G
Histidine	His	H
Isoleucine	Ile	I
Leucine	Leu	L
Lysine	Lys	K
Methionine	Met	M
Phenylalanine	Phe	F
Proline	Pro	P
Serine	Ser	S
Threonine	Thr	T
Tryptophan	Trp	W
Tyrosine	Tyr	Y
Valine	Val	V

1 INTRODUCTION: DIHYDROFOLATE REDUCTASE AND THERMOPHILES

1.1 General introduction of extremophiles

In 'normal' physiological conditions, there is a sufficient supply of oxygen (~20%), temperature is never too cold or too hot (~10 to 40 °C), and most of the damaging ultraviolet (UV) radiation is removed by ozone layer.(1) These conditions are ideal for a wide variety of life forms to survive. However, the planet Earth also consists of some 'extreme' environments where physical conditions are considered harsh for organism survival. For instance, the deepest part of the Pacific Ocean, the Mariana Trench, is under incredible pressure (1072 atm), is extremely cold (1 to 4 °C) and is too dark to perform photosynthesis. Other examples include the Dead Sea in the Mediterranean basin, where the concentration of salt is extremely high (23-30%), and the Sahara desert, which is dry, hot and exposed to intense UV radiation. Interestingly, life forms still exist in these 'extreme' places and are often categorised as 'extremophiles'. In fact, extremophiles are found in all kingdoms of organisms, such as several species of cacti and cockroaches that can tolerate relatively hot environments with strong UV radiation.(2)

A wide variety of extremophiles, especially prokaryotes, have been discovered in places that were previously considered uninhabitable.(3) Such discoveries have led to an interesting question: why would organisms choose to live in these extreme environments? Obviously, there is less competition in extreme conditions. In other words, it should be easy for extremophiles to thrive. However, another more complicated question comes to us spontaneously: how do life forms survive under extreme conditions? Indeed, it challenges our concept of the limits of life, and helps illustrate the comprehensive tree of life, thereby providing clues to how evolution has taken place. Moreover, the conditions of planet Earth have significantly changed with the evolution of life, thus the study of extremophiles and their relationships to the ecosystems has considerable value. We have also made useful discoveries, such as the enzymes from the temperature tolerant bacterium *Thermus aquaticus*, many of which have become extraordinarily powerful tools in all aspects of biology.(4) Lastly,

extremophiles also give us an idea of the physiology of life forms that could exist in outer space, where 'normal' conditions are similar to the extreme environments on earth.

Many extreme life forms have been discovered and can be categorised as follows:

Alkaliphiles refer to microorganisms living in natural habitats above pH 9 either persistently or over a prolonged period of time. Microbes have been found thriving in many alkaline environments, including the slag dumps of the Lake Calumet region in southeast Chicago, Octopus Spring in Yellowstone National Park, and the East African Rift Desert.(5, 6)

Acidophiles can withstand and even thrive in acidic environments (< pH 5). Although they might appear somewhat uncommon, acidophiles, such as *Lactobacillus plantarum*, have actually been used for centuries to pickle food by anaerobic fermentation. Other acidophiles have been found in a variety of habitats, including sulfuric pools and geysers and areas polluted by acid mine drainage.(7, 8)

Halophiles have an incredible ability to prevent desiccation as their natural habitat contains high salt concentration (>5-25%). Even though the term 'halophiles' has only been used in recent decades, some bacteria such as *Tetragenococcus halophilus* have been used in the fermentation processes of traditional Asian spices, including soy sauce, miso and fish sauce.(9, 10)

Barotolerant organisms and **barophiles** survive in aquatic habitats deeper than 2000 meters with pressure as high as over 600 atm. Studies of 'barotolerant' (tolerate high pressure) and 'barophilic' (dependent on high pressure) cultures of deep-sea bacteria show that distribution of these organisms is a function of depth. In July 2011, the depth record for life forms was rewritten, as xenophyophores were found at depths of up to 10641 meters within the Sirena Deep of the Mariana Trench, the deepest region

on Earth. The previous depth record was approximately 7500 meters in the New Hebrides Trench.(11)

Psychrophiles describe the microorganisms that survive in extremely cold habitats, such as polar and alpine ice, ranging from -15 to 5 °C. The biophysical properties of molecules isolated from psychrophiles have been extensively studied. One classical example is the study of antifreeze proteins, which lower the freezing point of water inside the cell.(12, 13)

Thermophiles, meaning 'heat-loving', have been found in sites at 50 °C and above. These organisms have been isolated from a number of marine and terrestrial geothermally-heated habitats, including shallow terrestrial hot springs, hydrothermal vent systems, sediment from volcanic islands, and deep sea hydrothermal vents, where temperature can be as high as 95-105 °C.(14) As a matter of fact, the upper temperature limit for life hasn't been completely confirmed yet. The previous record holder was a species of archaea called *Pyrolobus fumarii*. It was first discovered in 1997 in a black smoker hydrothermal vent at the Mid-Atlantic Ridge, setting the upper temperature threshold to 113 °C.(15) However, 6 years later, the upper temperature limit was extended; *Geogemma barossii*, a microbe from the same family found at a vent in the Pacific Ocean, survived and multiplied during a 10 hour period at 121 °C in an autoclave.(16)

A lot of research has been conducted on the survival mechanism for each type of extremophile. For example, acidophilic and halophilic prokaryotes have evolved to carefully regulate cytoplasmic pH (6.5-7.0)(17) and control the cellular osmotic pressure with the use of different ion (H^+ , Na^+ and K^+) pumps, respectively.(9, 18) Barotolerant bacteria regulate the fluidity of membrane phospholipids to compensate for pressure gradients between the inside of the cell and the environment.(19) Mechanisms developed by these extremophiles help maintain a mild environment inside the cytoplasm, thus intracellular proteins in these extremophiles do not need to

develop additional stability. In contrast, extremophiles found in extreme temperatures (i.e. psychrophiles and thermophiles) require a more complicated survival strategy, because essentially *all* of the intracellular proteins have to evolve to adapt to the extreme conditions. Indeed, their proteins have been shown to possess intriguing biophysical properties and have consequently become a major subject of research.

1.2 Thermophiles

In 1966, Thomas Brock made the remarkable discovery that microorganisms were growing in the boiling hot springs of Yellowstone National Park, Wyoming. Since Brock's discovery, thermophiles have been discovered in geothermal features all over the world including North and South America, New Zealand, Iceland, Italy, Japan and other geothermal regions of the world.(20) While boiling hot springs are far beyond the comfort zone of humans and many other organisms, these prokaryotes can survive at 50 °C and above. Scientists from different fields of research have taken an interest in thermophiles. Astrobiologists suggest that hot springs all over the world provide some of the best "doorways into early Earth". Microbial life is thought to have begun roughly 3 billion years ago, and the first evolutionary steps began in an anaerobic environment with strong ultraviolet radiation and water bodies which were hot and acidic. Therefore, the first organism was likely to be "polyextremophile", and could tolerate extreme temperature and acidity. Not only does this give insights into the origin of life on planet Earth, but the discovery of thermophiles also opens up a new realm of possibilities for life elsewhere in the universe. These prokaryotes represent the deepest branch and shortest lineage to the root of the phylogenetic tree; thus, they are considered to be the most ancient living organisms and closely related to the postulated "common ancestor" of all forms of life.(21-24)

Thermophiles, from the Greek meaning "heat-loving", are defined as organisms that thrive at relatively high temperatures of approximately 50 °C, a maximum of up to 70 °C or more, and a minimum of about 40 °C.(25) Thermophiles can be classified as

‘obligate’ and ‘facultative’.(25) Obligate thermophiles (also called extreme thermophiles) require high temperatures (60 °C) for growth, whereas facultative thermophiles (also called moderate thermophiles) can thrive at high temperatures, but also at lower temperature (below 50 °C).(26) Some extreme thermophiles (hyperthermophiles) require a very high temperature (80 °C to 105 °C) for growth.(27-29) Other bacteria would be damaged and even killed when exposed to the same temperatures.

Table 1.1 Upper temperature limits for growth of various organisms

Group	Upper temperature limits / °C
Animals	
Fish and other aquatic vertebrates	38
Insects	45-50
Ostracods (crustaceans)	49-50
Plants	
Vascular plants	45
Mosses	50
Eukaryotes	
Protozoa	56
Green algae	55-60
Fungi	60-62
Prokaryotes	
Bacteria	
Cyanobacteria	70-73
Anoxygenic phototrophic bacteria	70-73
Chemoorganotrophic bacteria	90
Archaea	
Hyperthermophilic methanogens	110
Sulfur-dependent hyperthermophiles	115

According to the studies of species distribution of thermal habitats at different temperatures, we can conclude that prokaryotes are capable of surviving at temperatures higher than those at which eukaryotes can grow (Table 1.1). As mentioned above, *Geogemma barossii*, discovered at a vent in the Pacific Ocean, is ranked as the most thermophilic organism, able to replicate at 121 °C.(16) Moreover, most natural thermal habitats vary significantly in conditions, making some thermophiles able to survive at extremely harsh conditions. For example, *Thiobacillus thiooxidans* and *Sulfolobus acidocaldarius* were discovered in hot acid soils in Yellowstone National Park(30) and are considered as acidophilic thermophiles that oxidise sulfur into sulfuric acid as a method to obtain energy.(31)

1.3 Survival mechanism

How do thermophilic organisms survive at high temperatures? Lower molecular weight metabolites and coenzymes become relatively unstable. For instance, NAD/P(H) is unstable at 95 °C ($t_{1/2}$ ~2 min).(32) Physical properties of biomolecules change dramatically as temperature increases. DNA and RNA denature due to hydrogen-bond disruptions between nucleotide bases, membrane permeability greatly increases with the fluidity of the phospholipid bilayer, and protein molecules often denature and/or aggregate. All of these changes render a survival challenge, thus biomolecules must evolve to achieve heat stability. Thermophiles can be discriminated from mesophiles based on several features. Firstly, thermophilic organisms can circumvent the thermal instability of their metabolites by using an alternative metabolic pathway or by utilising more stable alternative compounds than their mesophilic counterparts.(33) As mentioned above, NAD/P(H) is unstable at high temperature (>95 °C). As a result, in several extreme thermophiles, more thermostable non-heme iron proteins carry out part of the functions of NAD/P(H).(34, 35) Additionally, acetyl-CoA is directly converted to acetate instead of through a thermally unstable acetyl phosphate intermediate in some hyperthermophiles.(33) Secondly, thermal stability of the nucleic acid duplex structure can be increased by

higher GC content. However, in most of the thermophiles, including the hyperthermophilic archaea found in boiling hot springs, no difference GC ratio was observed.(36) Therefore, thermophiles adopt some alternative ways to enhance the DNA duplex thermal stability. At high temperatures, DNA undergoes denaturation by strand separation. However, it is known that duplex stability *in vitro* can be manipulated by addition of salts. The protection mechanism by salts could be explained as (i) the induction of structural changes to DNA, that render the critical sites of attack by hydroxyl radicals less accessible; and (ii) the stabilisation of the double helical regions between two close-set nicks on opposite strands, that hinders the effective double strand breakage of DNA.(37) For example, high concentrations of potassium inositol-1-1'-diphosphate(38) or tripotassium cyclic-2,3-diphosphoglycerate were found in some hyperthermophiles, and many protect the DNA duplex.(39) Additionally, in some thermophilic organisms, nucleic acids were stabilised by binding with cationic proteins. For example, the DNA polymerase of thermophiles can adequately bind and stabilise substrate DNA and make DNA elongation efficient at extreme temperatures.(40-42) Thirdly, some extremophile organisms minimise fluidity of their membrane at high temperatures by decreasing the ratio of unsaturated to saturated fatty acids. Ester linkages in membrane lipids of bacterial and eukaryotic cells are also replaced with more stable ether bonds in hyperthermophilic archaea, making archaeal ether lipid membranes thinner but exceedingly resistant to physical disruption.(43, 44)

In addition to nucleotides and membranes, protein molecules also have evolved to achieve extra heat-stability. Generally, protein molecules perform their physiological tasks by maintaining a specific three-dimensional conformation that is stabilised by a network of hydrogen and ionic bonds and hydrophobic interactions. However, heat increases the kinetic energy of atoms and causes rapid molecular vibrations, thereby disrupting all the crucial interactions responsible for the secondary and tertiary structure. Proteins from thermophilic organisms have evolved to retain their folded

structures and maintain their activities at high temperature, likely owing to their strong rigidity. While the thermophilic proteins and their mesophilic counterparts are structurally similar, several subtle biophysical modifications have evolved to enhance the stability of thermophilic proteins. These factors include (i) smaller and less numerous cavities in the protein core,(45) (ii) better packing, deletion or shortening of loops,(46) (iii) increased content of helices and strands,(47-49) (iv) an increase in polar surface area(47, 50, 51) or (v) reduction of the total surface area by oligomerisation,(52) (vi) docking of N and C termini and anchoring of loose ends,(53) (vii) enhanced hydrophobicity,(47) (viii) increased numbers of proline residues(47, 54, 55) and (ix) decreased numbers of thermolabile residues such as asparagine, glutamine, methionine or cysteine residues,(46) and (x) stronger hydrogen bonding(50, 51) (xi) salt bridges(46, 47, 56-60) and (xii) disulfide bridges.(61)

To what extent does each of the above-mentioned factors contribute to thermostability in thermophilic proteins? Szilágyi and Závodszy have performed a thorough comparative and statistical study by comparing the properties of 25 protein families with 64 mesophilic and 29 thermophilic protein subunits.(62) Each of these protein families was tested for hydrophobic cavities/packing of core region, hydrogen bonds, ion pairs, secondary structure and the polarity of surfaces. Amongst all the compared structural parameters, the only generally observed rule is an increase in number of ion pairs with increasing growth temperature. Other parameters do not show a clear trend; the number of hydrogen bonds and the polarity of buried surfaces exhibit no clear-cut tendency to change with increasing temperature. Proteins from extreme thermophiles are stabilised in different ways to moderately thermophilic ones. The preferences of these two groups are different with regards to the number of ion pairs, the number and size of cavities in the protein core, the polarity of exposed surface and the secondary structural composition.

The relationship between proteomics and thermostability has been further studied by Cambillau and Claverie.(63) They compared the overall amino acid composition in

mesophilic and thermophilic proteins and showed that hyperthermophilic proteins have a sharp increase in glutamic acid and lysine (charged residues) at the expense of mostly non-charged residues and glutamine. Also, alanine residues are replaced by medium and large aliphatic residues. The overall composition of aromatic residues (*e.g.* histidine) or other residues (*e.g.* proline, glycine or cysteine) showed no significant difference. The location of those charged and polar residues were also surveyed. They calculated the water accessible surface (WAS) of a group of proteins and observed a 3.5% decrease of polar residues on the surface and a 4.5% increase of charged residues. Of all individual residues, glutamine exhibits the largest difference between mesophiles and thermophiles, decreasing more than 2-fold in the WAS. Other polar residues (serine, threonine and asparagine) followed a similar trend in the WAS. The WAS percentage of aliphatic residues however showed little change at 6.0% surface area for mesophiles and 6.5% of the surface area in hyperthermophilic proteins. On the other hand the amount of alanine on the protein surface was decreased by 50% and the amount of histidine decreased 1.5 fold. It was concluded from this survey that the most important differences between mesophilic and thermophilic proteins occur at the surface of a protein.

While these studies provide us a general concept of factors that affect thermostability, it is still a challenge to enhance thermostability of a mesophilic protein by genetic engineering. Indeed, the mechanisms of thermal adaptation vary dramatically among thermophilic proteins, thus it is rather difficult to enhance protein thermostability in a systematic manner. Moreover, how these factors affect catalysis by an enzyme remains a matter of current debate.

1.4 Biotechnological applications of thermophilic proteins

In addition to their interesting biological backgrounds, thermophilic enzymes are particularly applicable in industry for large scale product preparation. Industrial processing at high temperature is advantageous, as it increases substrate solubility

while decreasing reaction time, viscosity and solvent volume by evaporation. Furthermore, high-temperature conditions eliminate the possibility of contamination caused by common mesophiles. The use of thermophilic enzymes as catalysts has its own benefit, as their structures are often highly rigid thus they are also particularly protease resistant.(64) Furthermore, thermophilic proteins can be easily purified simply by heat treatment, a method that is inapplicable to their mesophilic counterparts.(65)

Due to their superb properties, thermostable enzymes have been applied in different areas of industry, including detergent manufacturing and food preparation.(66) In particular, ~30% of global enzyme consumption is contributed by thermostable enzymes that are used in starch processing, which provides a natural source of glucose/fructose syrup, non-fermentable carbohydrates, and anti-staling agents in baking.(67) Hyperthermophilic α -amylases, which function optimally at 100 °C, are obtained from *Pyrococcus woesei*, *Pyrococcus furiosus*, *Thermococcus profundus* and *Thermococcus hydrothermalis* and are used in the process of starch breakdown. Glucose generated in this process can be further transformed into other important chemicals, including ethanol, amino acids and organic acids with the use of appropriate thermostable enzymes.(68) Protease is another important class of industrial enzyme. Today, proteases account for approximately 40% of the total enzyme sales in various industrial market sectors, such as detergent, food, leather and waste management.(69) Similarly, thermostable proteases are particularly popular because of their ability to withstand the harsh conditions during industrial processes, and (70, 71) proteases from *Thermotoga maritima*, *Thermotoga aggregans*, *Thermotoga celer* and *Thermotoga litoralis* have been used in the aforementioned processing.(72) Thermostable cellulases and related enzymes are also employed in the pulp and paper industry. Because the breakdown of wood to pulp requires a heated alkaline environment to disrupt the cell wall structure, an alkaliphilic thermostable xylanase could speed up this procedure by breaking down hemicellulose, a major component in cell walls.(73) For these purposes, hyperthermophilic xylanases from

Dyctioglomus sp., *Thermotoga* sp., and *Pyrococcus furiosus* have been cloned and successfully expressed in *Escherichia coli*.(74-76) Microbial lipases have many unique characteristics including stability in organic solvents, broad substrate specificity, and high enantioselectivity. These make lipases the most widely used group of biocatalysts for biotechnology. Lipases are often used as detergent and food additives, and are also involved in the pharmaceutical production and the pulp and paper industry.(77) To date, thermostable lipases from hyperthermophilic archaea have been isolated from *Pyrobaculum calidifontis*, *Pyrococcus furiosus* and *Pyrococcus horikoshii* are cloned in *Escherichia coli* for industrial use.(78-80) Another prominent application of thermostable enzymes is in the field of molecular biology. The discovery and use of DNA polymerase from *Thermophilus aquaticus* (Taq DNA polymerase) in the polymerase chain reaction (PCR) is a significant milestone in scientific research.(81) Many other DNA polymerases have also been isolated from thermophilic and hyperthermophilic archaea and are now commercially available. Other commonly used research enzymes include DNA ligases, proteases and restriction endonucleases.(82, 83) Given their wide applications, the pursuit and analysis of thermostable proteins/enzymes has become a growing field of research.

1.5 The effect of thermostability on catalysis

While thermophilic and mesophilic enzymes often have comparable catalytic activity at their optimal temperatures, thermophilic enzymes are often less active at lower temperatures.(84-86) For example, acylphosphatase from hyperthermophile *Pyrococcus horikoshii* (PhAcP) is less efficient at room temperature than its mesophilic homologues.(84) Comprehensive studies of activity, thermostability, and flexibility relationships of homologous enzymes from thermophiles, mesophiles, and psychrophiles demonstrated that enzyme flexibility often correlates with activity but is inversely related to its stability.(85-93) One popular hypothesis is that the extra stabilising interactions found in thermophilic enzymes enhance the enzyme's rigidity, which could be the cause of poor activity at low temperature. The flexibility is

restored with an increase in the temperature toward the optimum growth temperature of the organism. On the other hand, optimising local flexibility is a structural adaptation of psychrophilic enzymes to remain active at low temperatures.(85, 86, 94) However, this hypothesis could not explain some of the observations found in certain thermophilic enzymes. For example, a higher structural flexibility on the picosecond timescale has been observed for a thermostable α -amylase than its mesophilic counterpart.(95, 96) Moreover, a study of the millisecond-timescale flexibility of a hyperthermophilic rubredoxin at moderate temperature provided no evidence that enhanced conformational rigidity underlies the increased thermal stability.(97) In summary, the relationship between temperature adaptation and enzyme activity has not yet been clearly elucidated. Comparative studies between a well-studied mesophilic enzyme and its thermophilic/psychrophilic counterpart(s) might provide insights into this long-standing question.

1.6 Dihydrofolate reductase (DHFR)

Dihydrofolate reductase (DHFR) is a small enzyme that is found in all kingdoms of life and many have been well studied. Currently, over 30 DHFRs from all kingdoms of life and different physiological temperatures have been structurally or functionally characterised. Therefore, DHFR is a popular model used to study the relationship between enzyme structure, thermostability, and catalysis.

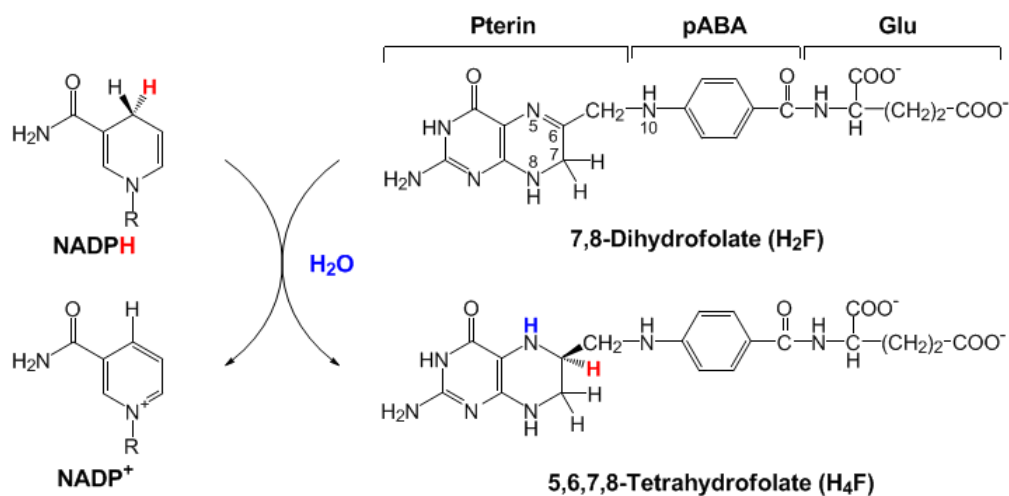


Figure 1.1 The DHFR-catalysed reaction.

DHFR plays a vital role in the cell by catalysing the NADPH-dependent reduction of 7,8-dihydrofolate (H_2F) to 5,6,7,8-tetrahydrofolate (H_4F) in the biosynthesis of amino acids and nucleic acids (Figure 1.1).^(98, 99) Both H_2F and H_4F belong to the family of folates (also known as vitamin B₉), and all of them consist of three functional moieties: a bicyclic pteridine, *p*-aminobenzoate, and a glutamate tail (Figure 1.1). H_4F is particularly important in cell growth and survival, because it participates in a complicated network of essential biosynthetic pathways by serving as a one-carbon unit carrier. A methyl, methylene or a formyl group can be added to the N5 and/or N10 positions of H_4F and subsequently transferred to different acceptors. In the biosynthesis of pyrimidines, for instance, a methylene group is added by the action of serine hydroxymethyl transferase to produce N⁵,N¹⁰-methylene- H_4F , which then becomes a carbon donor and a reducing agent in the formation of deoxythymidine monophosphate (dTMP). The C2 and C8 positions of purine nucleotide originate from the formyl groups transferred by H_4F (N¹⁰-formyl- H_4F). H_4F and its derivatives are also involved in the production of certain amino acids: methionine is generated as a methylated product of homocysteine through N⁵-methyl- H_4F during the cycle of *S*-adenosine methionine (SAM) regeneration (Figure 1.2). As illustrated by these examples, H_4F generated in the DHFR reaction is vital in the biosynthesis for multiple essential biomolecules and consequently cell replication and survival.

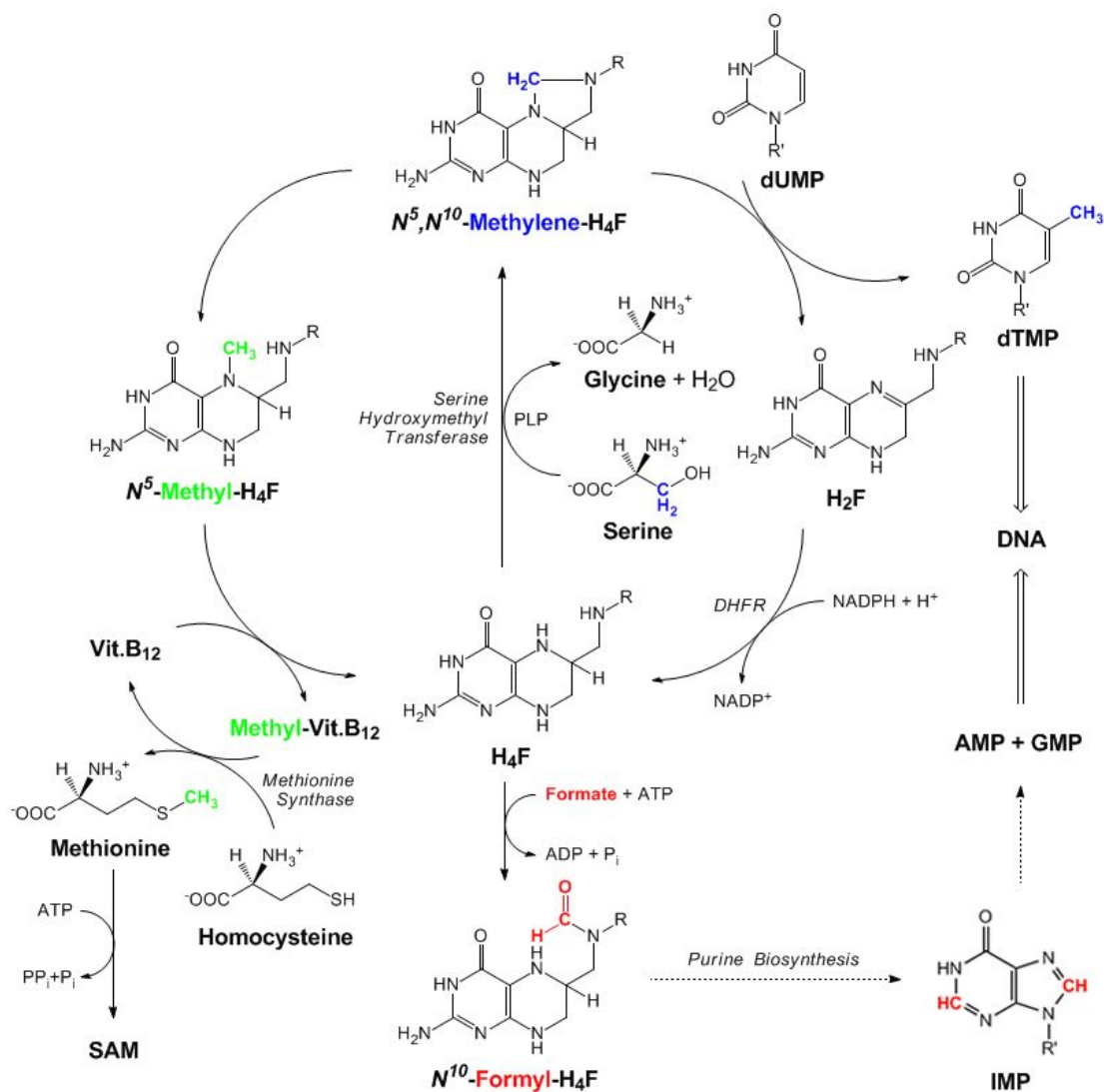


Figure 1.2 H₄F derivatives involved in purine bases, dTMP, methionine and glycine biosynthesis.

Whereas folates are indispensable for human survival and deficiency would cause symptoms such as anemia and depression,(100) humans actually lack a folate biosynthesis pathway and must obtain it from vegetables and fruits as a source of the vitamin. On the other hand, *de novo* biosynthesis of H₂F from GTP and shikimate can be found in other organisms, such as prokaryotes and plant cells.

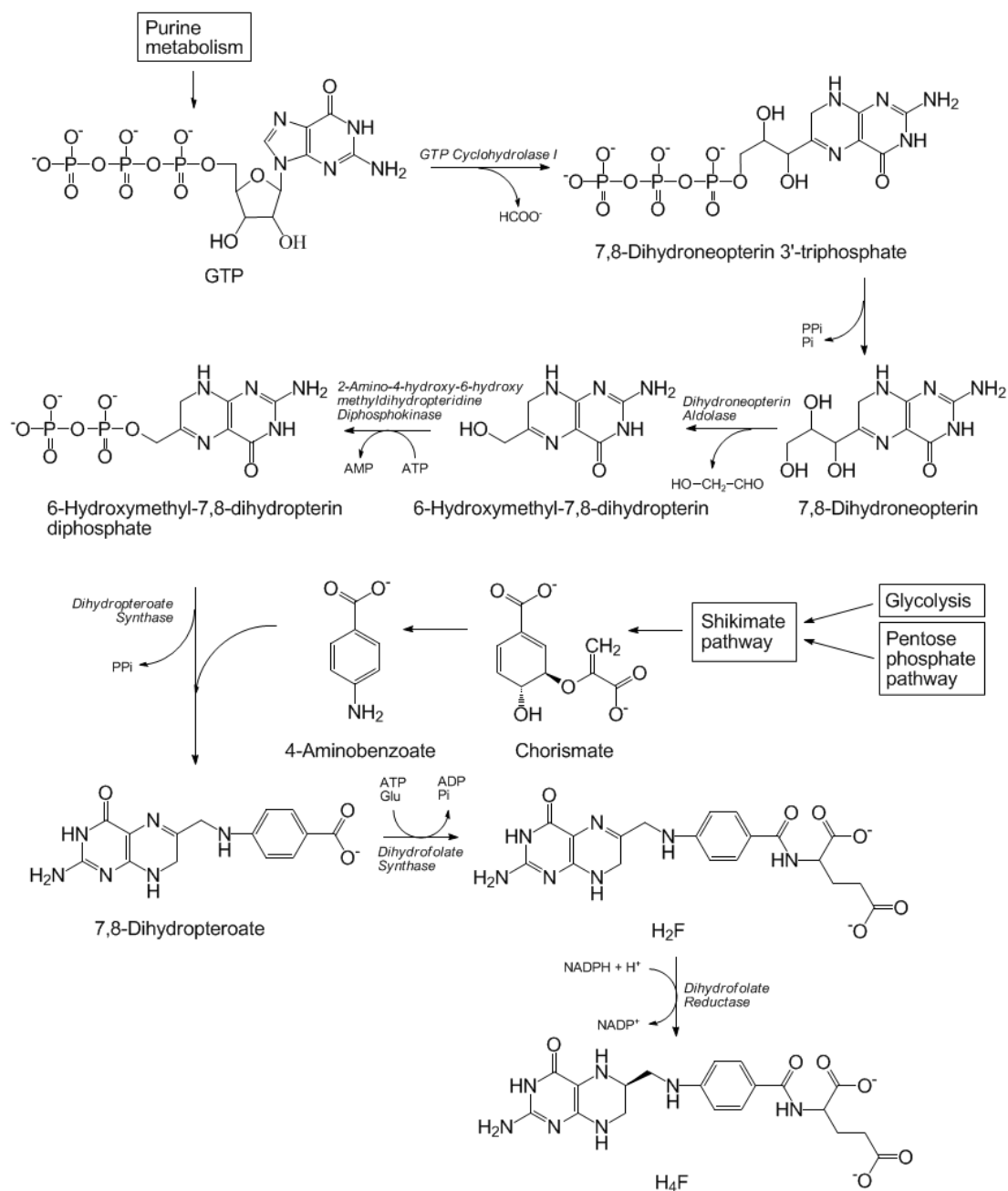


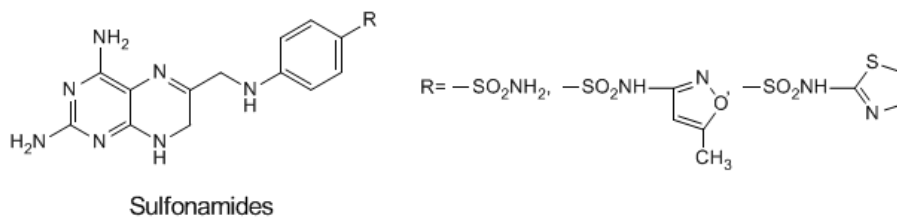
Figure 1.3 The folate biosynthesis pathway in plants, bacteria and lower eukaryotes.

As mentioned above, folates are tripartite molecules that are made up of a pterin, *p*-aminobenzoate and glutamate moieties. The first two are synthesised from GTP and chorismate, respectively. The first committed step catalysed by GTP cyclohydrolase I converts GTP into 7,8-dihydroneopterin 3'-triphosphate. The triphosphate motif is removed by a still unknown process (thought in some systems to first involve loss of

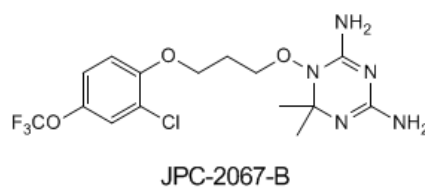
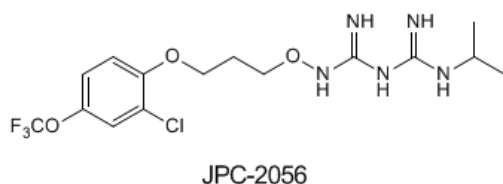
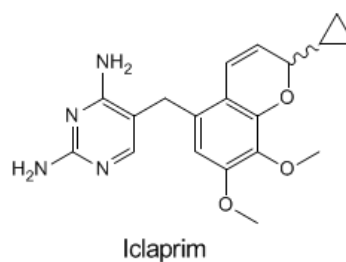
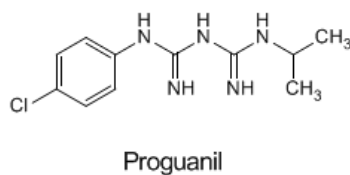
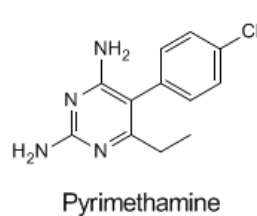
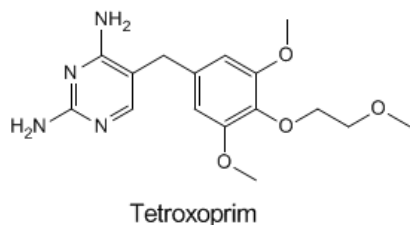
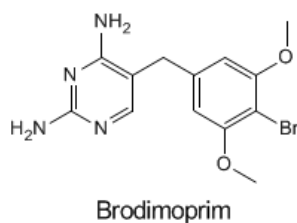
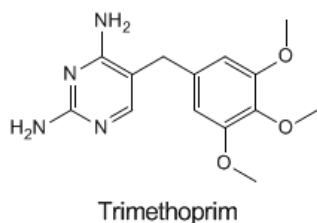
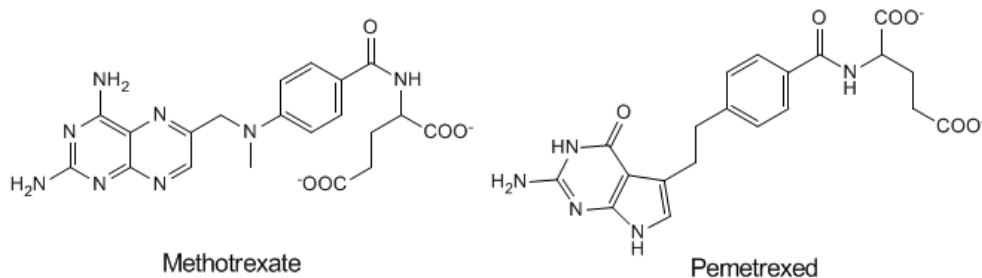
pyrophosphate then subsequent removal of the final phosphate), and the resulting 7,8-dihydroneopterin is converted to 6-hydroxymethyl-7,8-dihydropterin by dihydroneopterin aldolase (FolB). The consecutive action of the 2-amino-4-hydroxy-6-hydroxymethyldihydropteridine diphosphokinase (FolK), dihydropteroate synthase (FolP), dihydrofolate synthase (FolC), and dihydrofolate reductase (FolA) enzymes finally produces the final product, tetrahydrofolate (Figure 1.3).

The folate biosynthetic pathway is a well-established drug target for antimicrobial as well as antiparasite therapy. Sulfonamides (Figure 1.4A), the first synthetic antimicrobial and antiparasitic drugs with a broad action spectrum, act via inhibition of dihydropteroate synthase (Figure 1.3).^(101, 102) Other drugs act as inhibitors of dihydrofolate reductase and are used to treat a variety of diseases. Some of the classic examples include the chemotherapeutic agents methotrexate⁽¹⁰³⁻¹⁰⁶⁾ and pemetrexed (Figure 1.4B).^(107, 108) Methotrexate is a potent inhibitor of DHFR with an affinity 1000-fold stronger than folate and prevents tumor cell growth by prohibiting DNA synthesis.⁽¹⁰⁹⁾ Since it was clinically approved by the Food and Drug Administration (FDA) in 1943, methotrexate has been used to treat different neoplastic cancers including: leukemia, lymphoma and osteosarcoma.⁽¹⁰⁹⁾ Other DHFR inhibitors, such as trimethoprim,⁽¹¹⁰⁾ brodimoprim⁽¹¹¹⁾ and tetroxoprim,⁽¹¹²⁾ are antibiotics prescribed for bacterial infections, while pyrimethamine⁽¹¹³⁾ and proguanil⁽¹¹⁴⁾ are antiprotozoal compounds used to treat malaria. However, like the current situations of many other drugs, there is a noticeable drop in the efficacy of these DHFR inhibitors because pathogens have gained resistance. Even though DHFR inhibitors, such as the antibiotics iclaprim⁽¹¹⁵⁾ and the antimalarial drugs JPC-2056 and JPC-2067-B, have been developed relatively recently,⁽¹¹⁶⁾ there is still an urgent need to develop novel drugs thus it is worthwhile to further analyse the structure/activity relationship of DHFR.

A) Dihydropteroate synthase inhibitors



B) Dihydrofolate reductase inhibitors



1-(3'-(2-Chloro-4-trifluoromethoxyphenoxy)propyloxy)-5-isopropylbiguanide

4,6-Diamino-1,2-dihydro-2,2-dimethyl-1-(3'-(2-chloro-4-trifluoromethoxyphenoxy)propyloxy)-1,3,5-triazine

Figure 1.4 Structures of folate biosynthetic pathway inhibitors. A) Dihydropteroate synthase inhibitors. B) Dihydrofolate reductase inhibitors

1.7 Structure of DHFR from *Escherichia coli* (EcDHFR)

DHFR is arguably one of the most thoroughly investigated enzymes in terms of structural biology, experimental dynamics, thermal adaptation, and enzyme catalysis. Beginning with the first reported crystal of DHFR cloned from *Lactobacillus casei* (LcDHFR) in 1977,(117) approximately 250 structures of DHFR have been solved to date by the use of X-ray crystallography, solution NMR spectroscopy and neutron diffraction. Almost all of these characterised structures are small monomeric polypeptides that are similar in tertiary structure (with the exception of the dimeric DHFR from *Thermotoga maritima*, TmDHFR(118)). Moreover, these structures have been solved in the forms of apoenzyme and complexes with different ligands, such as substrates, inhibitors and cofactors. DHFR's from a wide variety of organisms, ranging from *Escherichia coli*,(119) *Geobacillus stearothermophilus*,(120) *Mycobacterium tuberculosis*,(121) *Thermotoga maritima*,(118) *Candida albicans*,(122) *Gallus gallus* (chicken)(123) to *Homo sapiens* (human),(124) have been characterised structurally. Among them, DHFR from *Escherichia coli* is most frequently studied, with ~50 crystal complexes reported. Hence, EcDHFR has become a paradigm in studying the relationship between enzyme catalysis, protein dynamics and thermal adaptation.

EcDHFR is a 18 kDa monomeric enzyme (159 residues), composed of four flanking α -helices, an eight stranded β -sheet and three mobile loops.(118) Each strand of the β -sheet is termed in consecutive order: β A (residues 1-8 in EcDHFR), β B (residues 39-43), β C (residues 58-63), β D (residues 73-75), β E (residues 89-95), β F (residues 108-116), β G (residues 132-141) and β H (residues 150-159) (Figure 1.5); whereas the α -helices are named based on their proximity to the β -strands: α B (residues 24-35), α C (residues 43-50), α E (residues 77-86), and α F (residues 96-104). The structure of EcDHFR can be categorised into three domains: the adenosine binding domain (ABD), the loop domain (LD) and the N-terminal domain (ND).(125) The adenosine moiety of the cofactor NADPH docks into the ABD, which comprises β B, C, D and E

strands and α C, E and F helices. As suggested by its name, the LD is formed by three important and flexible loops, namely the M20 (residues 10-24), the FG (residues 116-132) and GH (residues 141-150) loops. The active site is situated in the N-terminal domain, surrounded by the cleft area between α B and α C helices and the M20 loop.

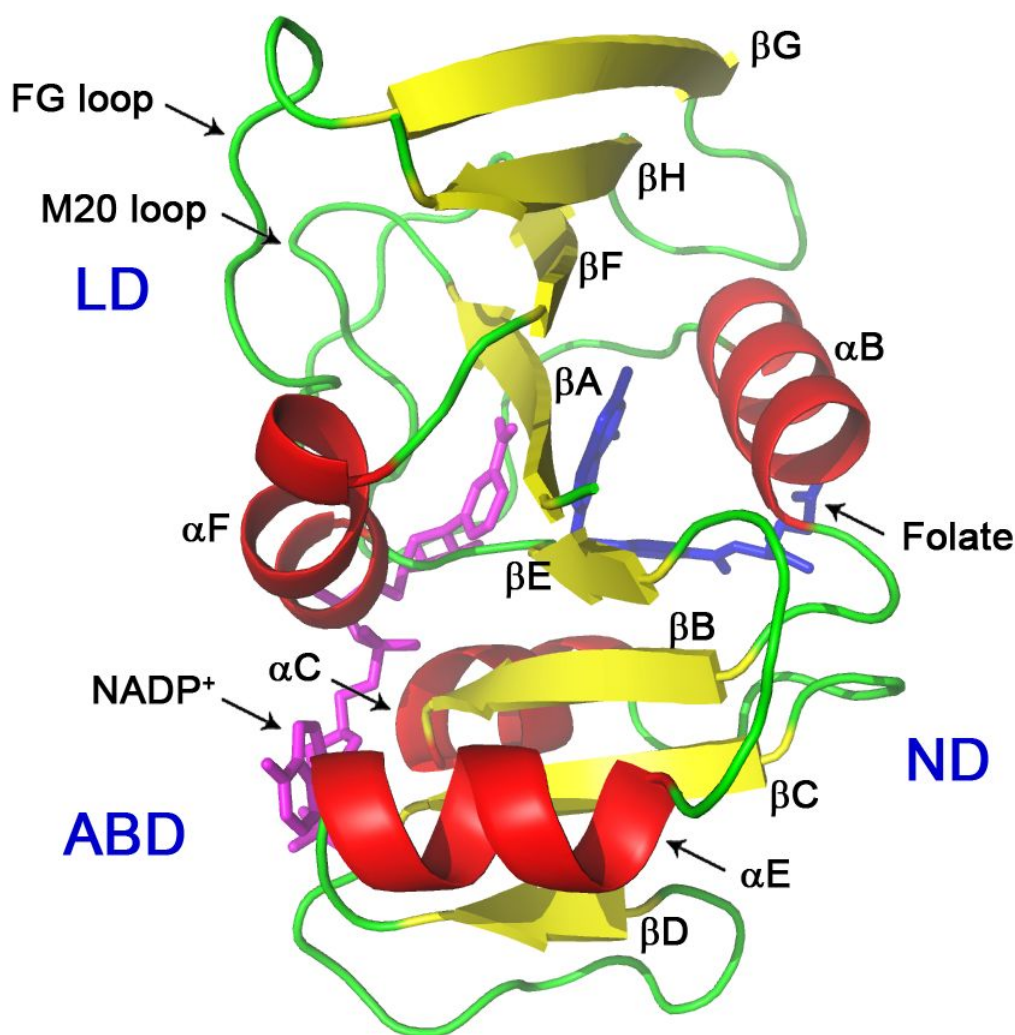


Figure 1.5 Structure of EcdHFR indicating the adenosine binding domain (ABD), N-terminal domain (ND), loop domain (LD), and the flexible M20 and FG loops (PDB 1RX2),(125)

In the active site of EcdHFR, the acidic residue Asp27 is the only ionisable residue. The presence of the carboxylate moiety appears to be significant, because different DHFR homologues contain either an aspartic or a glutamic acid residue at this

position. In EcDHFR, Asp27 coordinates with the substrate H₂F via a pair of hydrogen bonds with the N3 and C2-amino protons of the pterin ring.(125, 126) Furthermore, together with Trp22 and Thr113, Asp27 forms a network of hydrogen bonds with the pterin ring of H₂F.(127) A hydrogen bonding network is formed between the hydroxyl group of the Thr113, a fixed water molecule and the C2-amino group of the pterin ring. Trp22 forms another network of hydrogen bonds with the carboxylate group of Asp27 and the C4 carbonyl of the pterin ring via a water molecule (Figure 1.6). Replacing any of these three residues with ones that cannot form the hydrogen bond networks leads to a profound decrease in the rate of enzyme turnover and affinity for the substrate.(128, 129) Removal of a potential acidic proton in the active site, for example site directed mutagenesis of the Asp27 residue in EcDHFR to asparagine(130) or serine(131), has been shown to decrease the enzyme's hydride transfer rate greatly (300-fold) at physiological pH and reduce the binding affinity of the substrate. However, both variant enzymes were able to function at full catalytic efficiency when the substrate was fully protonated at low pH.(130-132)

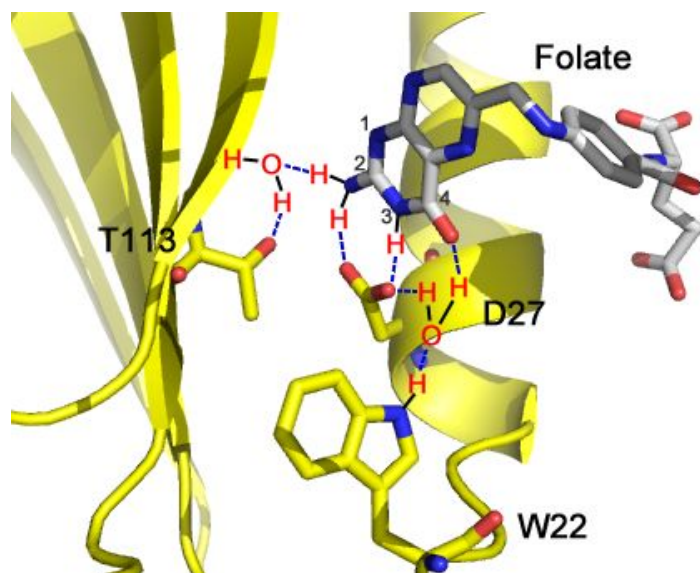


Figure 1.6 Active site hydrogen bonding network of EcDHFR, coordinating the substrate, active site residues and fixed water molecules (PDB 1RX2).

The hydride transfer step (the chemical step during the kinetic cycle; see below) for the EcDHFR catalysed reaction is pH dependent and the rate decreased with

increasing pH showing an inversion point at pH 6.5. It is generally accepted that the protonation event is responsible for the pH dependence of the chemical step, but there has been dispute of the actual proton source. Previously, this apparent pK_a was suggested to be attributed to Asp27, since it is the only residue in the active site that seems to be able to protonate the substrate. (133-136) Protonation of N5 was proposed to involve an adjacent water molecule, which is stabilised in the active site by the enol tautomer of the substrate's pterin ring. A proton is transferred from the water molecule to the O4 of the pterin ring and the proton of N3 is shifted to the carboxylate group of Asp27. Afterwards, the O4 proton is transferred to the N5 of the substrate setting the N5=N6 bond of the pterin ring ready for hydride transfer. The N3 proton is then transferred back from Asp27 (Figure 1.7).

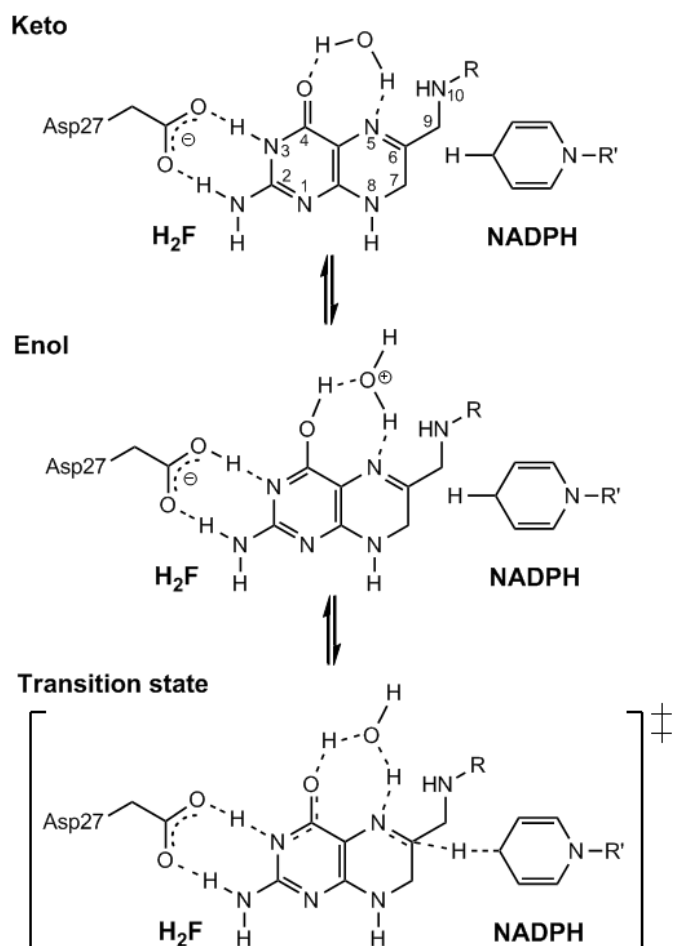


Figure 1.7 The mechanism of the proposed keto-enol tautomerisation. Hydrogen bonds are dashed. (Figure taken from reference (133))

However, water in this position has not been observed in various crystal structures of DHFR. This is contrary to the proposal that such a water molecule may be involved in the reaction. Additionally, Shrimpton and Allemann outlined the fact that the bond angles and lengths are not optimal for protonation of N5 from O4 *via* the water molecule.(137) An alternative mechanism has been suggested, involving protonation of the N5 atom of H₂F directly from solvent. Protonation in this mechanism is *via* O4 of the pterin ring to the lone pair of N5 through the water molecular at Site B (Figure 1.8).

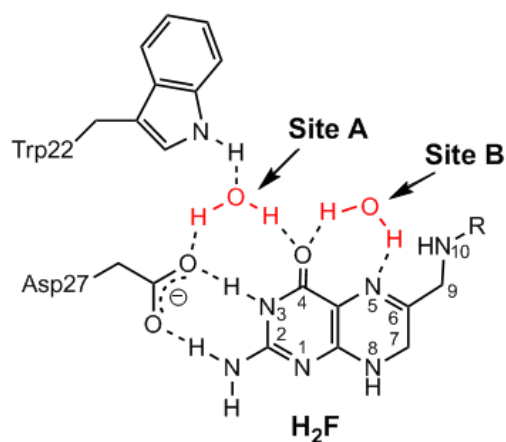


Figure 1.8 Hydrogen bonding network in the EcdHFR active site indicating potential water sites relative to the positioning of the substrate in the E·H₂F·NH complex.(127) Water molecules are coloured red. (Figure taken from reference (137))

It was previously shown through molecular dynamics simulations of EcdHFR that the N5 atom is solvent exposed with 50% and 80% H₂O contact in the closed and occluded states (different conformations during the kinetic cycle, see below) respectively.(126) Shrimpton and Allemann showed that water molecules are brought within hydrogen bonding distance of N5 with minimal conformational change (0.79 Å r.m.s deviation of backbone atoms). Occupancy of site B with water molecules was increased as the simulation time was increased from 210 ps to 1 ns. Additionally, and in favour of the hypothesis that hydride transfer and protonation are sequential events, when the hydride is transferred first, the M20 loop moves away from N5 and H₂O

access is increased, presumably to allow direct protonation from water.(137)

1.8 The kinetic cycle of EcDHFR.

Due to the biological and pharmacological importance of DHFR, this enzyme has been the subject of intensive kinetic investigations for decades. The full kinetic scheme of EcDHFR has been extensively studied and elucidated by Benkovic and coworkers.(125, 138-140) Under steady state conditions, the *E. coli* enzyme cycles through five key intermediates: $E \cdot H_2F \cdot NH$, $E \cdot H_4F \cdot N^+$, $E \cdot H_4F$, $E \cdot H_4F \cdot NH$, $E \cdot NH$ (Figure 1.9).(138) The chemical step refers to the step of hydride transfer, when the ternary Michaelis complex $E \cdot H_2F \cdot NH$ transforms to the ternary product complex $E \cdot H_4F \cdot N^+$. The oxidised cofactor subsequently releases from the product complex to yield the binary complex $E \cdot H_4F$, which binds a molecule of reduced cofactor forming the mixed ternary complex or product release complex, $E \cdot H_4F \cdot NH$. In preparation for the next cycle, the product H_4F is replaced with another substrate molecule H_2F via another binary complex $E \cdot NH$.

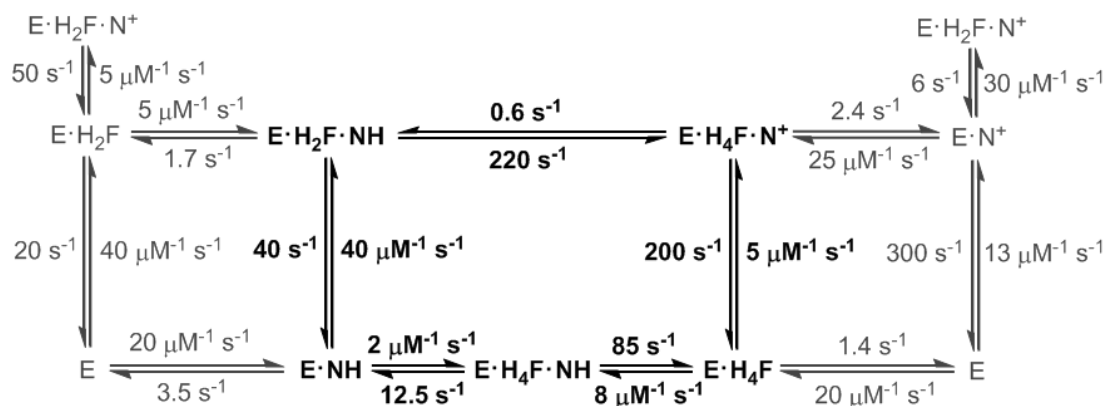


Figure 1.9 The complete kinetic scheme for conversion of H_2F to H_4F by EcDHFR at pH 7 and 25 °C. Where E = DHFR, NH = NADPH, N^+ = $NADP^+$, H_2F = dihydrofolate and H_4F = tetrahydrofolate. (Figure taken from reference (138))

There are several characteristic features of the EcDHFR catalytic cycle. Firstly, free enzyme is not regenerated during the cycle. Secondly, the rate of hydride transfer is highly dependent on pH with a single pK_a of 6.5.(138) As it is observed in many

enzymes, at neutral pH catalysis by EcDHFR is limited by product release rather than the chemical step. Under steady state conditions at 25°C and pH 7, the product release step of the cycle is rate limiting ($k_{\text{cat}} = 12.5 \text{ s}^{-1}$) while the step of hydride transfer ($k_{\text{H}} = 220 \text{ s}^{-1}$) is ~18-fold faster. However, when the pH of the reaction is raised to higher than 9, the chemical step becomes rate limiting under steady state conditions due to the decreased availability of protons needed to protonate the N5 position of H₂F.(138)

1.9 Loop and subdomain movements during the catalytic cycle

As described in Section 1.7, access to the active site is modulated by the flexible, largely conserved M20 loop.(141, 142) This loop lies directly over the active site, protecting it from solvent, and is primarily responsible for determining the conformation of the active site. The FG and GH loop play stabilising roles *via* hydrogen bonding interactions with the M20 loop. Sawaya and Kraut(125) published a set of crystal structures of EcDHFR analogous to the five key intermediates of the kinetic cycle (Section 1.8) determined by Benkovic and co-workers;(138) the holoenzyme E·NH, the Michaelis complex mimic E·Folate·N⁺, the ternary product complex mimic E·ddH₄F·ATP-ribose, the binary product complex mimic E·ddH₄F, the product release or mixed ternary complex mimic E·ddH₄F·NH and additionally a transition state analogue complex E·MTX·NH. The crystal structures suggest that the M20 loop is predominantly ‘closed’ over the reactants in the holoenzyme, Michaelis, and transition state complexes. During the remainder of the cycle, nicotinamide is not bound, thus the loop ‘occludes’ the nicotinamide-ribose binding pocket (Figure 1.10A). Besides the ‘closed’ and ‘occluded’ states, there are two more states which are ‘open’ and ‘disordered’, respectively.(125) In the ‘open’ M20 loop conformation, the *p*-aminobenzoylglutamate binding cleft is widened significantly and there is an 8 Å opening to the nicotinamide binding site, and this form displays characteristics intermediary to the ‘closed’ and ‘occluded’ states. In the ‘disordered’ state, the M20 loop’s motions render it unclear crystallographically and it appears in the X-ray structures of the apoenzyme.(125, 143)

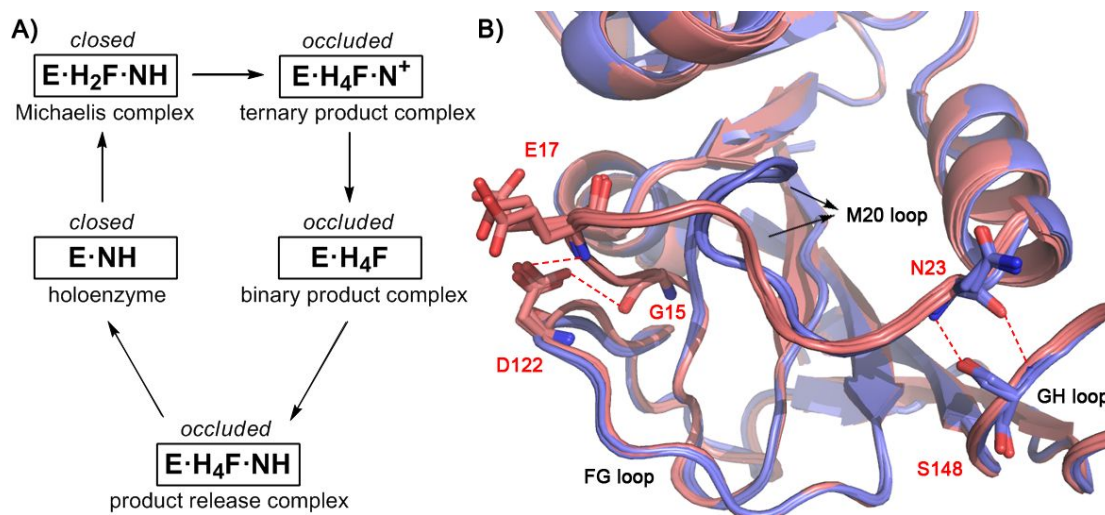


Figure 1.10 A) Conformational changes in the active site loops through the catalytic cycle of DHFR. B) Detailed view of the catalytically important M20 loop in the closed (red, PDB 1RA1 (holoenzyme), 1RA2 (Michaelis complex), 1RA3 (transition state complex)) and occluded (blue, 1RX4 (ternary product complex), 1RX5 (binary product complex), 1RX6 (product release complex)) conformations in EcDHFR. Hydrogen bonding interactions in the closed and occluded conformation are indicated.

Before the chemical step of the cycle, in the holoenzyme and Michaelis complex, M20 loop closes over the active site, shielding the reactants from solvent and providing an optimal environment for protonation of N5 of the dihydrofolate and hydride transfer to occur. This closed conformation is stabilised by hydrogen bonding to the neighbouring FG loop (G15-D122 and E17-D122). In the ternary and binary product complexes and product release complex, however, the M20 loop occludes the active site, preventing the nicotinamide ring of the cofactor NADP(H) from entering. In the occluded conformation, the hydrogen bonds between M20 loop and FG loop are disrupted. This occluded conformation is stabilised by a pair of hydrogen bonds between residue N23 on the M20 loop and S148 on the GH loop (Figure 1.10B). The chemical step of the reaction, hydride transfer from NADPH to dihydrofolate with concomitant protonation of dihydrofolate, occurs within the closed conformation.(125)

1.10 Principles of enzyme catalysis

Enzymes can achieve incredible rate accelerations of up to 21 orders of magnitude relative to uncatalysed reactions. For this reason, understanding enzyme mechanism has become the goal of many research groups for more than one century. Nevertheless, the precise mechanism by which enzyme can reach such an incredible rate accelerations has not been fully elucidated. Since hydrogen is a small particle with wave-like property, many enzymatic hydrogen transfer reaction are expected to proceed by quantum mechanical ‘tunnelling’, as evident by multiple studies. Given that hydrogen tunnelling is expected to be highly sensitive to the relative molecular properties of the surrounding environment,⁽¹⁴⁴⁻¹⁴⁷⁾ experimental and theoretical studies extrapolated from enzymes that catalyze hydrogen tunnelling, such as DHFR, can reveal valuable information on the mechanism of enzyme catalysis.

1.10.1 Semi-classical transition state theory

Previously, the enzyme catalysed reactions have been explained by semi-classical transition state theory (TST). This model ignores nuclear quantum effects typically. They only consider quantum mechanical effects on vibrational zero point energy (ZPE). By definition, the transition state (TS) is the transitory of molecular structure in which the molecule is no longer a substrate but not yet a product. All chemical reactions must go through the transition state to form a product from a substrate molecule (ground state, GS). The transition state is the least stable state. It has more free energy in comparison to the substrate or product. Generalised transition state theory provides a framework for the understanding of chemical reactions. The rate of the reaction can be related to the energy barrier between transition state and ground state by the Arrhenius equation.

$$k = A \exp\left(-\frac{\Delta E_a}{RT}\right)$$

where A is the Arrhenius pre-exponential factor, ΔE_a is the activation energy and R is the gas constant.

Kinetic isotope effect (KIE) is defined as the ratio of rate constants for the reactions involving the light (k_L) and the heavy (k_H) isotopically substituted reactants. It has long served as a probe for the mechanisms of both enzymatic and solution reactions. In semi-classical transition state theory, difference in vibrational zero point energy (ZPE = $1/2h\nu$) upon isotopic substitution is the primary contributor to the KIEs. Heavier isotopes have lower vibrational ZPEs at both ground state (GS) and transition state (TS), requiring different amounts of activation energy to reach the TS (Figure 1.11). The hydrogen KIE is particularly useful because the ratio of the masses of the isotopes is much larger than that of any other element, resulting in relatively high KIEs. A primary (1°) KIE is a KIE where the isotopically labelled atom is directly involved in bond cleavage or formation. It can be described as:

$$KIE = \frac{k_L}{k_H} = \frac{A_L}{A_H} \exp\left(\frac{\Delta ZPE}{RT}\right) = \frac{A_L}{A_H} \exp\left(\frac{1/2h\nu_L - 1/2h\nu_H}{RT}\right)$$

where ν is the vibration frequency of the transferring particle.

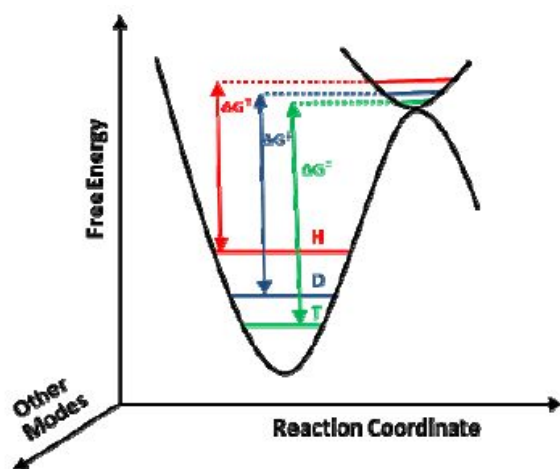


Figure 1.11 Semi-classical model of 1° KIEs. KIEs arise from the difference in ZPE between the reactants at the GS and the TS. (Figure taken from reference (148)).

In semi-classical models, the KIE is temperature dependent and is equal to unity at infinite temperature ($KIE = A_L/A_H = 1$). Additionally, this equation provides semi-classical upper limits on KIEs. Theoretical upper limits for H/D and H/T KIEs are 6.9 and 15.8 at 25 °C, respectively.(149) However, the vibration frequencies

orthogonal to the reaction coordinate presented at the transition state can deflate the primary KIEs from the maximum predicted values (Figure 1.11). The maximum KIE is obtained when the bond involving the isotope is completely broken in the transition state. In this case, the difference in activation energies is simply the difference in zero point energies of ground state.

1.10.2 Bell's tunnelling correction model

A transferring particle can be treated in terms of its location and momentum as a wave of energy (wave-particle duality).⁽¹⁵⁰⁾ This is the central concept of quantum mechanics. All particles have associated with them a wavelength, λ , which can also be described as the positional uncertainty, depending on mass according to the equation below. The equation is named after Louis de Broglie, who first proposed these ideas in his doctoral thesis.⁽¹⁵¹⁾

$$\lambda_B = \sqrt{h^2 / 2mE}$$

where h is Plank's constant, m is the mass of the transferred particle. E is its energy and λ_B is the de Broglie wavelength. From this expression, the lighter the particle in mass, the higher de Broglie wavelength it has, and therefore exhibits greater positional uncertainty.

Hydrogen has a relatively low mass, and thus a higher uncertainty in its position. For example, assuming an energy of 20 kJ mol⁻¹, protium has a de Broglie wavelength of 0.63 Å, and deuterium has a shorter de Broglie wavelength of 0.45 Å due to its increased mass.⁽¹⁴⁹⁾ Because this is comparable to the distance over which hydrogen must move in a typical reaction (< 1 Å), the wave properties of hydrogen are expected to play a role in its transfer between a donor atom and an acceptor atom. Therefore, Bell took into account the concept of particle "tunnelling" through the energy barrier of the reaction around the transition state.⁽¹⁵²⁾ According to Bell's tunnelling correction model, the potential for the occurrence of tunnelling depends on the properties of the particle and also on the width of the energy barrier. The narrower the

barrier in terms of width, the smaller the barrier in terms of height, and the smaller the particle in terms of its mass, the greater probability of tunnelling.

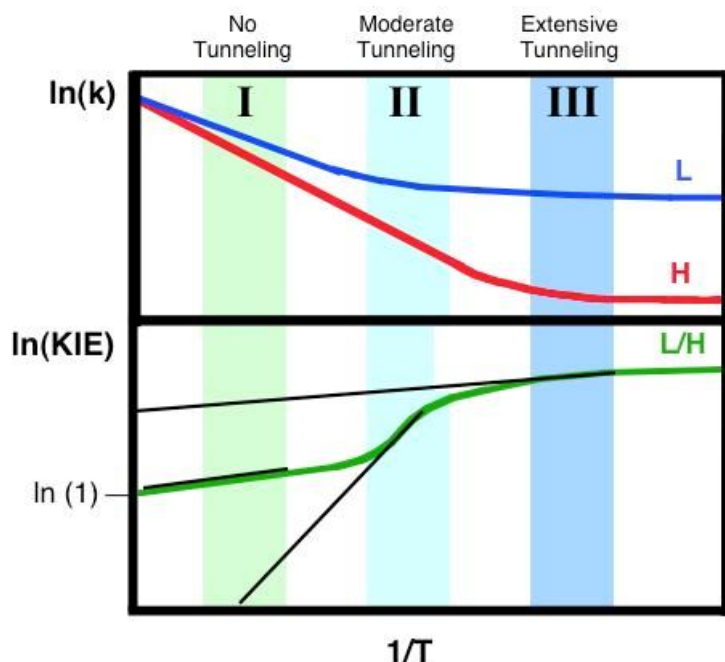


Figure 1.12 Arrhenius plot of rate (top) and KIEs (bottom) of light (blue) and heavy (red) isotopes.

Measurement of kinetic isotope effects (KIEs) is an excellent technique to infer the occurrence of tunnelling during an enzymatic reaction (Figure 1.12).^(149, 153-155) In Bell's tunnelling correction model, kinetic isotope effects arise not only from differences in the zero point energy (ZPE), but also due to the differences in the de Broglie wavelength (λ_B) of the transferred isotope. Since the de Broglie wavelength of protium is longer than that of deuterium, protium tunnels over greater distances than deuterium. Therefore, with the influence of the tunnelling effect, the upper limit of H/D KIE will be higher than 6.9 at 25 °C. At high temperatures (region I in Figure 1.12), reactions mostly take place by thermal activation which leads to temperature-dependent rates and KIEs. The tunnelling is negligible and the A_L/A_H is close to unity, as predicted by semi-classical models. At very low temperatures (region III in Figure 1.12), the particle transfer does not have enough thermal energy to react classically and tunnelling becomes dominant. Both k_H and k_D or E_a^H and E_a^D become temperature-independent, and the Arrhenius prefactor ratio will be higher

than unity. Between those two extremes lies the moderate tunnelling region II (Figure 1.12), where the lighter isotope mostly tunnels, but the heavy isotope reacts mostly by thermal activation, leading to a very steep temperature-dependent KIEs and the corresponding Arrhenius prefactor ratio much smaller than unity.(152)

1.10.3 Development of Bell's tunnelling correction model

Bell's tunnelling correction model inherits a limitation from semi-classical models, as it only takes into account the quantum mechanical effects in hydride transfer but not the whole system. Moreover, it ignores the influences of the polar medium and heavy-atom motions. Subsequent discovery of enzymes displaying greatly inflated KIEs,(156, 157) unusual temperature dependences of their KIEs,(155, 158) or ratios of Arrhenius prefactors outside the semiclassical limits(156) led to a collapse of the Bell model for hydrogen tunnelling and new theoretical frameworks developed to account for the experimental observations. These new models include rate-promoting motions or vibrations,(159-162) vibrationally enhanced ground state tunnelling,(163, 164) multi-dimensional tunnelling(165) and environmentally coupled tunnelling models.(149, 166) All of these models were premised on a contribution from quantum-mechanical tunnelling in all enzyme-catalysed hydride transfer. While H-tunnelling is considered strongly linked to the protein dynamics, the exact functional role(s) in driving tunnelling and therefore the overall enzyme-catalysed reaction is currently under considerable debate.(167-172)

The rate-promoting motions model and vibrationally enhanced ground state tunnelling model have been proposed by the research groups of Schwartz and Scrutton, respectively. The former model indicates that rate-promoting vibrations are directly linked to tunnelling by modulating the distance between reactants,(159-162) whereas the latter model states that tunnelling is promoted by a set of short-range vibrations which modulate the geometry of the active site and no long-range coupled motion is required.(163, 164) Truhlar and coworkers have proposed an alternative explanation

to the collapse of the Bell model; their computational work has led to the multi-dimensional tunnelling model, in which the protein motions and hydride transfer are correlated geometrically. They proposed that the free energy profile for hydride transfer reaction as a function of a reaction coordinate greatly depends on the geometrical parameters of the reactants. They also ascertained that although tunnelling makes only a small change in the primary KIE, it makes a large change in the secondary KIE.⁽¹⁶⁵⁾ Lastly, the environmentally coupled tunnelling model, proposed by Klinman and coworkers,^(149, 166) was developed based on Kuznetsov and Ulstrup's full tunnelling model.⁽¹⁷³⁾ In this model, enzyme motions that drive tunnelling are divided into two classes: slow motions (pre-organisational motions) that drive the enzyme active site into a tunnelling-ready conformation from which the reaction can occur, and fast gating motions (re-organisational motions) that squeeze the width of the potential-energy barrier and therefore alter the tunnelling possibility.⁽¹⁴⁹⁾ When an enzyme relies on gating dynamics, temperature-dependent KIEs are observed, whereas enzyme reactions occurring from tunnelling-ready conformations without additional barrier compression are characterised by temperature-independent KIEs.

1.11 Protein dynamics in EcDHFR

Numerous site-directed mutagenesis studies also have been done on EcDHFR to probe the change of flexibility and conformation in the M20, FG and GH loops during catalysis. As have been mentioned above, the hydrogen bond between Asp122 and Glu17 collaborates with the hydrogen bond between Asp122 and Gly15 playing a key role in stabilising the closed conformation. Substitution of residue Asp122 destroys the hydrogen bonds between these residues and leads to a substantial decrease in both the NADPH affinity and the hydride transfer rate. This indicates the importance of these hydrogen bonding interactions in formation of the transition state. In contrast, mutations in the GH loop residue Ser148, which forms hydrogen bonds with Asn23 in the occluded conformation, have little effect on the hydride transfer rate.^(174, 175)

Surprisingly, mutation of Gly121 (G121V), which is far from the active site (more than 19 Å) and expected to cause only slight alterations in the active site geometry, results in a 40-fold decrease in NADPH binding affinity and a striking 200-fold decrease in the hydride transfer rate.⁽¹⁷⁶⁾ Deletion of Gly121 has a similar effect on the kinetics.⁽¹⁷⁷⁾ It was interpreted as an introduction of an extra step with a slow conformational change prior to hydride transfer into the catalytic cycle. The reason for the reduced catalytic activity of EcDHFR-G121V is still under discussion.⁽¹⁷⁷⁻¹⁸⁰⁾

Many theoretical methods have been performed to study the protein dynamics during EcDHFR catalysis. Theoretical methods can identify motional correlations between different regions of the protein and simulate the dynamics of complexes such as the Michaelis complex which are too short-lived to sample through NMR. Benkovic, Wright and coworkers⁽¹⁸¹⁾ carried out model-free ¹⁵N relaxation measurements with the EcDHFR binary folate complex to investigate the protein backbone dynamics. Diverse dynamical features were seen in the DHFR backbone. Several residues also showed high amplitude, low order motions on a fast timescale, such as Gly67 and Asp69 at the adenosine binding domain, Lys38 and Val88 at the hinge between the adenosine binding domain and loop domain, and Glu120, Gly121 and Asp122 in the central portion of the FG loop. This indicates that a cluster of residues in the cofactor binding area, the M20 and FG loop have similar order parameters on the pico- to nanosecond timescale and is consistent with a network of correlated motions.

Following this work, a similar model-free ¹⁵N relaxation study of EcDHFR backbone dynamics was carried out with three different complexes in an attempt to elucidate the local motion of the polypeptide chain during the catalytic cycle.⁽¹⁸²⁾ There are significant differences in the backbone dynamics in the different complexes. In the occluded conformation complexes, residues in the M20 and FG loop and residues 67-69 in the adenosine binding loop display large amplitude motions on the pico- to nanosecond timescale. Formation of the closed conformation leads to attenuation of the motions in the M20 and FG loop, but results in increased flexibility in the

adenosine binding loop. The change of flexibility in various loops during the catalytic cycle reveals the key role of the M20 and FG loop in controlling the access to the active site, and also provides evidence for long-range motional coupling between the adenosine binding loop and distant regions of the protein.

Radkiewicz and Brooks(183) performed 10 ns duration molecular dynamics simulations on three ternary complexes from the catalytic cycle (Figure 1.13). The overall motions and atomic fluctuations were calculated in the three complexes: $E \cdot H_2F \cdot NH$, $E \cdot H_4F \cdot N^+$ and $E \cdot H_4F \cdot NH$. The simulations reveal enhanced flexibility in several loops, in general agreement with Benkovic and Wright's result.(181, 182) Particularly, in the complex $E \cdot H_2F \cdot NH$, motions of residues in the FG loop are strongly coupled to motions in the M20 loop and also distant regions such as the αC helix and adenosine binding loop. Such correlations were not seen in product complexes $E \cdot H_4F \cdot N^+$ and $E \cdot H_4F \cdot NH$, suggesting an involvement for such motions during the catalytic cycle. They also concluded that mutants might affect catalysis by altering the protein dynamics.

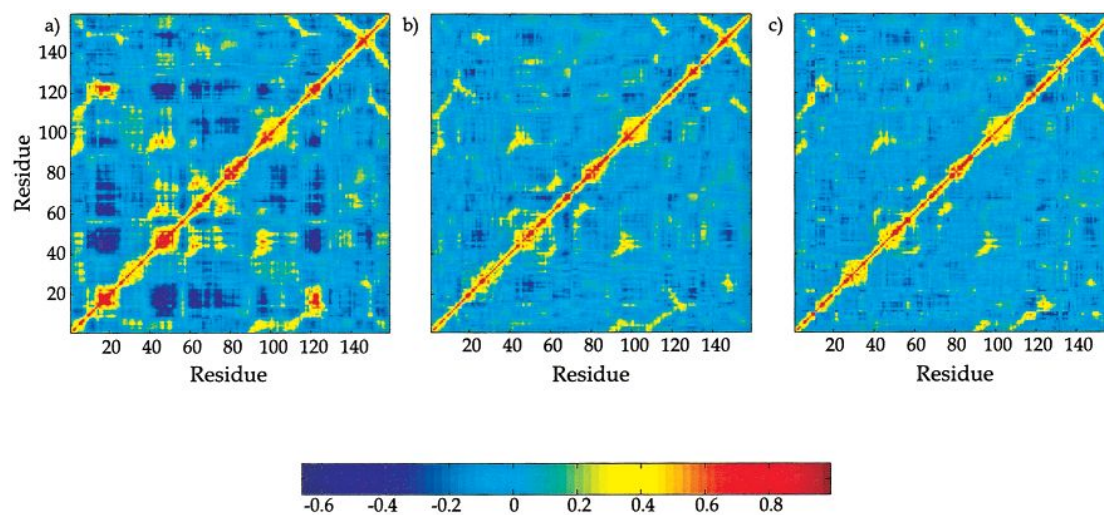


Figure 1.13 Residue-residue based map of correlated motions. Red and yellow indicate regions of positive correlation, and dark blue indicates regions of anti-correlation for; a) $E \cdot H_2F \cdot NH$, b) $E \cdot H_4F \cdot N^+$ and c) $E \cdot H_4F \cdot NH$. (Figure taken from reference (183)).

Later, Agarwal *et al.* (153, 184) combined the data from genomic analysis of sequence conservation, kinetic measurement of multiple mutations and mixed quantum/classical molecular dynamics simulations of hydride transfer together, and identified a network of coupled promoting motions in the DHFR-catalysed reaction (Figure 1.14). The promoting motions describe structural changes that occur from the Michaelis complex through to the transition state and on to the product, extend throughout the protein, range from a femto- to a millisecond timescale, and may play a key role in promoting hydride transfer. The simulations showed that several key residues in the active site participated in the network of promoting motions. It was suggested that motions of these side chains assist in directing the hydride donor toward the acceptor.

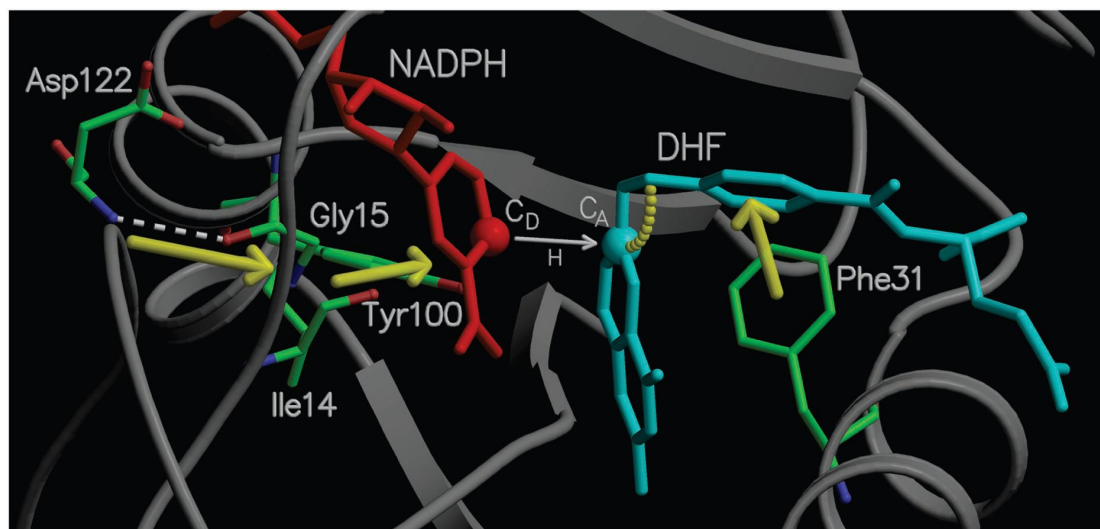


Figure 1.14 Diagram illustrating the network of coupled promoting motions as proposed by Agarwal *et al.*, 2002. (153) Where C_D is the hydride donor carbon C^4 of NADPH. C_A is the acceptor carbon C^6 of the substrate. H indicates the direction of hydride transfer. The directions of promoting motions are indicated in yellow. (Figure taken from reference (153)).

1.12 Contribution of protein dynamics to catalysis in EcdHFR

The above section (Section 1.11) suggested that protein dynamics are involved in the DHFR-catalysed reaction. The location and timescales of the motions observed

together with the availability of large amounts of detailed structural and mechanistic data make EcDHFR a good paradigm for understanding the relationship between dynamics and catalysis.(125, 138, 185, 186)

Benkovic and Wright *et al.* have engineered an EcDHFR N23PP/S148A mutant which cannot form the occluded conformation due to loss of hydrogen bonding between the M20 and GH loops.(187) They interpreted that the hydride transfer rate and steady-state turnover rate were reduced because of the elimination of the millisecond timescale motions of the M20 loop in the Michaelis complex. They therefore concluded that millisecond timescale protein motions contribute significantly to enzyme catalysis.

However, results obtained from some other studies strongly contradict this conclusion. A subsequent computational study of this mutant by Warshel and coworkers suggested that the reduced rate constant is not because of the abrogation of millisecond timescale fluctuations but a consequence of changes to the reorganisation free energy of the reaction brought about by altering of the electrostatic preorganisation within the active site.(188) The temperature dependence of kinetic isotope effects measured in our group showed the nature of the chemistry in the N23PP/S148A mutant is essentially the same as in the wild type enzyme.(189) We therefore proposed that the conformational fluctuations do not seem to be directly involved in the chemical step of the reaction. The subtle conformational changes brought about by amino acid substitutions change the equilibrium of the conformational state of the enzymes and therefore affect the reaction rate constants. This conclusion aligns well with our previous work on the effect of cosolvents. These results showed that viscosity of the cosolvents, which affects the long-range motions(190) clearly does not link to the reaction rates of EcDHFR,(191) TmDHFR(192) and MpDHFR (psychrophilic DHFR from *Moritella profunda*)(193). It is therefore shown that long-range motions do not couple directly to hydride transfer of the reaction. The studies performed on adenylate kinase also obtained the same conclusion.(170) Warshel and coworkers simulated the

dynamic coupling on a millisecond timescale and found that the millisecond timescale conformational dynamics were not 'remembered' during the chemical step.

Recently, Wright *et al* backtracked a little on their previous views based on a new algorithm that identified functional dynamic contact networks from X-ray crystallography.(194) This algorithm was performed on EcDHFR-N23PP/S148A, EcDHFR-G121V and other enzymes. They concluded that the reduced hydride transfer rate in different mutants resulted from increased nonproductive, frustrated conformational heterogeneity in the active site rather than loss of protein motions on the millisecond timescale.

Recently, studies of protein motions have been further advanced by analysing 'heavy' enzymes, in which atoms are replaced by heavy isotopic labels. The studies performed on heavy isotope-labelled human purine nucleoside phosphorylase(195) and HIV-1 protease(196) by Schramm and coworkers further suggested that only femtosecond timescale fast motions are involved in catalysing the reaction. Femtosecond timescale changes to the bond vibration frequencies did not affect KIEs and steady-state kinetic parameters but decreased the single-turnover rate constants. However, the studies combining experimental results, simulations and theoretical analyses on heavy isotope-labelled EcDHFR performed in our group suggested that there was no significant role for promoting motions in driving tunnelling.(197) The slower rate of the heavy enzyme related to the differences in environmental coupling to the hydride transfer step. Our previous pH work on EcDHFR also suggested the lack of a role for short-range promoting motions in the DHFR-catalysed reaction. We measured the change of temperature dependence of KIE with pH and observed a sharp transition from the temperature-dependent KIE of EcDHFR to temperature-independent between pH 7.5 and 8. This result suggested that the factor which directly influences the hydride transfer is the conformational ensemble of the enzyme prior to reaction, not enzyme motions or conformational changes.(198)

Mulholland and coworkers' studies on various enzymes' dynamics (including DHFR) using theoretical approaches supported our conclusion.(199, 200) They found cues to explain the principles of enzyme catalysis simply by using the transition state theory and suggested that kinetic isotope effects with complex temperature dependences result from multiple conformations of the enzyme with different reactivity. Direct driving motions of proteins are not necessary to explain the experimental observations.

In summary, protein dynamics was proposed to be at the heart of enzyme catalysis, although its role remains hotly debated. More experimental study and theoretical analysis of different enzymes will provide us with more clues to answer this long-standing question.

1.13 Hyperthermophilic DHFR from *Thermotoga maritima* (TmDHFR)

A method to test the validity of different theoretical frameworks is to compare the reactivity of enzyme homologues, such as DHFR, that are isolated from organisms in extreme environments. *Thermotoga maritima* is a hyperthermophilic organism that belongs to the order Thermotogales. It was first discovered in the sediment of a marine geothermal area near Vulcano, Italy, and generally resides in hot springs as well as hydrothermal vents. The ideal environment for the organism is a water temperature of 80 °C, though it is capable of growing in water at 55-90 °C.(201) The DHFR from *T. maritima* (TmDHFR) is a hyperthermophilic enzyme, whose thermal melting temperature is 82 °C, much higher than other DHFRs.(202) This enzyme is unique, as it is the only chromosomally encoded DHFR known to exist as a homodimer, with no structured monomers existing in equilibrium or during unfolding experimentally (Figure 1.15a).(203-205) Computational chemistry revealed the thermal unfolding of the monomeric subunits and their dimerisation are not step-wise processes where each subunit folds and then associates to form the dimer. This feature

likely contributes to the exceptional thermostability, as the dimer interface is most resistant to thermal denaturation when compared to other regions of the enzyme.(206) Each monomeric subunit of TmDHFR has the eight β -strands and four α -helices in similar positions and lengths to those described above. Additionally there is a ninth β -strand;(118) the FG loop is extended and runs anti-parallel with the ninth β -strand on the other monomer, forming the dimer interface and a hydrophobic core. Amino acid residues Lys129 from one monomer and Glu136 and Glu138 from the other form salt bridges across the dimer interface (Figure 1.15b).(118)

Our group has extensively characterised bacterial DHFRs from the mesophile *Escherichia coli* (EcDHFR),(137, 154, 179, 191, 198) the hyperthermophile *Thermotoga maritima* (TmDHFR)(155, 192, 202, 206-210) and the psychrophile *Moritella profunda* (MpDHFR)(193, 211, 212) by comparing their physical and chemical properties. The changes of reaction rates and kinetic isotope effects (KIEs) with temperature, pH and solvent, as well as the thermostability have been systematically measured.

Catalytic efficiency of the hyperthermophilic TmDHFR is relatively poor – k_{cat} is 10 to 100 fold lower than those of its mesophilic and psychrophilic counterparts.(202) As mentioned above, catalytic efficiency of the mesophilic EcDHFR has been shown to rely heavily on the flexibility of the M20 and FG loops.(183) In contrast, the dimer interface of TmDHFR is composed of the corresponding loops, which form a tightly packed hydrophobic core (Ile15, Val19, Trp22, Tyr125, Phe127 in one subunit and Tyr140 in the other) and key intermolecular ion pairs (Lys129 of one subunit interacts with Glu136 and Glu138 of the other).(118) It seems that the intersubunit interactions constrain free movement of these loops, thus preventing proper closure of the active site and leading to the poor activity of TmDHFR.(118) The “M20 loop” of TmDHFR adopts an open conformation making the active site of TmDHFR more accessible to solvent.

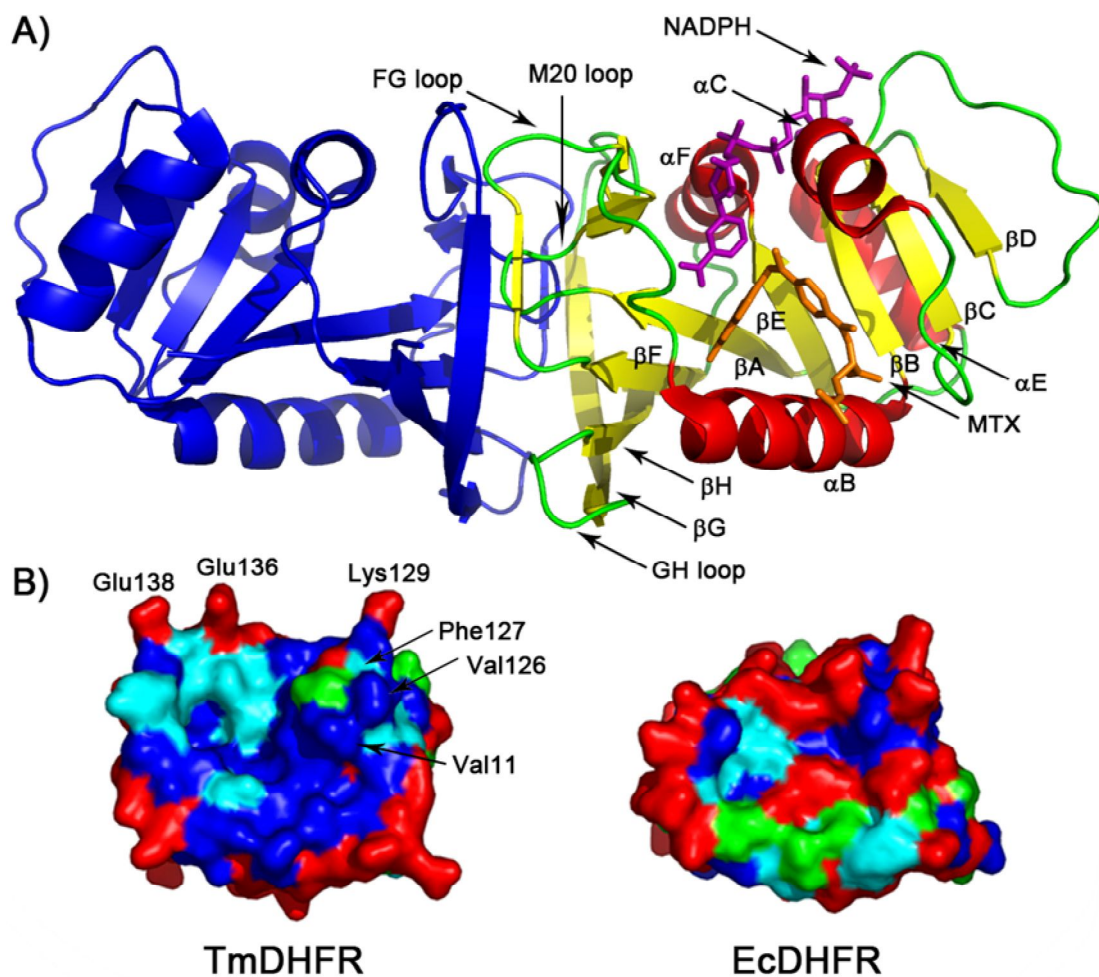


Figure 1.15 A) Structure of TmDHFR bound to methotrexate and NADPH (PDB 1D1G). The two monomers are shown in different colours for clarity. B) View of the dimer interface of TmDHFR indicating the central hydrophobic core and the more polar perimeter: red for charged residues, green for polar uncharged residues, blue for hydrophobic aliphatic residues, and cyan for aromatic residues. Val11, Val126, Phe127, Lys129, Glu136, and Glu138 are highlighted. The corresponding surface of EcDHFR is also displayed.

The distinctive quaternary structures also lead to the different reaction mechanisms of TmDHFR at physiological pH. Modulation of the substrate pK_a by the M20 loop of EcDHFR allows preprotonation and leads to increased reactivity with respect to hydride transfer. Computational studies suggested that the proton is donated directly from bulk solvent to N5 of H_2F . (126, 137, 213) In TmDHFR, the “M20 loop” is fixed in the open conformation, which exposes the active site to solvent and prevents

efficient modulation of the pK_a of its substrate. Therefore its hydride transfer and protonation occur in a concerted transition state and binding energy may be required to induce electron flow from the cofactor to C6 and N5 of H_2F to facilitate protonation.(214)

Computer simulations have shown that the hydride transfer catalysed by TmDHFR is also dominated by quantum-mechanical tunnelling, and that both inter- and intramonomeric correlated motions are present.(215) These motions may relate to the biphasic temperature dependence of the KIEs of TmDHFR,(208) which show a break point at approximately 25 °C. Below 25 °C the KIE increases with decreasing temperature, while above 25 °C the KIE is temperature independent.(155) This behaviour is different from those of EcDHFR and MpDHFR, whose KIEs are monophasic. Their KIEs are temperature dependent over the measured temperature range. Furthermore, a site-directed mutant, TmDHFR-V11D, was developed which could 'switch' between the dimeric and monomeric forms by the addition of the non-denaturing detergent 3-[(cholamidopropyl)dimethylammonio]-1-propane-sulfonate (CHAPS).(209) Interestingly, unlike the wild type TmDHFR, TmDHFR-V11D exhibited a monophasic temperature dependence of the KIE on hydride transfer, which indicates that the temperature dependence of the KIE of TmDHFR could be influenced by intersubunit interactions.(208) Kinetic experiments performed on TmDHFR-V11D also showed that monomerisation has a mild effect on the rate of hydride transfer, but reduces the steady-state turnover by ~20-fold. Therefore, even when unconstrained by the dimer interface, the loop regions of TmDHFR do not seem to carry out the functions ascribed to them in the monomeric EcDHFR. Instead, constraints on the position of the loops due to dimerisation prevent proper closure of the active site, leading to the reduced activity of TmDHFR.(207)

1.14 Moderately thermophilic DHFR from *Geobacillus stearothermophilus* (BsDHFR)

Another thermophilic DHFR homologue was found in the rod-shaped, Gram-positive, spore-forming bacterium, *Geobacillus stearothermophilus* (Figure 1.16, originally termed *Bacillus stearothermophilus* in 1920,(216) but following a reclassification in 2001 it is officially a member of the genus *Geobacillus*(217)). This thermophilic species is widely distributed in soil, hot springs, ocean sediment, and is a cause of spoilage in food products.(217) It will grow within a temperature range of 30-75 °C,(218) and over a range of pH from 2 to 11.

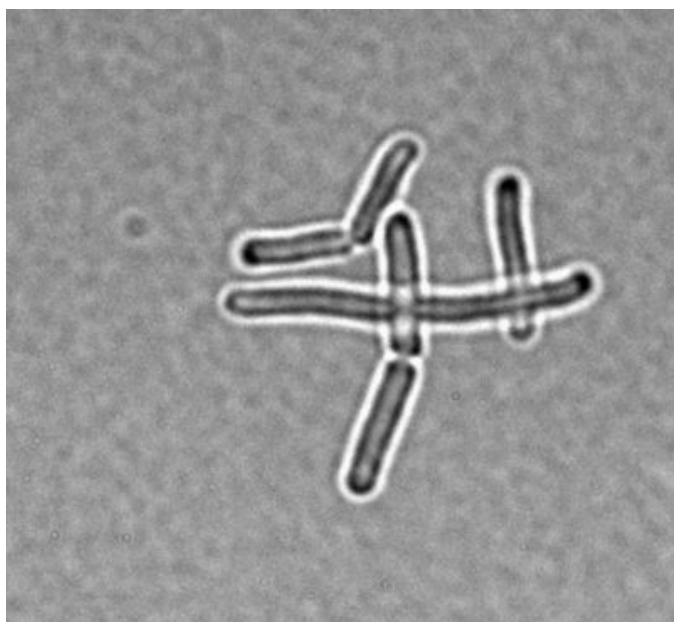


Figure 1.16 Bright micrograph of *Geobacillus stearothermophilus*. Photograph by Afave Biosystem, 2011.

The optimal growth temperature of *G. stearothermophilus* is 60 °C, thus DHFR from this species (BsDHFR; this abbreviation is used for consistency with previous literature) is moderately thermophilic, with a melting temperature at 67 °C,(219) lying between those of EcDHFR and TmDHFR.

The first crystal structure of BsDHFR was reported by the Klinman group (2005).⁽¹²⁰⁾ Different from the dimeric TmDHFR, BsDHFR is the first monomeric DHFR isolated from a thermophilic organism. As with all chromosomal DHFRs, the structure of BsDHFR is highly conserved and aligns well with that of mesophilic EcDHFR (Figure 1.17B). The M20 loop in BsDHFR is in the closed conformation in the absence of ligand binding. As yet other conformations of BsDHFR have not been identified. All elements of secondary structure are superimposable with the closed conformation of EcDHFR except for helix E, which in BsDHFR is tilted 20° from the adenosine binding site. The M20 loop in BsDHFR does not align well with apo-EcDHFR since its M20 loop is disordered (not shown).^(125, 143)

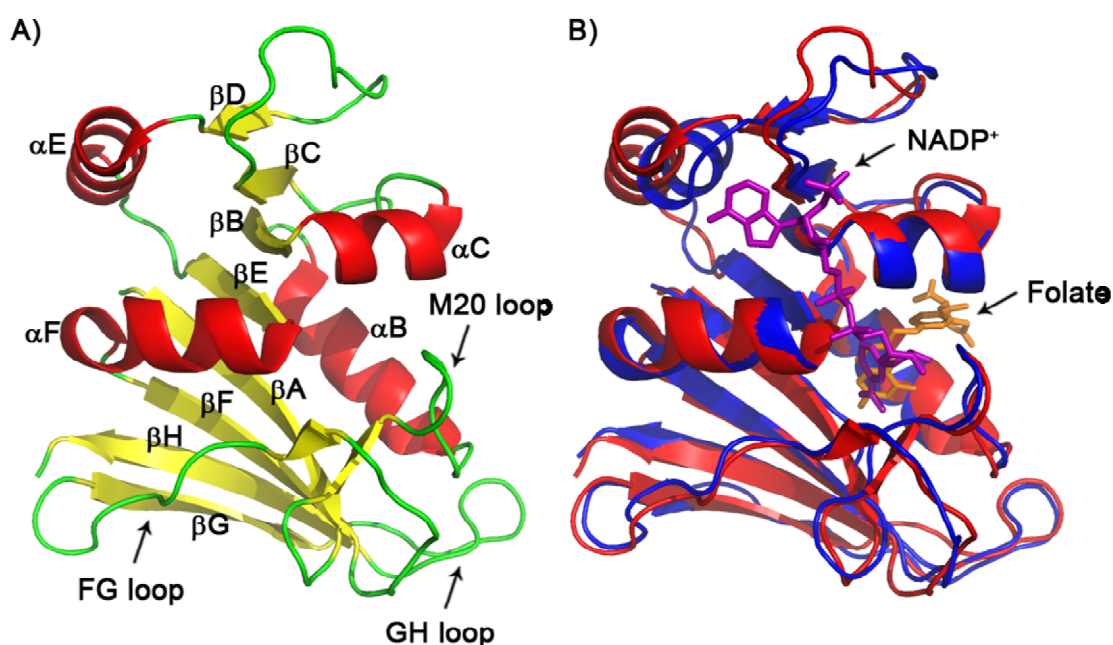


Figure 1.17 A) Crystal structure of apo-BsDHFR (1ZDR) and B) Overlay of apo-BsDHFR (red) and closed conformation of EcDHFR (blue, 1RX2).

In contrast to the mesophilic EcDHFR, BsDHFR showed a higher content of secondary structural elements and more proline residues in loop regions, which has been proposed to contribute to its thermostability. The effect on kinetic behaviour caused by these structural adaptations has been inspected. Preliminary results have shown a decreasing trend in efficiency of hydride transfer with increasing thermophilicity, when comparing the kinetic data of BsDHFR to published data of

EcDHFR and TmDHFR. For TmDHFR, the reaction turnover rate is at least partially limited by hydride transfer at all values of temperature and pH studied.(202) However, the hydride transfer step of BsDHFR becomes rate-limiting only at elevated temperature (60 °C) or pH (pH 9). BsDHFR has been characterised at pH 9 by the Klinman group, although the corresponding values at a physiological relevant pH (i.e. pH 7) have not yet been reported. The hydride transfer measurement showed a moderate value for the activation energy (E_a) and a temperature dependence of the primary deuterium kinetic isotope effect (KIE) that lies just outside the lower limit for semiclassical behaviour. Additionally, the KIEs of BsDHFR, EcDHFR and TmDHFR at 25 °C are almost identical. E_a values are much closer for EcDHFR and BsDHFR than TmDHFR.(120)

The structural flexibility of BsDHFR was first studied by Meinhold et al.(220) The dynamics of BsDHFR and EcDHFR were studied over a physiological temperature range on the sub-nanosecond timescale using the elastic incoherent neutron scattering (INS) technique. Contrary to expectation, this investigation indicated that thermophilic BsDHFR is more flexible than its mesophilic counterpart EcDHFR. Their study also hypothesised that the highly mobile fraction of BsDHFR might involve the relatively nonstructured loops of the protein, while the functional core remains relatively rigid at high temperature.

Meinhold's hypothesis has been verified by the Klinman group. Precise structural flexibility of BsDHFR (219) was investigated using a mass spectrometric technique, which measures the rate of hydrogen-deuterium exchange in the backbone of the enzyme when it is introduced into a deuterated buffer.(221) The adenosine binding domain (ABD) and α B helix showed the highest flexibility as they exhibited the highest solvent exchange. Most of the loop domain (LD) including M20, FG and GH loops is relatively rigid with intermediate solvent accessibility. The most rigid place was in the protein core (β A and β F), showing an insignificant extent of hydrogen-deuterium exchange.(219) In contrast, at the same temperature in EcDHFR,

the protein core showed higher flexibility, and other regions are either unchanged or more flexible in BsDHFR. It is likely that the reduced motions in the BsDHFR protein core which relates to cofactor and substrate binding play some role in catalysis. However, it is difficult to distinguish whether it is related to the binding and positioning of cofactor and substrate or the subsequent rate of hydride transfer.(221)

1.15 Investigations on the effect of catalysis due to thermal adaptation

The ultimate aim of this thesis is to compare DHFR homologues across a wide temperature range to analysis their ability to function at various temperatures. For this purpose, two main lines of experimentation were adopted.

Firstly, the thermophilic enzymes TmDHFR and BsDHFR were investigated in an aim to understand the relationship between thermal adaptation, enzyme catalysis and the functional role of enzyme dynamics. The tertiary structure of TmDHFR is similar to that of other DHFRs, but it is the only characterised homologue that forms a stable dimer.(118) The dimer interface of TmDHFR is largely made up of the C-terminal regions of the enzyme and certain loops that are crucial for the catalysis in EcDHFR.(118) In this thesis, we present our analysis on the effect of dimerisation by incorporating the residues of the dimer interface of TmDHFR into EcDHFR in a goal to create an artificial dimeric EcDHFR variant. By comparing the kinetic and structural properties of these hybrid enzymes with its parental homologues, the effect of structural rigidity and intersubunit interactions on thermostability and catalysis can be distinguished.

Secondly, previous studies showed that both thermostability and kinetic behaviour of BsDHFR lie between the mesophilic and hyperthermophilic homologues. Interestingly, the overall structure of this enzyme appears to be relatively flexible, yet contains a rigid protein core. This enzyme has been studied for almost a decade, but the step of hydride transfer has never been characterised at a physiologically relevant

pH. By extending the characterisation of BsDHFR at physiological pH in line with the studies already performed on MpDHFR, EcDHFR and TmDHFR, a more complete picture on the general trend of thermophilicity on catalysis can be built. Furthermore, the temperature dependence of the kinetic isotope effect on hydride transfer at pH 7 will provide information on quantum mechanical tunnelling under physiological conditions. In the environmentally coupled model of hydrogen tunnelling, protein motions control binding of substrate and cofactor to generate a tunnelling ready conformation and modulate the width of the activation barrier and hence the reaction rate. Changes to the composition of the reaction medium are known to perturb protein motions.^(188, 190) Therefore, the measurement of kinetic parameters in various cosolvents will give us more clues about the promoting motions in driving the catalysis.

2 MATERIALS AND METHODS

2.1 Materials

All chemicals were purchased from Sigma-Aldrich UK, Fisher Scientific Ltd, unless otherwise stated. IPTG, ampicillin, NADP⁺ and NADPH were purchased from Melfold. All restriction enzymes were purchased from New England Biolabs (Hitchin, UK). All oligonucleotides were purchased from Eurofins MWG Operon (Ebersberg, Germany). The DNA fragments were purchased from Epoch Biolabs (Texas, USA).

2.2 Media

2.2.1 Luria-Bertani (LB) medium

LB medium was prepared by dissolving tryptone (10.0 g), yeast extract (5.0 g), and sodium chloride (10.0 g) in 950 mL of deionised water. The pH was adjusted to 7.0 before taking the total volume to 1 L. The solution was then sterilised in an autoclave at 121 °C, 15 lb.(sq. in.)⁻¹ for 20 minutes.

2.2.2 Luria-Bertani agar (1.5 % w/v)

To prepare culture plates, trypton (1.0 g), yeast extract (0.5 g), sodium chloride (1.0 g) and agar (1.5 g) were dissolved in 95 mL of deionised water. The pH was adjusted to 7.0 before taking the total volume to 100 mL. The solution was then sterilised in an autoclave at 121 °C, 15 lb.(sq. in.)⁻¹ for 20 minutes. The liquid LB agar was cooled to about 50 °C and the antibiotic ampicillin was then added to a final concentration of 0.1 mg/mL. LB agar (~10 mL) was aseptically poured into 90 mm Petri dishes and allowed to set before being stored at 4 °C.

2.3 Solutions

2.3.1 Rubidium chloride solutions for preparation of ultra-competent cells

Rubidium chloride solution 1 (Rb1) was prepared by dissolving potassium acetate (246 mg), rubidium chloride (1.56 g), calcium chloride (22 mg), manganese chloride (629 mg) and glycerol (15 mL) in 80 mL of deionised water. The pH was adjusted to 5.8 with dilute acetic acid before taking the total volume to 100 mL with deionised water. The solution was then filter-sterilised and stored at 4 °C.

Rubidium chloride solution 2 (Rb2) was prepared by dissolving 3-(N-morpholino)propane sulfonic acid (MOPS) (105 mg), calcium chloride (416 mg), rubidium chloride (78 mg) and glycerol (7.5 mL) in 40 mL of deionised water. The pH was adjusted to 6.8 with dilute potassium hydroxide before taking the total volume to 50 mL. The solution was then filter-sterilised and stored at 4 °C.

2.3.2 dNTPs

Stock solutions of each dNTPs were purchased from Promega (Madison, WI USA) at a concentration of 100 mM. These were diluted to a working concentration of 10 mM each with sterile deionised water and stored at -20 °C.

2.3.3 Ethidium bromide solution

Stock ethidium bromide solution was prepared by dissolving 8.1 g of ethidium bromide in 100 mL of deionised water to give a stock concentration of 25 mM. The solution was stored in the dark at 4 °C. Immediately prior to gel staining, 48 µL of the stock solution was added to 200 mL of deionised water to give a working concentration of 6 µM.

2.3.4 TAE buffer stock (50x) for agarose gels

EDTA (0.5 M) was prepared by dissolving 14.6 g in 50 mL of deionised water and the pH adjusted to 8.0 with 5 M NaOH. The total volume was taken to 100 mL and the solution used immediately for preparation of TAE buffer stock (50x).

Tris base (242 g), glacial acetic acid (57.1 mL) and 0.5 M EDTA (100 mL, pH 8.0) were mixed with 800 mL of deionised water until completely dissolved. The total volume was taken to 1 L with deionised water, and the solution was stored at room temperature. The buffer was diluted 1:49 with deionised water immediately prior to use.

2.3.5 10% (w/v) sodium dodecyl sulfate (SDS)

Sodium dodecyl sulfate (10 g) was fully dissolved in 90 mL of deionised water. The total volume was taken to 100 mL. The solution was stored at room temperature.

2.3.6 Sodium dodecyl sulfate polyacrylamide gel electrophoresis (SDS PAGE) running buffer

2.3.6.1 Anode buffer

Tris base (24.3 g) was dissolved in 950 mL of deionised water. The pH was adjusted to 8.9 before taking the total volume to 1 L.

2.3.6.2 Cathode buffer

Tris base (12.1 g), tricine (17.9 g) and 10% (w/v) SDS (2 mL) were dissolved in 950 mL of deionised water. The pH was confirmed to be 8.25-8.3 before taking the total volume to 1 L.

2.3.7 Protein loading dye

0.5 M Tris-HCl, (1.25 mL, pH 6.8), glycerol (3 mL), 0.6% (w/v) bromophenol blue (1 mL) and 10% (w/v) SDS (2 mL) were mixed and the total volume taken to 10 mL with deionised water. β -mercaptoethanol was added to a final concentration of 10% immediately prior to use.

2.3.8 Protein staining buffer

Coomassie brilliant blue (0.5 g), Methanol (90 mL), acetic acid (20 mL) and 90 mL of deionised water were mixed.

2.3.9 Protein destaining buffer

Methanol (450 mL), acetic acid (100 mL) and 450 mL of deionised water were mixed.

2.3.10 Potassium phosphate stock solution

Dibasic (174.2 g) and monobasic (136.1 g) potassium phosphate were separately dissolved in 950 mL of deionised water. The total volume of each was taken to 1 L with deionised water for use as stock solutions.

2.3.11 Protein dialysis buffer

1 M Monobasic potassium phosphate (12.3 mL), 1 M dibasic potassium phosphate (7.7 mL), and β -mercaptoethanol (1.4 mL) were added to 3.98 L of deionised water. Buffer was prepared fresh each time and dialysis was performed at 4 °C.

2.3.12 Inclusion body dissolving buffer

Urea (255.3 g) was dissolved in 300 mL of deionised water and the total volume was taken to 500 mL.

2.3.13 Inclusion body refolding buffer

Tris base (6.1 g), sodium chloride (5.8 g) and arginine (69.7 g) were dissolved in 900 mL deionised water. The pH was adjusted to 8.0 before taking the volume to 1 L.

2.4 DNA manipulation

2.4.1 Purification of plasmid DNA

XL1-Blue Ultracompetent cells (Stratagene, California, USA) were used for the preparation of new plasmid constructs. Single colonies were picked from selective LB agar plates and grown overnight at 37 °C in 10 mL LB media containing 0.1 mg/mL ampicillin, whilst shaking at 150 RPM in an Innova 43 shaker (New Brunswick Scientific, Hertfordshire, UK). The cells were precipitated by an Eppendorf 5810R centrifuge (Eppendorf AG, Hamburg, Germany) at 3200 RCF and a QIAprep spin miniprep kit (QIAGEN, Crawley, UK), which is based on the Brinbiom and Doly method,(222) was then adopted. The plasmid was purified *via* alkaline lysis of bacterial cells followed by adsorption of DNA onto a silica membrane in the presence of a high concentration of salt. EconoSpin All-in-1 mini spin columns were used for DNA/RNA extraction (Epoch Biolabs, Texas, USA). The plasmid was eluted in low salt buffer provided in the kit and stored at -20 °C.

2.4.2 Quantification of oligonucleotides and plasmid DNA

All plasmid DNA and oligonucleotides were quantified using a NanoDrop 1000 spectrophotometer (Thermo Scientific, Waltham, Massachusetts, USA). Absorbance measurements were taken at 260 nm and 280 nm. An absorbance value (260 nm) of 1.0 equates to 50 µg of double stranded DNA (dsDNA) or 30 µg of oligonucleotide. The ratio of absorbance at 260 and 280 nm was used to assess the purity of DNA and RNA. A ratio of ~1.8 is generally accepted as pure for DNA.

2.4.3 DNA sequencing

Plasmid DNA was isolated from the appropriate cloning strain of competent cells using the miniprep plasmid purification technique outlined in Section 2.4.1 to give pure DNA at a concentration of ~100 ng/μL. DNA sequencing of plasmid constructs was verified by automated DNA sequencing (Molecular Biology Unit, Cardiff University).

2.4.3 Polymerase chain reaction (PCR) and site-directed mutagenesis

The polymerase chain reaction (PCR) is a biochemical technique in molecular biology used to amplify a single or a few copies of a piece of DNA generating thousands to millions of copies of a particular DNA sequence. PCR site-directed mutagenesis is a method that uses the PCR reaction to make specific and intentional changes to the DNA sequence of a gene. The PCR reaction was first developed in 1983 by Kary Mullis,⁽⁸¹⁾ and has now become a common and indispensable technique for a variety of applications. In 1993, Mullis was awarded the Nobel Prize in Chemistry along with Michael Smith for his talented work on PCR.

The PCR reaction and site-directed mutagenesis both rely on thermal cycling, consisting of cycles of repeated heating and cooling of the reaction for DNA melting and enzymatic replication of the DNA. Primers (short DNA fragments) containing corresponding sequences along with a DNA polymerase are key components which enable selective and repeated amplification. As PCR progresses, the DNA generated is itself used as a template for replication, setting in motion a PCR reaction in which the DNA desired is exponentially amplified.

For the PCR reaction and site-directed mutagenesis, Phusion High-Fidelity DNA Polymerase (New England Biolabs, Hitchin, UK) was used. All PCR reactions and site-directed mutagenesis were carried out using a Biometra TGradient Thermocycler (Biometra, Göttingen, Germany). The primers used are shown in Table 2.1.

Oligonucleotide primers are generally 20-40 nucleotides in length and ideally have a GC content of 40-60%. A computer program such as PrimerX can be used to design or analyse primers.

Table 2.1 Primer design. The codons of the amino acids that were changed are highlighted. For all mutations, the first primer in the sequence is the forward and the second is the reverse.

Primers for BsDHFR mutants
<p>BsDHFR L20M</p> <p>5' GT AAG GAT AAC CGC ATG CCG TGG CAC CTG C 3'</p> <p>5' G CAG GTG CCA CGG CAT GCG GTT ATC CTT AC 3'</p> <p>BsDHFR A104Q</p> <p>5' C GCA GAG CTG TTT CGC CAG ACC ATG CCG ATT GTC 3'</p> <p>5' GAC AAT CGG CAT GGT CTG GCG AAA CAG CTC TGC G 3'</p> <p>BsDHFR P122E</p> <p>5' CT AAG ATC TTT GCA TCT TTC GAA GGG GAT ACT TTC TAT CCA C 3'</p> <p>5' G TGG ATA GAA AGT ATC CCC TTC GAA AGA TGC AAA GAT CTT AG 3'</p> <p>BsDHFR P129D</p> <p>5' GGG GAT ACT TTC TAT CCA GAT ATT TCT GAT GAC GAA TGG 3'</p> <p>5' CCA TTC GTC ATC AGA AAT ATC TGG ATA GAA AGT ATC CCC 3'</p>
Primers for creation of hybrid Xet-1, Xte-1, Xet-2 and Xte-2
<p>EcDHFR SpeI</p> <p>5' CAA AAA CTG TAT CTG ACT AGT ATC GAC GCA GAA GTG G 3'</p> <p>5' C CAC TTC TGC GTC GAT ACT AGT CAG ATA CAG TTT TTG 3'</p> <p>TmDHFR SpeI</p> <p>5' GAG CTT TTC GTC ACT AGT GAA CCG TAC GTG TTC G 3'</p> <p>5' C GAA CAC GTA CGG TTC ACT AGT GAC GAA AAG CTC 3'</p> <p>Xet-1 XhoI</p> <p>5' G GAG ATG AGG CGT CTC AAC GAA AGA GGC 3'</p>

5' G CCT CTT TCG TTG AGA CGC CTC ATC TCC 3' (step 1)

5' G ATG AGG CGT CTC GAG GAA AGA GGC ACA C 3'

5' G TGT GCC TCT TTC CTC GAG ACG CCT CAT C 3' (step 2)

Xte-1 XhoI

5' GTA TTC AGC GAA TTC CTC GAG GCT GAT GCG CAG AAC TC 3'

5' GA GTT CTG CGC ATC AGC CTC GAG GAA TTC GCT GAA TAC 3'

Xet-1 SpeI TV

5' G CAA AAA CTG TAT CTG ACT GTT GAA CCG TAC GTG TTC GG 3'

5' CC GAA CAC GTA CGG TTC AAC AGT CAG ATA CAG TTT TTG C 3'

Xte-1 SpeI TH

5' GAT GAG CTT TTC GTC ACT CAT ATC GAC GCA GAA GTG G 3'

5' C CAC TTC TGC GTC GAT ATG AGT GAC GAA AAG CTC ATC 3'

Xet-2 XhoI LD

5' CG GTA TTC AGC GAA TTC CAC AAC GAA AGA GGC ACA CTT TTT C 3'

5' G AAA AAG TGT GCC TCT TTC GTT GTG GAA TTC GCT GAA TAC CG 3'

Xte-2 XhoI HN

5' G GAG ATG AGG CGT CTC GAT GCT GAT GCG CAG AAC TC 3'

5' GA GTT CTG CGC ATC AGC ATC GAG ACG CCT CAT CTC C 3'

Primers for Xet-1 and Xte-1 mutants

Xet-1 L24S

5' GCC ATG CCG TGG AAC TCG CCT GCC GAT CTC GC 3'

5' GC GAG ATC GGC AGG CGA GTT CCA CGG CAT GGC 3'

Xet-1 W30N

5' G CCT GCC GAT CTC GCC AAT TTT AAA CGC AAC ACC 3'

5' GGT GTT GCG TTT AAA ATT GGC GAG ATC GGC AGG C 3'

Xet-1 E101T

5' GGC GGC GGT CGC GTT TAT ACA CAG TTC TTG CCA AAA GC 3'

5' GC TTT TGG CAA GAA CTG TGT ATA AAC GCG ACC GCC GCC 3'

Xte-1 E27A

5' GAG AGC TGG AGC TCA TTT GCG GAC AGA AAA AAT TTC AG 3'

5' CT GAA ATT TTT TCT GTC CGC AAA TGA GCT CCA GCT CTC 3'

Primers for creation of Hybrid Xbt-1 and Xtb-1

BsDHFR insert

5' TT TAA CTT TAA GAA GGA GAT ATA CAT 3'

5' AGT GAC ATA CAG GCG ATC 3'

BsDHFR vector

5' AAG ATC TTT GCA TCT TTC CC 3'

5' AT TGC AAC GAT ATG ACT AAT CAT 3'

TmDHFR insert

5' TT TAA CTT TAA GAA GGA GAT ATA CAT 3'

5' AGT GAC GAA AAG CTC ATC TA 3'

TmDHFR vector

5' GTC GAA CCG TAC GTG TT 3'

5' CGC AAG AAC GAA AAT CAC TTT 3'

Primers and DNA fragments for creation of Xet-3 and Xte-3

Xet-3 insert

5' GTC ATC CCG GCA GTG GTG GAA GGC GAC ACC CAT TTC CCG GAT TAC GAG
CCG GAT GAC TGG GAA CTT GTA TTC ATG GAA TTC CAC GAT GCT GAT GCG CAG
AAC TCT CAC GGC TAT CTT TTT CTC 3'

Xet-3 vector

5' ATT CTG GAG CGG CGG TAA 3'

5' CGT CAG ATA CAG TTT TTG CG 3'

Xet-3 DR11SG

5' GCG TTA GCG GTA TCT CGC GTT ATC GG 3'

5' CC GAT AAC GCG AGA TAC CGC TAA CGC 3' (step 1)

5' G TTA GCG GTA TCT GGC GTT ATC GGC ATG 3'

5' CAT GCC GAT AAC GCC AGA TAC CGC TAA C 3' (step 2)

Xte-3 insert

5' CAT GAA GAC TAC GAA TTC GGA AAG GGA ATA CCT TTT TTC GAT GAG TTC
GAA GGT TAC TTT CCT TTG AAA TCG CTG GAG AGC AGG CGT TTG AAC GAA
AGA AGC ACA TGC TTT GAG AAA TAT T 3'

Xte-3 vector

5' CT GTA GAA AAA TCG CAC C 3'

5' A GTG ACG AAA AGC TCA TC 3'

Xte-3 SG13DR

5' GCG ATG GAC GTC GAC GGA AAG ATA GCC 3'

5' GGC TAT CTT TCC GTC GAC GTC CAT CGC 3' (step 1)

5' CG ATG GAC GTC GAC AGA AAG ATA GCC TC 3'

5' GA GGC TAT CTT TCT GTC GAC GTC CAT CG 3' (step 2)

Primers for creation of hybrid Hbt-3

5' GAT CGC CTG TAT GTC ACT GTG ATC TTT GCA TCT TTC C 3'

5' G GAA AGA TGC AAA GAT CAC AGT GAC ATA CAG GCG ATC 3' (step 1)

5' C GTT GCA ATG GAC GTG AAT CGC GTC ATC G 3'

5' C GAT GAC GCG ATT CAC GTC CAT TGC AAC G 3' (step 2)

5' GAC GAG AAG AAT CCT TAC GGA CAC GCT TTC ATT ATT TAC 3'

5' GTA AAT AAT GAA AGC GTG TCC GTA AGG ATT CTT CTC GTC 3' (step 3)

5' CA ATG GAC GTG AAT GGC GTC ATC GGT AAG G 3'

5' C CTT ACC GAT GAC GCC ATT CAC GTC CAT TG 3' (step 4)

5' C TAT CCA CCT ATT TCT GGT GAC GAA TGG GAG ATC G 3'

5' C GAT CTC CCA TTC GTC ACC AGA AAT AGG TGG ATA G 3' (step 5)

5' GTC ACT GTG ATC TTT GCA GTT TTC CCA GGG GAT ACT TTC 3'

5' GAA AGT ATC CCC TGG GAA AAC TGC AAA GAT CAC AGT GAC 3' (step 6)

The required components were assembled on ice and the reactions quickly transferred to a thermocycler preheated to the denaturation temperature (98 °C). All components should be mixed and centrifuged prior to use. It is important to add Phusion DNA polymerase last in order to prevent any primer degradation caused by the 3'->5'

exonuclease activity. 30 μL of mineral oil was added to the top of the aqueous phase to prevent evaporation during the reaction cycle.

Table 2.2 Components of the PCR reaction

Component	50 μL reaction	Final concentration
Nuclease-free water	to 50 μL	
5X Phusion HF buffer	10 μL	1X
10 mM dNTPs	1 μL	200 μM
10 μM forward primer	2.5 μL	0.5 μM
10 μM reverse primer	2.5 μL	0.5 μM
Template DNA	variable	< 250 ng
DMSO (optional)	1.5 μL	3%
Phusion DNA polymerase	0.5 μL	1.0 unit/50 μL PCR

Table 2.3 Temperatures and durations of the PCR cycle

Cycle step	2-step protocol		3-step protocol		cycles
	Temp.	Time	Temp.	Time	
Initial denaturation	98 °C	30 s	98 °C	30 s	1
Denaturation	98 °C	5-10 s	98 °C	5-10 s	25-35
Annealing	-	-	45-72 °C	10-30 s	
Extension	72 °C	15-30 s/kb	72 °C	15-30 s/kb	
Final extension	72 °C	5-10 min	72 °C	5-10 min	1
	4 °C	hold	4 °C	hold	

Annealing temperatures required for use with Phusion tend to be higher than with other PCR polymerases. Typically, primers greater than 20 nucleotides in length anneal for 10-30 seconds at 3 °C above the T_m of the lower T_m primer. If the primer length is less than 20 nucleotides, an annealing temperature equivalent to the T_m of the

lower primer should be used. When primers with annealing temperatures ≥ 72 °C are used, a 2-step thermocycling protocol is recommended.

When the site directed mutagenesis was completed, the PCR product solution was incubated at 37 °C for 1 hour with *DpnI*, which is a specific endonuclease for methylated and hemimethylated DNA. The DNA isolated from the XL1-Blue *E. coli* cell lines is *dam*⁺ methylated, while the DNA elongated in the PCR cycles is not methylated. Treatment with *DpnI* therefore selectively digests template DNA, ensuring only mutated DNA was left intact. Ultracompetent *E. coli* XL1 Blue cells were then transformed with 2 μ L of the PCR product solution.

2.4.4 Restriction digestion of DNA and controls

For each restriction digest, the manufacturer's guidelines were followed with regard to operating buffers, temperatures and denaturation steps.

NdeI/BamHI digestion was used for excision of the BsDHFR gene from the pPCR-Script vector. Digestion was performed at 37 °C for 3 hours and all restriction endonucleases were removed by agarose gel electrophoresis. *NdeI/SpeI* or *NdeI/XhoI* digestions were used for the excision of the N-terminal gene from EcDHFR and TmDHFR or Xet-1 and Xte-1 respectively and then swapped to construct hybrid enzymes. *SrfI* was used for the treatment of the pPCR-Script plasmid.

2.4.5 DNA visualisation, isolation and purification

Agarose gels were prepared by w/v ratio (usually 1.5%) with 1X TAE buffer (Section 2.3.4). Gels were run at constant amperage of 80 mA for 60 mins and stained in 250 mL 6 μ M ethidium bromide for 20 minutes whilst stirring. DNA bands were visualised using a Syngene GeneFlash UV light box (Syngene, Cambridge, UK), ensuring limited exposure of DNA to UV light. The appropriate bands were identified by comparison with a molecular weight ladder, cut from the agarose gel using a clean scalpel blade,

and stored in a sterile eppendorf. DNA was extracted from the gel according to the manufacturer's instructions using the QIA quick gel extraction kit (QIAGEN, Crawley, UK) and stored at -20 °C.

2.4.6 Cloning of BsDHFR gene into cloning vector pPCR-Script

The gene encoding BsDHFR with *Nde*I and *Bam*HI restriction sites at the 5'- and 3'-end, respectively, was purchased from Epoch Biolabs (Texas, USA) and blunt end ligated into the pPCR-Script plasmid at the *Srf*I restriction site. The pPCR-Script Amp cloning kit (Stratagene, Edinburgh, UK) was used according to the manufacturer's instructions. By incubating the ligation mixture together with *Srf*I, ligation efficiency is increased as undigested plasmid is eventually cut by the restriction enzyme while the new plasmid construct remains intact as the BsDHFR insert disrupts the *Srf*I site. Ultracompetent *E. coli* XL1 Blue cells were then transformed with 2 µL of the ligation mixture.

*Nde*I

CAT ATG ATT AGT CAT ATC GTT GCA ATG GAC GAG AAT CGC GTC ATC
GGT AAG GAT AAC CGC CTG CCG TGG CAC CTG CCA GCC GAT CTG GCG
TAT TTT AAA CGC GTG ACG ATG GGT CAT GCC ATT GTA ATG GGT CGT
AAA ACG TTT GAA GCG ATC GGG CGT CCG CTG CCG GGT CGT GAT AAC
GTT GTT GTT ACC GGG AAC CGT AGC TTT CGT CCG GAA GGC TGC CTG
GTA CTG CAT AGC CTG GAA GAA GTG AAA CAG TGG ATT GCC AGC CGT
GCG GAC GAA GTG TTC ATT ATT GGT GGC GCA GAG CTG TTT CGC GCG
ACC ATG CCG ATT GTC GAT CGC CTG TAT GTC ACT AAG ATC TTT GCA
TCT TTC CCA GGG GAT ACT TTC TAT CCA CCT ATT TCT GAT GAC GAA
TGG GAG ATC GTG AGT TAT ACC CCA GGC GGG AAG GAC GAG AAG AAT
CCT TAC GAA CAC GCT TTC ATT ATT TAC GAG CGC AAG AAA GCT AAA
TAA GGA TCC

*Bam*HI

2.4.7 Subcloning of BsDHFR gene into expression vector

The new plasmid construct formed by ligation of the BsDHFR gene and pPCR-Script (Section 2.4.6) was subjected to *NdeI/BamHI* restriction endonuclease treatment (Section 2.4.4). The pJGetit plasmid containing the EcDHFR gene was also treated with *NdeI/BamHI* digestion. Following each digestion, plasmid and insert were separated *via* agarose gel electrophoresis, visualised, and the insert isolated and purified (Section 2.4.5).

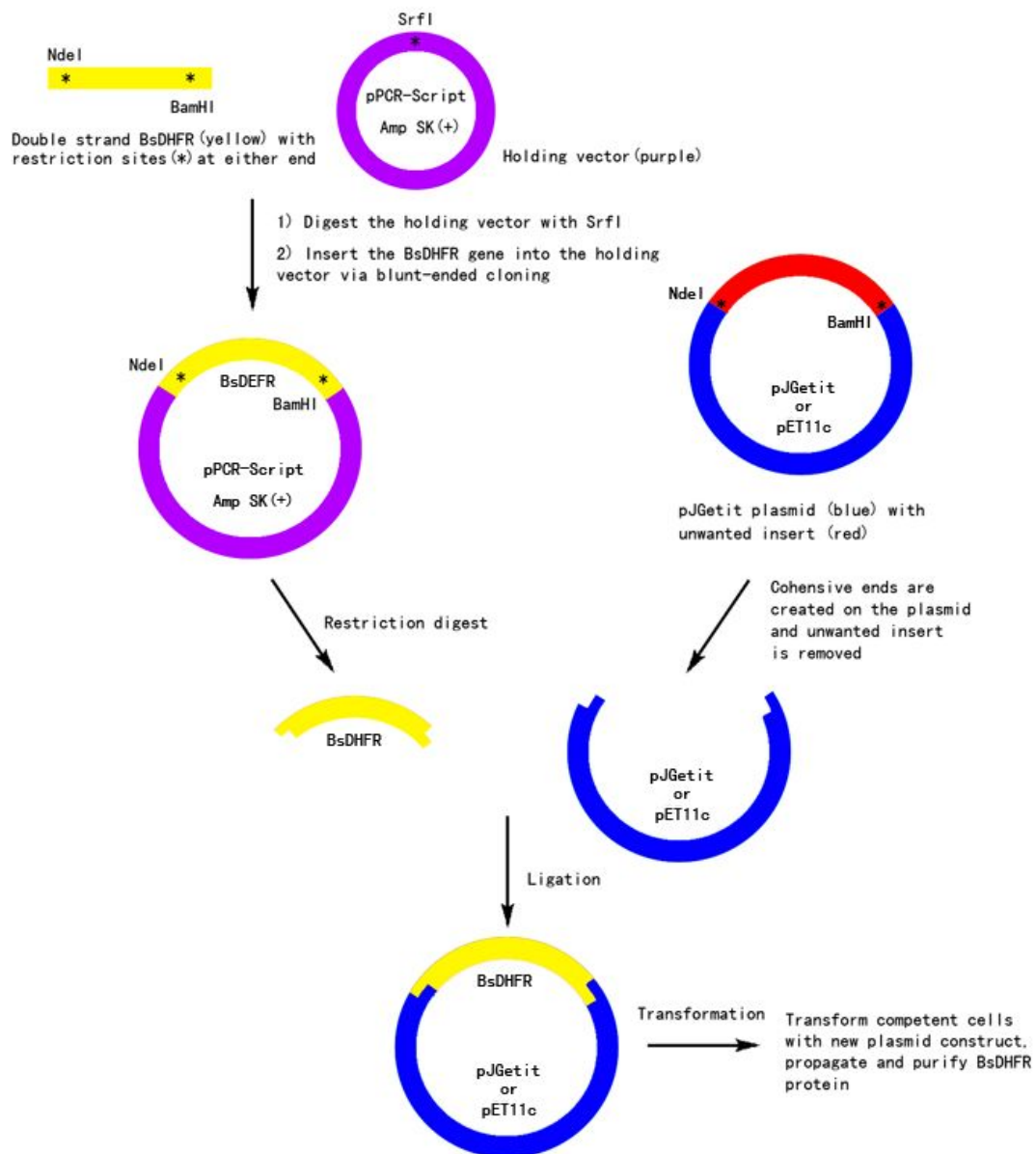


Figure 2.1 Procedure for the creation of an expression vector for BsDHFR

The Quick Ligation Kit (New England Biolabs, Hitchin, UK) was used for the ligation. Typically, 50 ng of vector was combined with a 3-fold molar excess of insert and the volume adjusted to 10 μ L with dH₂O. 10 μ L of 2X Quick Ligation Reaction Buffer followed by 1 μ L of Quick T4 DNA Ligase were added and mixed thoroughly. The reaction was centrifuged briefly and incubated at room temperature (25 °C) for 5 minutes. The reaction was chilled on ice, and then used for transformation (Figure 2.1).

2.4.8 EcDHFR/TmDHFR and BsDHFR/TmDHFR Hybrid construction

2.4.8.1 Construction method 1

Nucleotides 337-342 (EcDHFR) and 364-369 (TmDHFR) were mutated to form *SpeI* sites in both genes (Section 2.4.3). Both constructs were then *NdeI/SpeI* digested (Section 2.4.4), and the small fragments swapped and ligated to form hybrids. The *SpeI* sites were then mutated to reform the native sequences, generating a first pair of hybrids (Xet-1, Xte-1) (Figure 2.2).

XhoI sites were then incorporated at nucleotides 424-429 (Xet-1) and 448-453 (Xte-1). Both constructs were *NdeI/XhoI* digested, and the small fragments swapped and ligated as above to allow the β H strand of the original protein to be re-incorporated, forming a second pair of hybrids (Xet-2, Xte-2) (Figure 2.2).

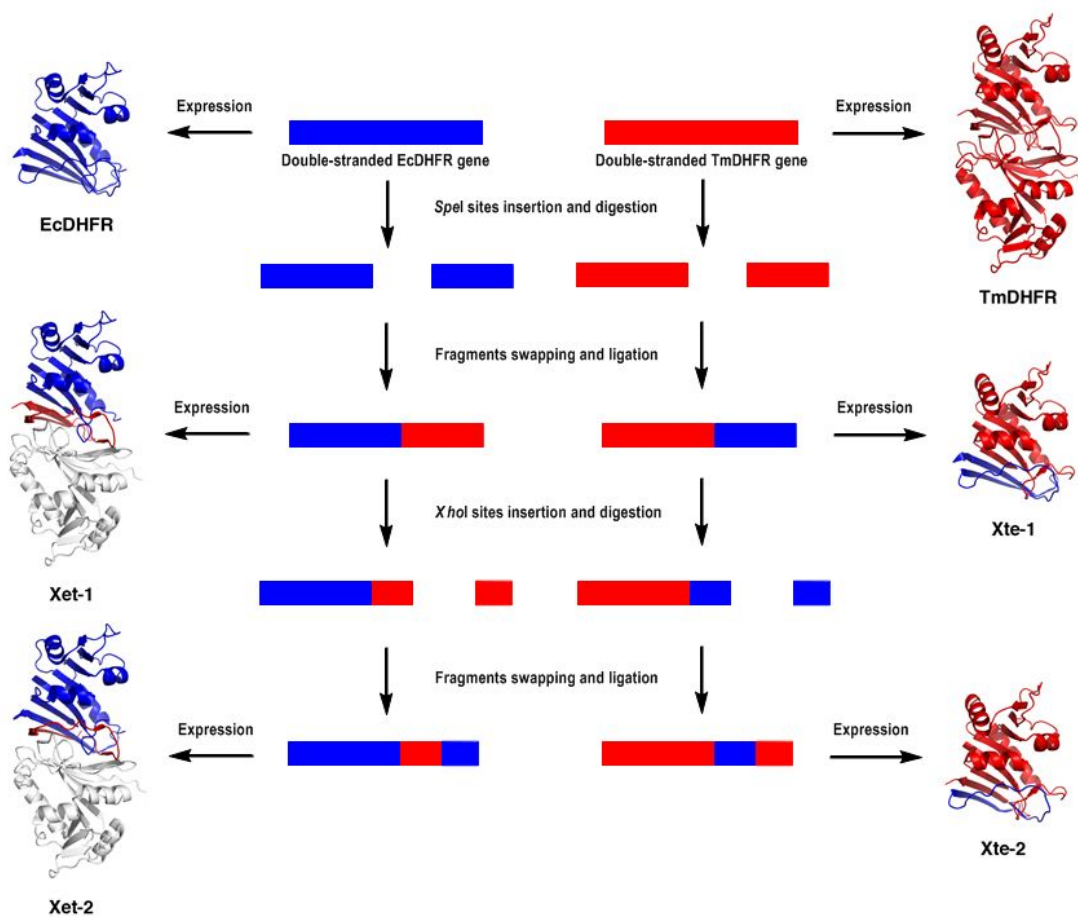


Figure 2.2 Procedure for the hybrid enzyme construction method 1

2.4.8.2 Construction method 2

The DNA sequences encoding the N-terminal regions of BsDHFR (nucleotide 1-345) and TmDHFR (nucleotide 1-366), as well as the vector plus C-terminal regions of both enzymes were PCR-amplified (Section 2.4.3). The small fragments were treated with T4 Polynucleotide Kinase (New England Biolabs, Hitchin, UK) to transfer and exchange P_i from the γ position of ATP to the 5'-hydroxyl terminus of polynucleotides. Typically, up to 300 pmol of 5' termini in a 50 μ L reaction containing 1x T4 Polynucleotide Kinase Buffer, 1 mM ATP and 10 units of T4 Polynucleotide Kinase was used for phosphorylation. The reaction was incubated at 37 $^{\circ}$ C for 30 minutes. The generated fragments were then swapped and ligated to form hybrids Xbt-1 and Xtb-1 (Figure 2.3).

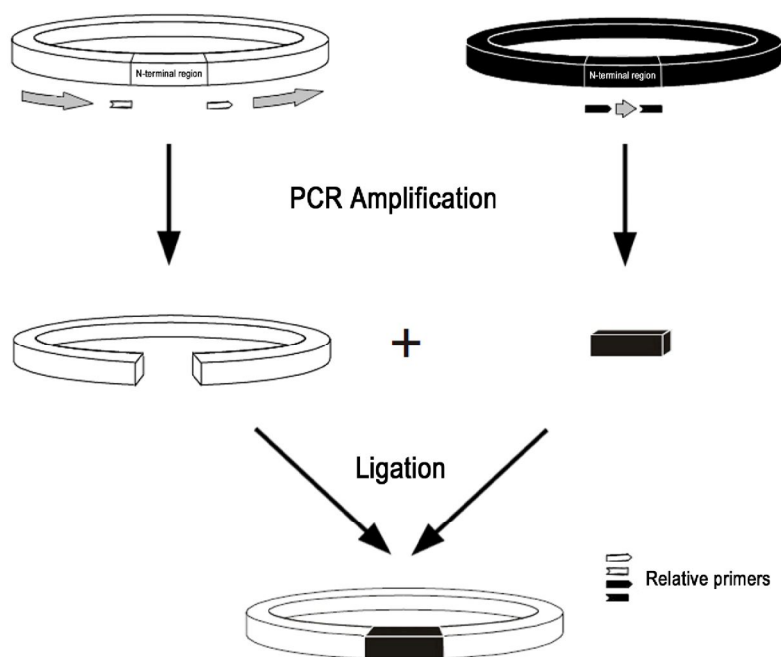


Figure 2.3 Procedure for the hybrid enzyme construction method 2

2.4.8.3 Construction method 3

The dimer interface of TmDHFR mainly consists of aliphatic and aromatic residues which form a stable hydrophobic core, but many of these are replaced by ionic and polar residues in EcDHFR or BsDHFR. In the third method used, hybrids were generated by only replacing the residues directly involved in forming the dimer interface. Specifically, 10 residues in EcDHFR were substituted with the corresponding hydrophobic residues found in TmDHFR to create Xet-3 (D11S and R12G in the M20 loop, and H114V, D116P, E118V, S134L, S137M, S150G, C152L and E154L in the C-terminal region). Correspondingly, 10 residues in TmDHFR were also substituted with the residues in EcDHFR to create Xte-3 (S13D, G14R, V124H, P126D, V128E, L147S, M150S, G157S, L159C, and L161E). Additionally, 6 residues in BsDHFR were substituted with the residues in TmDHFR to create Xbt-3 (E10V, R12G, K116V, S120V, E152G, and D132G) (Figure 2.4).

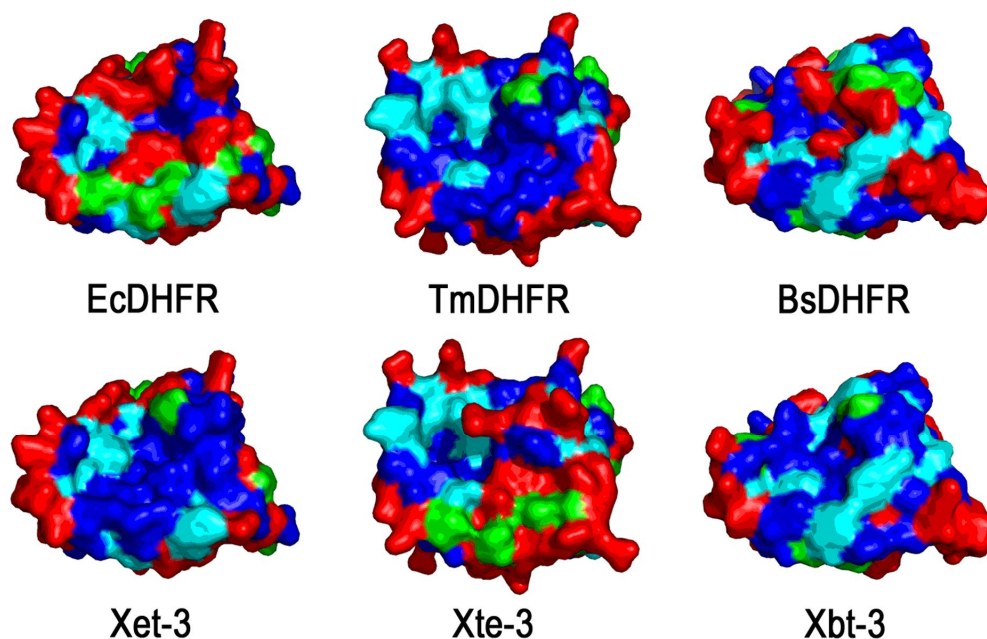


Figure 2.4 The dimer interface of TmDHFR and the corresponding regions of EcDHFR, BsDHFR and hybrid Xet-3, Xte-3, Xbt-3. Red = charged residues, green = polar uncharged residues, blue = hydrophobic aliphatic residues, cyan = aromatic residues.

Typically, for the construction of Xet-3, A DNA fragment encoding the mutated C-terminal region of EcDHFR (5'-GTCATCCCGGCAGTGGTGGAAGGCGACAC CCATTTC~~CCCGATTACGAGCCGGATGACTGGGAACTTGTATTCATGGAATTC CACGATGCTGATGCGCAGAACTCTCACGGCTATCTTTTTCTC~~-3'; changes underlined) was purchased from Epoch Biolabs (Texas, USA). A second fragment was obtained from a pJGetit-based vector harbouring the gene encoding wild type EcDHFR, using the primers 5'-ATTCTGGAGCGGCGGTAA-3' (forward) and 5'-CGTCAGATACAGTTTTTGCG-3' (reverse) under standard PCR conditions (Section 2.4.3). This second fragment was made up of the N-terminal sequence of EcDHFR plus the vector. The two fragments were ligated by T4 DNA ligase to form a pJGetit-based vector harbouring a gene encoding a partial EcDHFR-TmDHFR hybrid. The N-terminal mutations, D11S and R12G, were generated using the Phusion Site-Directed Mutagenesis Kit following the manufacturer's instructions (Section 2.4.3). The final product was excised from the pJGetit-based vector and subcloned

into pET11c at the restriction sites *Nde*I (5') and *Bam*HI (3'). The hybrid Xte-3 and Xbt-3 can be constructed by the similar way.

2.4.9 Preparation of XL1 Blue, BL21(DE3) and BL21-CodonPlus(DE3)-RP cells

XL1-Blue Ultracompetent cells (Stratagene, California, USA) were used for the preparation of new plasmid constructs following site directed mutagenesis and ligation of the appropriate plasmid and insert. BL21(DE3) competent cells (Stratagene, California, USA) were used for expression of BsDHFR and BL21-CodonPlus (DE3)-RP competent cells (Stratagene, California, USA) were used for the expression of hybrid enzymes.

A wire loop of competent cells was streaked on non-selective plates. As a negative control, competent cells were also streaked on an ampicillin plate. Both plates were incubated at 37 °C overnight. Non-selective LB medium (100 mL) was inoculated with a single colony from the non-selective plate and incubated at 37 °C until an optical density at 600 nm of 0.6 was reached after which the cells remained on ice. Cells were harvested in an Eppendorf 5810R centrifuge (Eppendorf AG, Hamburg, Germany) at 3200 RCF, 4 °C for 20 minutes and the supernatant solution discarded. Cells were resuspended in 25 mL Rb1 solution (Section 2.3.1), incubated on ice for 20 minutes and the centrifugation step repeated. Rb2 solution (Section 2.3.1) (5 mL) was used to resuspend the washed cell pellet and the cells aliquoted (50 µL) into sterile Eppendorf tubes and flash frozen in liquid nitrogen for storage at -80 °C. Transformation efficiency was determined and expressed as cfu/µg DNA used.

2.4.10 Transformation protocol and controls

The appropriate competent cells were allowed to thaw on ice. The DNA solution was thawed on ice and 2 µL transferred to the competent cells, mixing with the pipette tip

under sterile conditions. The cell/DNA mixture was incubated on ice for 30 minutes, heat shocked at 42 °C for 40 seconds and returned to ice for a minimum of 2 minutes. Non-selective LB medium (250 µL) was added to the cell/DNA mixture and incubated at 37 °C for 1 hour then plated on agar plates containing ampicillin (0.1 mg/mL) and incubated at 37 °C overnight.

When transforming cells, a positive control was always included whereby plasmid of a known concentration was used to transform the competent cells and the transformation efficiency calculated. A negative control was also included whereby sterile water was used in substitution for the DNA solution.

2.5 BsDHFR and hybrid enzymes production and purification

2.5.1 Large scale expression

The T7 expression system present in the pET vectors was adopted. This expression system was originally developed by Studier at Brookhaven National Laboratories (Studier and Moffatt, 1986).(223) The pET plasmids contain an expression cassette in which the gene of interest is inserted behind an extremely strong promoter from the *E. coli* bacteriophage T7. In the absence of the T7 polymerase, this promoter is completely shut off. For expression, the pET plasmids are transformed into bacterial strains that typically contain a single copy of the T7 polymerase on the chromosome in a lambda lysogen (the most commonly used lysogen is known as DE3). The T7 polymerase is under the control of the Lac-UV5 lac promoter. When cells are grown in media without lactose, the lac repressor (lacI) binds to the lac operator and prevents transcription from the lac promoter. When lactose is the sole carbon source, or when the lactose analog isopropyl- β -D-1-thiogalactopyranoside (IPTG) is added to the media, lactose or IPTG binds to the repressor and induces its dissociation from the operator, permitting transcription from the promoter.

Specifically, BL21(DE3) or BL21-CodonPlus(DE3)-RP competent cells were transformed with the appropriate DNA solution (section 2.5.5) and incubated overnight on ampicillin selective agar plates at 37 °C. A single colony was picked and used to inoculate 100 mL of ampicillin selective LB medium, incubating at 37 °C overnight whilst shaking at 150 RPM in an Innova 43 shaker (New Brunswick Scientific, Hertfordshire, UK). The overnight pre-culture (10 mL per 500 mL final culture) was subcultured into ampicillin selective LB medium and incubated at 37°C whilst shaking as previously described, until an optical density at 600 nm of 0.6 AU was reached. The incubation temperature was lowered to 30 °C. IPTG (0.5 mM) was then added and incubation continued overnight.

2.5.2 Protein identification: SDS-PAGE protocol

Gel buffer was prepared by dissolving Tris base (36.42 g) in 60 mL deionised water. 3 mL 10% SDS was added and the pH adjusted to 8.45 before adjusting the volume to 100 mL. Resolving gel (10%) was prepared by mixing 30 % acrylamide (3.33 mL), gel buffer (3.33 mL), 50% glycerol (2.6 mL), and 0.62 mL deionised water. Stacking gel (4%) was prepared by mixing 30 % acrylamide (667 µL), gel buffer (1.25 mL), and 3 mL deionised water.

Immediately prior to pouring the gel, 100 µL 10% ammonium persulfate (APS) and 50 µL N',N',N',N'-tetramethylethylenediamine (TEMED) were added for the resolving gel whilst 50 µL of 10% APS and 20 µL of TEMED were added for the stacking gel. Solutions were stirred gently to initiate polymerisation. When the resolving gel had been poured it was covered with a layer of isopropanol and allowed to polymerise. Isopropanol was then removed with blotting paper, the stacking gel poured, and a comb was inserted to create wells for sample loading.

The Mini-PROTEAN 3 Cell (Bio-Rad, California, USA) was used to identify the protein of interest and to monitor its purification. The resolving gel was used to

separate the proteins by their molecular weight and the stacking gel was used to concentrate the samples. Samples were resuspended in 100 μ L of protein loading dye (Section 2.3.7) and heated to 90 °C for 5 min. 15 μ L of the protein solution was then loaded into the gel wells. The anode (Section 2.3.6.1) and cathode buffer (Section 2.3.6.2) were added into the corresponding tanks. Gels were allowed to run at 150 V for 60 min.

Gels were stained in 100 mL protein staining buffer (Section 2.3.8) overnight whilst stirring. Protein bands were visualised after destaining the gels using protein destaining buffer (Section 2.3.9).

2.5.3 Protein purification

There are several methods for the purification of proteins based on the proteins' specific properties. The most efficient way is affinity chromatography. This method can achieve a high level of selectivity and thus purity but is not suitable for all proteins. Proteins can also be separated based on other physical properties such as charge via ion-exchange chromatography and size via size exclusion or 'gel filtration' chromatography. There are also some other properties which can be exploited for the purification of certain proteins, for example, the use of high temperatures in the purification of thermostable proteins, and extraction of insoluble proteins from inclusion bodies.

2.5.3.1 Inclusion body dissolving and refolding

The recombinant hybrid enzymes (Xet-1, Xte-1, Xet-2, Xte-2, Xbt-1, Xtb-1, Xet-3, and Xte-3) expressed segregated into inclusion bodies, thus the proteins need to be refolded before purifying by fast protein liquid chromatography (FPLC).

The general refolding protocol is as follows: the pellet from 0.5 L cell culture was resuspended in 30 mL potassium phosphate buffer (50 mM, pH 7) and disrupted by

sonication. The supernatant was decanted and the precipitate washed with 30 mL 1% Triton X-100, followed by 30 mL 2 M urea. Then the inclusion bodies were dissolved in 40 mL 8 M urea at 4 °C. The mixture was stirred slowly at 4 °C overnight. The insoluble proteins were removed by centrifugation. Refolding was then performed by dropwise 5 fold dilution of the denatured proteins into refolding buffer (Section 2.3.13). The urea and arginine were removed by dialysis.

2.5.3.2 Anion exchange chromatography

Ion exchange chromatography separates proteins based on their net surface charge. Usually, when the mixture of proteins is loaded onto the column, the conditions of the buffers are selected to let the desired protein bind to the resin. Unwanted proteins will pass through the column at different rates.

Xte-1 (theoretical pI 4.97), Xet-2 (theoretical pI 6.18), Xte-2 (theoretical pI 5.46), Xtb-1 (theoretical pI 6.63) and Xet-3 (theoretical pI 4.99) were purified using a diethylaminoethyl (DEAE) anion exchange column (~80 mL CV). The DEAE column was pre-equilibrated with 50 mM Tris-HCl (pH 8.0) and proteins eluted with a 0 to 1 M NaCl gradient. A two-stage NaCl gradient was applied to the column, from 0.0-0.5 M NaCl over 3 CV, followed by 0.5-1.0 M NaCl over 1 CV. The absorbance was monitored at 280 nm and fractions (typically 10 mL) were collected. SDS-PAGE analysis of each fraction was used to determine the point of elution of the desired protein. Proteins were dialysed as described above (Section 2.3.11).

2.5.3.3 Cation exchange chromatography

BsDHFR (theoretical pI 6.97) and its mutants (BsDHFR L20M, BsDHFR A104Q, BsDHFR L20M/A104Q, BsDHFR P122E, BsDHFR P129D, and BsDHFR P122E/P129D), Xet-1 (theoretical pI 9.04), Xbt-1 (theoretical pI 9.10), Xte-3 (theoretical pI 7.81), and Xbt-3 (theoretical pI 7.88) were purified using a

SP-Sepharose cation exchange column (~ 20 mL CV). Before the purification of wild type BsDHFR, the supernatant from the centrifuged cell extract was heat-precipitated at 55°C for 20 min and then centrifuged. The column for purification of BsDHFR and its mutants was pre-equilibrated with 50 mM citric acid (pH 5.0) and that for hybrids Xet-1, Xbt-1, Xet-3, and Xbt-3 was pre-equilibrated with 50 mM potassium phosphate (pH 7.0), and proteins eluted with a 0 to 1 M NaCl gradient. A two-stage NaCl gradient was applied to the column, from 0.0-0.5 M NaCl over 5 CV, followed by 0.5-1.0 M NaCl over 1 CV. The fractions were analysed by SDS-PAGE and proteins were dialysed as described above (Section 2.3.11).

2.5.3.4 Ni-Sepharose affinity chromatography

Polyhistidine-tagged (His-tag) Xet-1 and Xte-1 plasmids were prepared by inserting Xet-1 and Xte-1 genes into the pET19b vector (between *NdeI* and *BamHI* restriction sites). The His-tag hybrids were expressed as normal and can be purified by HisTrap FF Ni-Sepharose affinity column (~1 mL CV), because the string of histidine residues can strongly bind to immobilised metal ions, such as nickel, under specific buffer conditions. The HisTrap column was pre-equilibrated with 20 mM sodium phosphate, 0.5 M NaCl, 20 mM imidazole (pH 7.4) and then eluted with a 0 to 0.5 M imidazole gradient. A two-stage imidazole gradient was applied to the column, from 0.0-0.25 M imidazole over 10 CV, followed by 0.25-0.5 M imidazole over 1 CV. The fractions were analysed by SDS-PAGE and proteins were dialysed as described above. The column was then washed with 7 CV of 0.5 M imidazole buffer. The fractions were analysed by SDS-PAGE and proteins were dialysed as described above (Section 2.3.11).

2.5.3.5 Size exclusion chromatography

Size exclusion chromatography is commonly used as a final polishing step in a series of chromatographic procedures. The basic principle of size exclusion chromatography is

the passage of a mixture of proteins through a gel filtration resin packed in a column. The proteins are retarded to different degrees when passing through the column to give different retention times. Larger molecules are retarded to a lesser degree due to their inability to enter the small pores of the particles in the gel matrix. Smaller molecules become temporarily trapped in the pores of the particles as they diffuse between the stationary and mobile phase and thus have a longer retention time.

Size exclusion chromatography was performed using a Superdex 75 10/300 GL column (GE Healthcare) at a flow rate of 0.5 mL min⁻¹. Enzyme concentrations of 20-600 μM were used in 100 mM potassium phosphate (pH 7.0) containing 100 mM NaCl.

2.5.4 Protein storage

Final buffer concentration following dialysis and dilution with storage solution was 2.5 mM K₂PO₄, 2.5 mM β-ME. The protein/storage solution was flash frozen in liquid nitrogen and immediately stored at -20 °C.

2.5.5 Enzyme concentration determination

Potassium phosphate (100 mM, pH 7) buffer was used, which had been filtered and degassed on a vacuum pump (Vacuubrand GMBH +CO KG, MD4C, Wertheim, Germany). The Beer-Lambert law was used to calculate the concentration (mg/mL) of the protein solution.

$$A = \epsilon \cdot c \cdot l, \text{ and therefore } c = A \cdot df / \epsilon \cdot l$$

where: ϵ = extinction coefficient, A = absorbance at given wavelength, c = sample concentration in mg/mL, l = pathlength of the cuvette in cm and df is the dilution factor. Average extinction coefficients for proteins at 210 ($\epsilon = 20$ mL/mg/cm), 215 ($\epsilon = 15$ mL/mg/cm) and 220 nm ($\epsilon = 10$ mL/mg/cm) were used. To convert to a micromolar concentration, the concentration in mg/mL was divided by the molecular weight of the protein, multiplied by 10⁶.

2.6 Cofactor preparation

2.6.1 Preparation of dihydrofolate

Zakrzewski's method for the preparation of dihydrofolate (H₂F) was followed, as modified from Futterman, whereby folate is reduced with sodium dithionite.(224) Folic acid (400 mg) was dissolved in a minimal volume of 0.1 M NaOH and added to 80 mL 10% aqueous ascorbic acid (pH 6.0). Any fluctuation in pH was corrected to pH 6.0. The mixture was stirred under N₂ and sodium dithionite (4.4 g) added. The reaction was cooled on ice for 5 minutes and the pH slowly taken to 2.8 by drop-wise addition of 1 M HCl. The precipitate was centrifuged at 4 °C, 27000g for 5 minutes. The solid pellet was resuspended in 80 mL of fresh 10% ascorbic acid solution (pH 6.0), cooled on ice for 5 minutes and the pH reduced to 2.8 with 1 M HCl. The centrifugation step was repeated and the solid pellet re-suspended in ~20 mL of acetone, purged with N₂ and recentrifuged. This washing step was carried out twice with acetone and once with diethyl ether. The product was stored at -20 °C in an N₂-purged, foil-wrapped container. Product purity was assessed by ¹H NMR spectroscopy (500 MHz, D₂O/NaOD).

2.6.2 Preparation of NADPD

A pET11c plasmid harbouring the gene encoding alcohol dehydrogenase from *Thermoanaerobacter brockii* (TbADH) was purchased from ATG Biosynthetics GmbH (Merzhausen, Germany). *E. coli* BL21(DE3) cells were transformed with this plasmid and grown in LB media containing ampicillin (100 mg/mL) to an OD₆₀₀ of 0.6. IPTG was added to a final concentration 0.5 mM, and cells were grown for a further 4 h. Cells were harvested by centrifugation, resuspended in Tris-HCl (50 mM, pH 8) containing β-mercaptoethanol (5 mM) and disrupted by sonication. The clarified lysate was diluted two fold with the same buffer and incubated at 80 °C for 30 min to precipitate *E. coli* proteins. The clarified solution was purified by

anion-exchange chromatography on diethylaminoethyl resin (GE Healthcare) eluting with a 0–1M NaCl gradient to yield >95 %-pure TbADH as judged by SDS-PAGE. The pure TbADH was freeze-dried for storage.

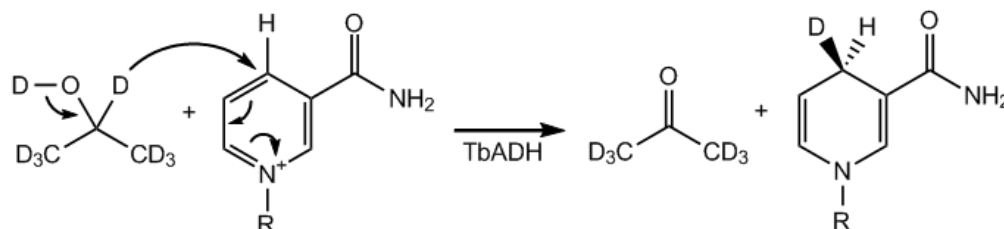


Figure 2.5 Reaction scheme for the enzymatic 4R stereospecific reduction of NADP^+ with d8-isopropanol.

NADPD was prepared by reducing NADP^+ with d8-isopropanol as the deuteride source and TbADH as the catalyst, using a modification of the method of Jeong and Gready (Figure 2.5).(225) NADP^+ (7 mg) and freeze-dried TbADH (1 mg) were dissolved in Tris-HCl (2 mL, 25 mM, pH 9) and d8-isopropanol (0.2 mL) was added. The reaction mixture was incubated at 40 °C for 15 min and purified by a modification of the method of Orr and Blanchard,(226) using anion exchange chromatography on a 250×4 mm SAX-10 column with an ICS-3000 FPLC system (Dionex).

2.7 Enzyme kinetics

2.7.1 Buffers for kinetics

2.7.1.1 Potassium phosphate buffers

Temperature dependence of k_{cat} and K_M at pH 7 was determined in 100 mM K_iPO_4 buffer containing 100 mM NaCl and 10 mM β -mercaptoethanol. Buffer was made freshly each day.

For determination of the salt dependence of k_{cat} and K_M , the above buffer was

modified to contain the appropriate concentration of NaCl, KCl, or KF. The salt was always added as a solid to a fresh batch of buffer, followed by pH correction to pH 7.

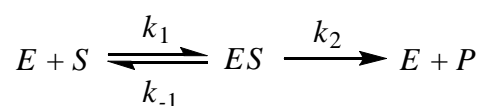
2.7.1.2 MTEN buffer

In order that a wide range of pH values could be sampled, MTEN buffer was used for the pH dependence of k_{cat} and K_M . The $\text{p}K_a$ values of the components used in this buffer allowed for a pH profile ranging from pH 4-10. MTEN buffer contains 50 mM MES, 25 mM Tris, 25 mM ethanolamine, 100 mM NaCl and 10 mM β -mercaptoethanol.

Due to the fact that there is a relatively large change in pH (-0.027) per 1 °C rise in temperature when using Tris as a buffer system, the pH was corrected at each experimental temperature. Standard pH calibration solutions were also used at the appropriate temperature (100 mM sodium borate for pH 9 and 100 mM potassium phosphate for pH 7).

2.7.2 Steady-state kinetics via UV spectroscopy

The term "steady state" refers to a period of time in enzyme kinetics where the concentration of enzyme-bound intermediates is constant. An enzyme-catalysed conversion of substrate (S) into product (P), *via* enzyme-bound substrate complex (ES) can be represented schematically as:



Only when the rate of formation of product is equal to the rate of consumption of substrate can the velocity of the enzyme-catalysed reaction be defined in the steady state.

$$\frac{d[ES]}{dt} = 0$$

Under the steady state condition, the concentrations of product and substrate have not

been significantly altered to affect the enzyme turnover. This means that either the rate of consumption of substrate or the rate of formation of product is changing in a linear fashion. Experimentally, a good approximation of the steady state rate can be achieved by making the concentration of substrate much greater than the concentration of enzyme, such that the concentration of substrate does not greatly change but remains linear over a longer period of time.

The catalytic rate constant (k_{cat}) of the reaction can be calculated from the reaction velocity, which is dependent on the concentration of enzyme.

$$V_{max} = k_{cat}[E]_0$$

where V_{max} is the maximal velocity of the reaction, and $[E]_0$ is the total enzyme concentration.

The Michaelis-Menten equation describes how the velocity of the reaction changes with the substrate concentration and the total enzyme concentration.

$$v = \frac{[E]_0[S]k_{cat}}{K_M + [S]}$$

where v is the apparently velocity of the reaction, and K_M is the substrate concentration at half maximal velocity.

This can be illustrated by plotting the substrate concentration against the enzyme velocity. At low substrate concentration the velocity of the reaction increases linearly with $[S]$. At high substrate concentration, the enzyme will be saturated, and velocity will tend towards a limiting value (V_{max}).

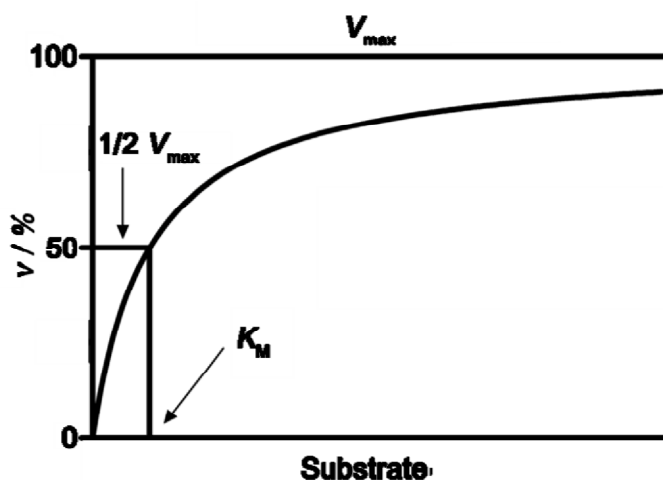


Figure 2.6 An example of a Michaelis-Menten plot illustrating a saturation curve for an enzyme showing the relation between the concentration of substrate and rate.

Steady state kinetics was performed on a Jasco V-660 spectrophotometer (Essex, UK) with the cofactor and substrate in excess concentrations relative to the enzyme. The cuvette used had a 10 mm path length. The temperature of the reaction was controlled by pre-incubating the reaction buffer at the appropriate temperature, and the temperature in the cuvette was monitored immediately prior to data acquisition.

When measuring the steady state turnover rate of the enzyme, the oxidation of cofactor was monitored at 340 nm where a linear decrease in absorbance was recorded over time ($\epsilon_{340}(\text{cofactor} + \text{substrate}) = 11,800 \text{ M}^{-1} \text{ cm}^{-1}$)(139). The temperature dependence of the steady state rate constants was studied between 10 and 65 °C at pH 7. The pH dependence at 20 °C was studied between 4 and 10. Typically, enzyme (0.02-0.05 μM) was incubated with the cofactor (0.5-300 μM for K_M (NADPH) measurements, otherwise 200 μM , 0.5-100 μL) in the appropriate assay buffer for 1 minute. The reaction was started by addition of the appropriate concentration of substrate (0.5-200 μM for K_M (H_2F) measurements, otherwise 100 μM , 0.5-100 μL).

A linear fit was applied to the decrease in absorbance signal using the software

provided (Spectra Analysis, Spectra Manager Version 203.02 JASCO Corporation). Initial velocities were recorded from 5-40 seconds and rates were calculated from the change in absorbance with time using the Beer-Lambert law.

2.7.3 Pre-steady-state kinetics

The study of the first few milliseconds of a reaction is called pre-steady-state kinetics. Pre-steady-state kinetics is concerned with the formation and consumption of enzyme-substrate intermediates until their steady-state concentrations are reached.

Pre-steady-state kinetics was performed on a Hi-Tech Scientific stopped-flow spectrophotometer (TgK Scientific, Bradford-on-Avon, UK). The reaction was monitored using Fluorescence Resonance Energy Transfer (FRET) under single turnover conditions over time scales ranging from 0.1-1 second. Tryptophan residues (for example, active site W22, EcDHFR numbering) were excited at 292 nm. This in turn excites the cofactor at 340 nm, which emits at 450 nm and is detected (using a 400 nm cut-off filter on the detector). Alternatively the cofactor may be excited directly at 340 nm and the reaction monitored at 450 nm as above.

The temperature of the reaction was controlled by pre-incubating the buffer at the appropriate temperature. The temperature in the reaction cell was monitored *via* internal temperature sensors on the stopped-flow instrument. The temperature range studied at pH 7 was 10-50 °C. At 20 °C the pH was varied from 4 to 10. Typically, 40 µM of enzyme was incubated with the appropriate concentration of cofactor (16 µM) in the appropriate assay buffer for 10 minutes in one syringe to avoid hysteretic behaviour. H₂F (400 µM) was incubated in the second syringe. The reaction was started by rapid mixing of the solutions from the two syringes.



Figure 2.7 Example of a stopped flow instrument (A) and the principle of its mechanism (B).

A single exponential fit ($Y = -A \cdot \exp(-k \cdot X) + C$) was applied to the decrease in signal using the software provided. This provided an estimate of the rate constant for the reaction. In order to minimise operator and equipment error each rate constant was the average of 3-4 measurements as calculated by the software, and this was repeated 3-4 times to give individual rate constants with which errors could be propagated. The reported rate constants are therefore the average of 9-16 individual runs.

The activation energy (E_a^H) and the preexponential factors (A_H) of the reaction were calculated by fitting the kinetic data to empirical Arrhenius equation:

$$k_H = A_H \exp\left(-\frac{E_a^H}{RT}\right)$$

$$\text{Therefore } \ln k_H = -\frac{E_a^H}{R} \cdot \frac{1}{T} + \ln A_H$$

where R is the molar gas constant and T is the absolute temperature. Plotting the natural logarithm of the rate constant as a function of the reciprocal of absolute temperature gives a straight line. The activation energies (E_a^H) can be derived from the slope and the preexponential factors (A_H) can be derived from the intercept.

2.8 Circular Dichroism spectroscopy

Circular dichroism (CD) refers to the differential absorption of left and right circularly polarised light. It is exhibited in the absorption bands of optically active chiral molecules. This technique is now used to investigate the secondary structures of proteins.

When the protein exists in its folded form, secondary structural elements have a characteristic CD absorbance (Figure 2.8). CD spectra can be used to estimate the percentage of a protein that is in the α -helix, β -sheet or random coil conformations. α -Helices show negative peaks at 222 nm and 208 nm of similar magnitude, whereas β -sheets are characterised by a negative peak at ~216 nm and a positive peak around 195 nm of similar magnitude. Random coils exhibit a strong negative peak at ~220 nm followed by a strong positive peak at ~218 nm. At the near UV range (>250 nm), the CD spectrum provides information on the tertiary structure. The absorption, dipole orientation and the nature of the surrounding environment of the phenylalanine, tyrosine, cysteine and tryptophan residues give signals in the 250-300 nm region. The CD absorbance of secondary structural elements in proteins is sensitive to environmental changes such as temperature, denaturing agents and pH. Therefore it is also widely used to study how the secondary structure of a molecule changes as a function of temperature, various denaturing agents or pH.

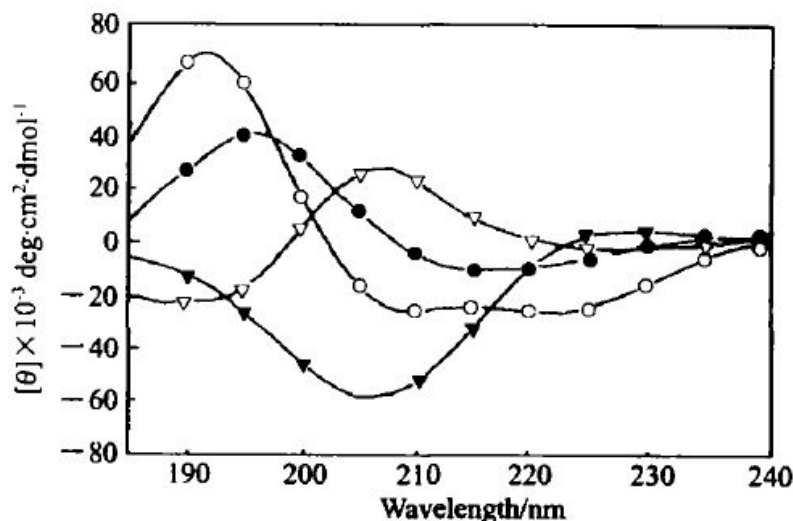


Figure 2.8 Circular dichroism (CD) spectra of polypeptides in the α -helical (\circ), β -sheet (\bullet), β -turn (∇) and P2 (\blacktriangledown) conformation. (Figure taken from reference (227))

All circular dichroism spectroscopy in this thesis was carried out using a ChirascanTM spectrophotometer (Applied Photophysics Limited, UK).

2.8.1 Buffers for thermal denaturation experiments

Potassium phosphate buffer (10 mM, pH 7) was sterilised with a 0.2 μ M syringe filter and degassed *via* vacuum pump. A blank run was always taken of the buffer alone and of buffer plus the appropriate concentration of ligands used in the experiment.

2.8.2 Calculation of mean residue ellipticity (MRE)

Calculating the signal obtained from CD experiments into mean residue ellipticity was performed using:

$$\Theta_{\text{MRE}} = \Theta / 10 \cdot n \cdot c \cdot l$$

where Θ = CD signal in millideg, n = number of backbone peptide bonds (*i.e.* number of amino acid residues minus 1), c = Molar concentration of sample, and l = path length of cuvette used in cm.

Typically a 0.1 cm path length cuvette was used to monitor the CD spectrum of DHFR, usually from 190-400 nm. The concentration of enzyme used was ~10 μ M.

2.9 Errors and their propagation

2.9.1 Standard deviation and standard error of the mean

All errors in this work are reported as the standard error of the mean which is defined as the standard deviation of the values in the sample divided by the square root of the sample size.

$$\sigma_M = \frac{\sigma}{\sqrt{n}}$$

$$\sigma = \sqrt{\frac{\sum (X - M)^2}{(n - 1)^2}}$$

where X is each value measured in the sample, M is the mean of the sample and n is the sample size.

2.9.2 Propagation of errors

In this thesis the effect of the uncertainty of values directly measured experimentally (X or Y) upon the uncertainty of a function based upon them (Z) was calculated using the following equations. The equation used is dependent upon the treatment of X and Y in order to obtain the value of Z .

$$\text{If } Z = X + Y \text{ or } Z = X - Y \text{ then } \Delta Z = \sqrt{\Delta X^2 + \Delta Y^2}$$

$$\text{If } Z = X * Y \text{ or } Z = X / Y \text{ then } \Delta Z = Z \sqrt{\left(\frac{\Delta X}{X}\right)^2 + \left(\frac{\Delta Y}{Y}\right)^2}$$

$$\text{If } Z = \ln X \text{ then } \Delta Y = \frac{\Delta X}{X}$$

$$\text{If } Z = e^X \text{ then } \Delta Y = \Delta X * e^X$$

where X and Y are independently measured values, ΔX and ΔY are their errors or uncertainty, and Z is the calculated value and ΔZ is its propagated error.

3 PREPARATION AND CHARACTERISATION OF WILD TYPE BsDHFR

3.1 Introduction

Many techniques are used to investigate the structural and functional aspects of enzymes. Effects of various environmental factors on enzyme catalysis may result from alteration(s) to the structural integrity of a protein. Structural differences of a protein caused by increasing temperature, ligand addition and buffer replacement can be monitored through the use of circular dichroism spectroscopy. Kinetic rates measured with enzymes are also sensitive to variations of these environmental factors. In the reaction catalysed by DHFR, the steady-state turnover rate of H₂F and NADPH is measured spectrophotometrically at 340 nm. At this wavelength the reduced form of cofactor (NADPH) has a maximal absorbance, whereas the absorbance of the oxidised form (NADP⁺) is sufficiently low to be ignored. The reaction rate is calculated from the change of absorbance of NADPH over time using the Beer-Lambert law ($A = \epsilon \cdot c \cdot l$) and the composite extinction coefficient for the reaction (11800 M⁻¹ cm⁻¹)(139).

The overall aim of the work described in this chapter was to clone the BsDHFR gene into a pET vector and express it with the T7 expression system to produce large amounts of pure, functional BsDHFR for used in structural and steady state kinetic studies. A wide range of changes were made to the BsDHFR catalysed steady state reaction such as changes in temperature, ligands, pH, salts and co-solvents.

3.2 Results and Discussion

3.2.1 Expression of BsDHFR

The gene encoding *Geobacillus stearothermophilus* DHFR (BsDHFR) with *Nde*I and *Bam*HI restriction sites at the 5'- and 3'- end, respectively, was purchased from Epoch Biolabs (with codons optimised for high level expression in *E. coli*), and ligated into the pPCR-Script Amp SK(+) vector *via* blunt-ended cloning. The BsDHFR gene was

excised from the cloning vector pPCR-Script Amp SK(+) by simultaneous digestion with *Bam*HI and *Nde*I restriction endonucleases (Figure 3.1). The modified pET expression vector pJGetit containing the EcDHFR gene was treated with the same restriction enzymes to ensure compatible ‘sticky’ ends for ligation with the BsDHFR gene. The restriction digestion process was followed *via* agarose gel electrophoresis.

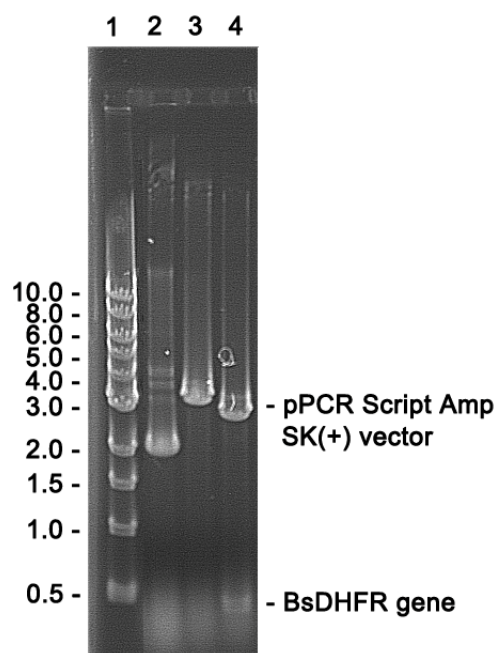


Figure 3.1 Agarose gel showing the digestion of the pPCR-Script Amp SK(+) plasmid. 1) 1 kb DNA ladder; 2) the plasmid; 3) digested with *Nde*I; 4) digested with *Nde*I/*Bam*HI.

Both the BsDHFR gene and the linearised expression vector were extracted from the agarose gel following electrophoresis, and then ligated with T4 DNA ligase. XL1-Blue competent cloning cells were transformed with the ligation products. The new plasmid construct was purified from these cells and sequenced for confirmation of integrity. BL21(DE3) competent cells were used for the expression.

3.2.2 Purification of BsDHFR

In this work, the purification of BsDHFR mostly followed the published procedure that has been described for production of BsDHFR, except the pH for the ion

exchange chromatography.(120) We chose pH 5 instead of 7 to get better binding of the enzyme to the SP-Sepharose column. Typically, 86 mg of pure protein was obtained from 1 L of culture. BsDHFR is a moderate thermophilic DHFR, thus purification of this enzyme involves heat treatment, in which crude mixture of protein is incubated at 55 °C for 20 min. At this temperature, BsDHFR remains folded and soluble in solution, while most of the *E. coli* proteins precipitated (lane 3, Figure 3.2).

Followed by heat treatment and centrifugation, the supernatant solution was applied to a SP-Sepharose column (sulfopropyl cation exchange chromatography column) which bound BsDHFR. The enzyme was eluted with a 0 to 1 M NaCl gradient, leading to essentially pure protein as judged by SDS-polyacrylamide gel electrophoresis. The final purified product showed a single band of ~18 kDa by gel electrophoresis under denaturing conditions, coincident with the molecular mass of 18694.55 Da calculated from the primary sequence (lane 4, Figure 3.2). After the salt was removed by dialysis in 10 mM potassium phosphate buffer at pH 7, the BsDHFR was flash frozen in liquid nitrogen, lyophilised and stored at -20 °C. This process did not affect the activity or stability of the enzyme.

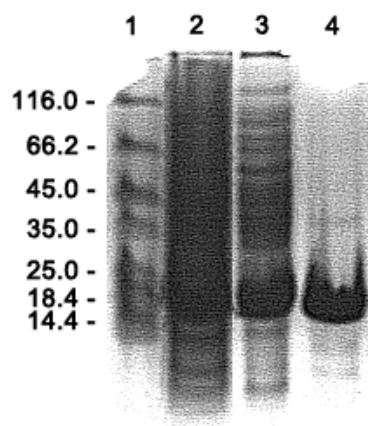


Figure 3.2 SDS-PAGE gel of BsDHFR purification: 1) molecular mass standards in kilodaltons; 2) supernatant solution of the crude cellular lysate; 3) supernatant solution following the heat precipitation step; 4) pool of fractions from cation exchange chromatography.

3.2.3 Sequence analysis of BsDHFR

The amino acid sequence alignment of BsDHFR, MpDHFR, EcDHFR and TmDHFR showed that the sequences of DHFR with different thermostability are highly conserved, especially the N-terminal region (Figure 3.3). The sequence of BsDHFR shares 43.9, 37.8 and 27.4% identity with MpDHFR, EcDHFR and TmDHFR, respectively. In particular, many residues participating in binding of substrate (Phe 31 and Ile 96) and cofactor (Ala 7, Ile 14, Arg 44, Thr 46, Ile 96 and Gly98) are fully conserved.

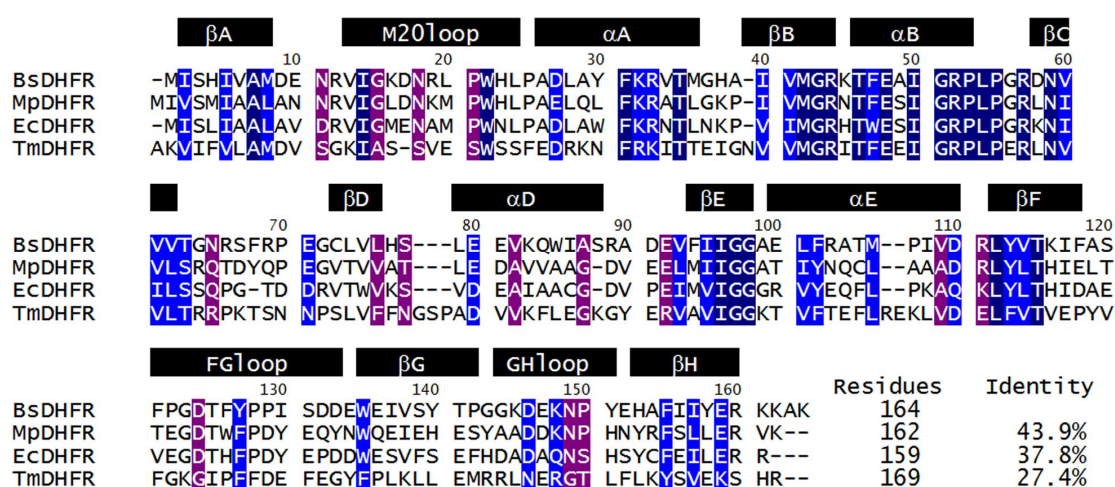


Figure 3.3 Sequence alignment (created using ClustalW) of BsDHFR, MpDHFR, EcDHFR and TmDHFR. Dark blue, light blue and purple indicate conserved, strongly similar and weakly similar residues, respectively. Tertiary structure, sequence lengths and levels of identity to BsDHFR are also indicated.

While BsDHFR shows the highest sequence identity to the psychrophilic analogue MpDHFR, biophysical properties of these enzymes are vastly different. Fast hydrogen-deuterium exchange (HDX) experiments suggested that all residues in apo-MpDHFR are very flexible at room temperature.⁽¹⁹³⁾ However, BsDHFR is much more rigid under the same conditions, especially in the protein core and loop subdomain.⁽²¹⁹⁾ The rigid structure of BsDHFR may be ascribed to the additional proline residues (11 in BsDHFR and 8 in MpDHFR, 7 of which are conserved) which are believed to enhance the thermostability of BsDHFR.⁽¹²⁰⁾ The insertion of proline

residues increases rigidity of the loop regions, thereby reducing conformational entropy of the folded enzyme.(47, 54, 55)

Another factor that may contribute to the thermostability of BsDHFR is the absence of thermolabile residues in water-accessible regions. Asparagine, glutamine, methionine and cysteine are considered thermolabile, because they tend to undergo deamidation (asparagine and glutamine) or oxidation (methionine and cysteine)(228) at high temperatures. These amino acids are less common in thermophilic proteins, or they are buried within the protein to prevent unwanted side reactions.(46) Understandably, there are 5 asparagine residues and 1 glutamine residue in BsDHFR, but 9 and 5 in MpDHFR, respectively. Moreover, several residues involved in the binding of cofactor are different to those in MpDHFR. Noticeably, Gln 104 in MpDHFR, which is conserved in many DHFRs, is substituted with Ala in BsDHFR. This substitution reduces the binding ability of NADPH and might be the reason for the large K_M value of BsDHFR for NADPH which will be discussed in Chapter 5.

3.2.4 Size exclusion chromatography analysis of BsDHFR

To determine the oligomerisation state of the native protein under neutral conditions, BsDHFR was analysed by size exclusion chromatography and compared with monomeric EcDHFR and dimeric TmDHFR (Figure 3.4). The elution volume of a 100 μ M solution of BsDHFR (~12.4 mL) at pH 7 was close to that of EcDHFR (~12.5 mL) but observably greater than that of TmDHFR (~11.0 mL), indicating that the apparent molecular weight of BsDHFR was close to the expected value for monomer. This value was in good agreement with the molecular mass as measured by Kim et al (18694.6 \pm 0.8 Da).(120) No obvious oligomerisation has been observed at concentrations up to 600 μ M (not shown). Reduction of the protein concentration did not significantly influence the apparent molecular weight (Figure 3.4).

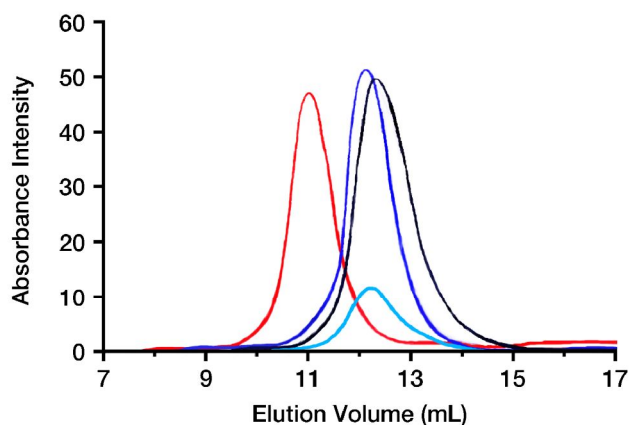


Figure 3.4 Size exclusion chromatography of BsDHFR (blue), EcDHFR (black), and TmDHFR (red) at 100 μM and BsDHFR at 10 μM (cyan) in 100 mM potassium phosphate (pH 7.0) containing 100 mM NaCl.

3.2.5 Circular dichroism analysis of BsDHFR

Far-UV circular dichroism (CD) spectroscopy of BsDHFR showed characteristics of a folded structure with secondary structural elements. There is a broad negative peak at 222-208 nm for BsDHFR (Figure 3.5A), which is wider and blue shifted when compared to the CD spectra for MpDHFR,(211) EcDHFR(179) and TmDHFR.(202) At 20 °C, there is a minimum mean residue ellipticity of $-5966 \text{ deg}\cdot\text{cm}^2\cdot\text{dmol}^{-1}$ at 206 nm, compared to $-5970 \text{ deg}\cdot\text{cm}^2\cdot\text{dmol}^{-1}$ at 216 nm for MpDHFR, $-9150 \text{ deg}\cdot\text{cm}^2\cdot\text{dmol}^{-1}$ at 218 nm for EcDHFR and $-11000 \text{ deg}\cdot\text{cm}^2\cdot\text{dmol}^{-1}$ at 222 nm for TmDHFR, and a maximum below 190 nm, compared to at 192 nm for MpDHFR, 195 nm for EcDHFR and 196 for TmDHFR. Moreover, in the cases of BsDHFR and MpDHFR, the 208 nm band is of larger magnitude and more prominent than the 222 nm band, while for EcDHFR and TmDHFR signals at these wavelengths are reversed, indicating a difference in the percentage of secondary structure elements.(227, 229)

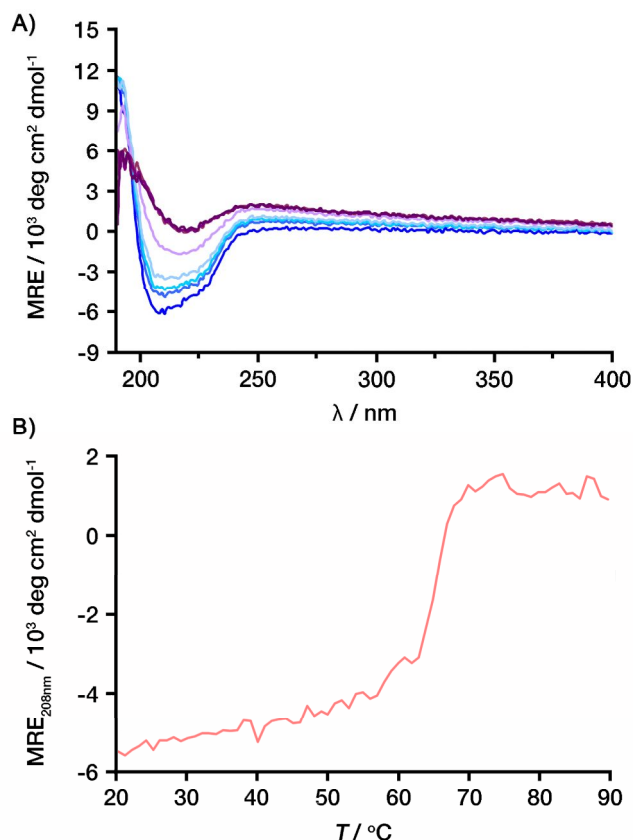


Figure 3.5 A) Effect of temperature on the CD spectrum of BsDHFR in 10 mM potassium phosphate buffer at pH 7. Spectra are shown at 10 °C intervals between 20 °C (darkest blue) and 90 °C (darkest purple); B) temperature dependence of the mean residue ellipticity of BsDHFR at 208 nm.

3.2.6 Thermal unfolding of BsDHFR

The thermal melting point (T_m) of BsDHFR was measured by monitoring the change in mean residue ellipticity (MRE) at 208 nm with increasing temperature. The temperature dependence of the MRE of BsDHFR exhibited small linear variations of the signal between 20 and 58 °C, and a very sharp loss of secondary structure between 58 and 70 °C (Figure 3.5B). At temperatures higher than 70 °C, the denatured protein started to precipitate. T_m was determined as 66.2 ± 0.4 °C, which is similar to the value previously reported.⁽²¹⁹⁾ This value is ~ 17 °C lower than that of the hyperthermophilic TmDHFR (~ 83 °C),⁽²⁰²⁾ ~ 15 °C higher than that of the mesophilic EcDHFR (~ 51 °C),⁽¹⁷⁹⁾ and ~ 29 °C higher than that of the psychrophilic MpDHFR

(37.5 ± 0.8 °C).(211) The thermal denaturation of BsDHFR was not reversible due to aggregation of the denatured protein (not shown).

3.2.7 Environmental factors influencing the stability of BsDHFR

G. stearothermophilus can be found in many warm environments, such as sand, ocean vents and hot springs,(217) and can thrive at temperatures as high as 75 °C,(218) *In vitro*, however, in 10 mM potassium phosphate at neutral pH, BsDHFR starts to denature at only 58 °C and up to 70 °C, the protein unfolds completely. Therefore, there should be some environmental factors *in vivo* that provide the extra thermostability to maintain its folded structure at very high temperature.

3.2.7.1 Effect of salts on BsDHFR thermostability and specific activity

In order to investigate the effect of salts on the thermostability and specific activity of BsDHFR, the melting temperature and the specific activity of BsDHFR were measured in the presence of increasing concentration of sodium and potassium chloride as well as potassium fluoride. The effect of ionic strength on the secondary structure was monitored by CD spectroscopy. Even in the presence of 2 M salts (NaCl, KCl and KF), no major differences in the shape or intensity in the protein CD spectrum were observed, suggesting that in this concentration range, Na⁺, K⁺, Cl⁻ and F⁻ ions do not change the secondary structure of the structure (Figure 3.6). The melting temperature of BsDHFR was also measured by monitoring the change in MRE at 208 nm as a function of NaCl, KCl and KF. All of these salts showed similar influences on the thermostability of BsDHFR. The melting temperature of BsDHFR increased sharply when the salt concentration was increased from 0.1 to 0.5 M, and plateaued at higher concentrations (>0.5 M) (Table 3.1). Eventually, the enzyme showed maximum stability when the salt concentration reached 2 M, leading to a ~8 °C increase in the melting temperature.

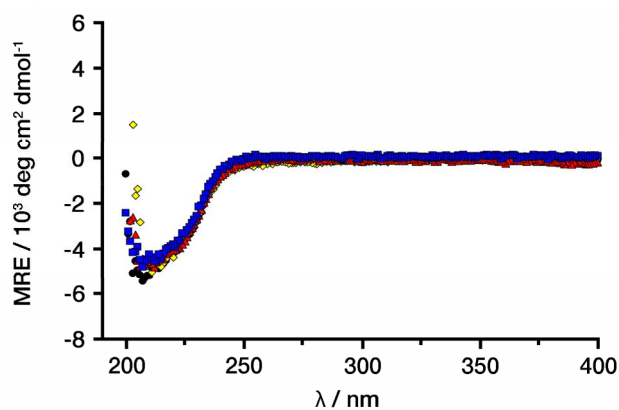


Figure 3.6 CD spectra of BsDHFR at 20 °C with no added salt (black), 2 M NaCl (yellow), KCl (red) and KF (blue) at pH 7.

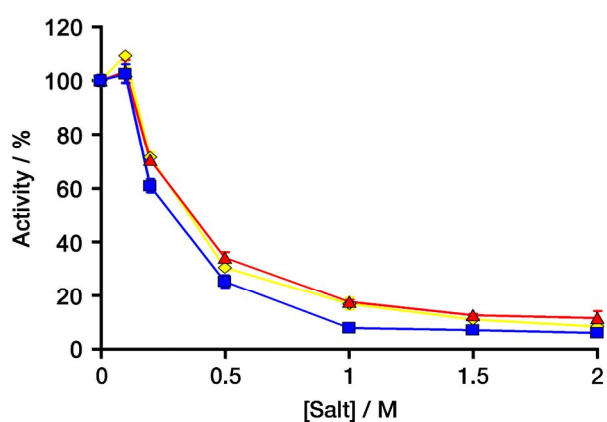


Figure 3.7 Effect of ionic strength on the specific activity of the BsDHFR-catalysed reaction at 20 °C. The buffer was 100 mM K_iPO_4 , pH 7 in the presence of NaCl (yellow), KCl (red) and KF (blue).

Table 3.1 Effect of salts on the melting temperature of BsDHFR.

[Salt] / M	T_m (NaCl) / °C	T_m (KCl) / °C	T_m (KF) / °C
0	66.2 ± 0.4		
0.1	66.8 ± 0.2	66.9 ± 0.2	66.8 ± 0.2
0.2	67.2 ± 0.2	67.9 ± 0.2	67.5 ± 0.1
0.5	67.6 ± 0.2	68.3 ± 0.2	68.6 ± 0.2
1	69.5 ± 0.2	70.1 ± 0.2	71.0 ± 0.3
1.5	71.5 ± 0.4	71.7 ± 0.4	73.8 ± 0.8
2	73.4 ± 0.3	73.8 ± 0.3	74.6 ± 0.3

Nevertheless, buffers with high ionic strength are not likely to represent the naturally functioning environment of BsDHFR, since the optimal growth NaCl concentration of *Geobacillus stearothermophilus* is relatively low *in vitro* (0.5% w/v, ~85 mM).(230) In order to test the influence of salts on the activity of BsDHFR, the steady-state rate of the enzyme catalysed reaction was measured at saturated concentrations of substrate and cofactor. The temperature for the measurement was 20 °C and the buffer used was 100 mM K_iPO₄ at pH 7. The ionic strength of the solution was varied by adding increasing concentrations of NaCl, KCl and KF. A significant decrease in the specific activity of the enzyme was noted when the ionic strength was raised higher than 0.2 M (Figure 3.7). Lower concentrations of NaCl seemed to enhance the specific activity of the enzyme (~9%), while concentrations higher than 0.2 M appeared to greatly inhibit the BsDHFR catalysed reaction (Figure 3.7). At 1 M NaCl, the activity of BsDHFR was nearly 80% lower than that in buffer without salt. At 2 M NaCl, the enzyme lost over 90% of its initial activity. This effect was also observed by Kim *et al.*(120) Low concentrations of KCl and KF also slightly increased the specific activity, and showed inhibitory effects with increasing concentrations. The inhibitory effect of KF was strongest.

3.2.7.2 Effect of substrate and cofactor binding on the thermostability of BsDHFR

Although the presence of salt increases the thermostability of BsDHFR, high concentrations of salt inhibit the BsDHFR activity greatly. Therefore, the presence of various salts may not be the main factor that stabilises BsDHFR *in vivo*. Substrates and cofactors can stabilise enzymes through binding to their active sites, as this enhances the packing of the structure and therefore the entire rigidity. A more rigid structure will enhance the capability to resist thermal denaturation and thus increase the melting temperature of the protein. This effect is postulated as a possible mechanism to enhance thermostability of a protein and has been seen in many thermophilic enzymes.(231-233) In order to investigate the extent of the thermal

stabilisation of substrate and cofactor molecules on the structure of BsDHFR, the T_m of the enzyme was measured in the presence of NADPH or H₂F. Adding one equivalent of NADPH greatly enhanced the thermostability of BsDHFR and increased the melting temperature by 5 °C (71.2 ± 0.4 °C). The presence of H₂F also slightly increases the melting temperature 2 °C (68.2 ± 0.4 °C), providing a mild thermal stabilisation of the enzyme.

Beside salts, substrate and cofactor binding, glycerol and sucrose also have been shown to stabilise enzymatic action under elevated temperature.(234) Their effects together with other organic solvents on the tertiary structure and activity of BsDHFR will be discussed in another section.

3.2.8 Influence of temperature on the steady state kinetics of BsDHFR

The rate of the BsDHFR catalysed turnover of NADPH and H₂F could be measured by UV-spectroscopy. The steady-state rate was calculated by measuring the specific activity of the enzymes (defined as the amount of product formed by an enzyme in a given amount of time under given conditions) at saturating condition for substrate and cofactor.

The steady-state rate constant (k_{cat}) for the reduction of H₂F by NADPH catalysed by BsDHFR at pH 7 increased in an exponential fashion up to 65 °C (Figure 3.8A). The k_{cat} for the BsDHFR-catalysed reaction was similar to its mesophilic and psychrophilic counterparts (EcDHFR and MpDHFR) and much greater than that of the hyperthermophilic TmDHFR at 25 °C. k_{cat} was maximal at 70 °C (243 ± 12 s⁻¹), slightly higher than the optimal growth temperature of *G. stearothermophilus* (60 °C).(218) At the respective optimal growth temperatures of 60 °C for *G. stearothermophilus*, 2 °C for *M. profunda*, 37 °C for *E. coli* and 80 °C for *T. maritima*, the steady-state rate constant of BsDHFR (183 ± 8 s⁻¹) was approximately 37 times

higher than that of MpDHFR ($\sim 5.0 \text{ s}^{-1}$),⁽²¹¹⁾ 5 times that of EcDHFR ($\sim 37 \text{ s}^{-1}$)⁽¹¹⁹⁾ and 38 times that of TmDHFR ($\sim 4.8 \text{ s}^{-1}$).⁽²⁰²⁾ Above $70 \text{ }^\circ\text{C}$, k_{cat} decreased markedly as expected for an enzyme with a T_m of $66.2 \pm 0.4 \text{ }^\circ\text{C}$.

Table 3.2 Temperature dependence of the steady-state reaction catalysed by BsDHFR, EcDHFR, MpDHFR and TmDHFR at pH 7 as well as the primary KIE of BsDHFR-catalysed reaction.

t / $^\circ\text{C}$	BsDHFR $k_{\text{cat}}(\text{H}) / \text{s}^{-1}$	BsDHFR KIE	EcDHFR ^[a] $k_{\text{cat}}(\text{H}) / \text{s}^{-1}$	MpDHFR ^[b] $k_{\text{cat}}(\text{H}) / \text{s}^{-1}$	TmDHFR ^[a] $k_{\text{cat}}(\text{H}) / \text{s}^{-1}$
5	nd	nd	nd	5.9 ± 0.2	nd
10	7.02 ± 1.95	1.34 ± 0.16	nd	8.2 ± 0.4	nd
15	9.29 ± 2.23	1.44 ± 0.15	8.5 ± 1.2	10.8 ± 0.5	nd
20	16.2 ± 2.8	1.66 ± 0.07	12.6 ± 1.4	14.8 ± 0.8	nd
25	21.6 ± 1.6	1.90 ± 0.19	16.4 ± 3.6	18.7 ± 0.8	0.10 ± 0.01
30	32.7 ± 1.4	2.02 ± 0.20	24.0 ± 3.0	25.3 ± 1.1	0.18 ± 0.01
35	48.6 ± 6.8	2.27 ± 0.36	32.0 ± 5.0	32.5 ± 1.9	0.24 ± 0.02
40	66.7 ± 3.9	2.43 ± 0.19	44.9 ± 6.1	39.6 ± 1.8	0.31 ± 0.02
45	87.3 ± 2.3	2.54 ± 0.09	53.9 ± 5.6	28.8 ± 0.8	0.42 ± 0.04
50	116 ± 5	2.56 ± 0.16	nd	nd	0.59 ± 0.04
55	145 ± 8	2.75 ± 0.22	nd	nd	0.77 ± 0.05
60	183 ± 8	2.96 ± 0.14	nd	nd	1.00 ± 0.08
65	236 ± 18	3.08 ± 0.25	nd	nd	1.35 ± 0.07
70	243 ± 12	nd	nd	nd	1.70 ± 0.14
75	nd	nd	nd	nd	2.03 ± 0.20

[a] Data taken from ref. (202) and reported per monomer subunit for TmDHFR. [b] Data taken from ref. (211).

The primary KIE was estimated by measuring the steady-state rate of the BsDHFR catalysed reaction using deuterium-labelled cofactor, 4-(R)-NADPD (NADPD).

Across the temperature range studied (10-65 °C), the steady-state rate constant with NADPD is lower than that with NADPH, giving an increasing KIE against temperature (Figure 3.8B). The temperature dependence of the KIE indicates that a physical step is rate limiting at 10 °C, and that the hydride transfer step becomes gradually more rate limiting as the temperature is increased, as was also reported by Kim *et al.*(120) This behaviour is in contrast to both the *M. profunda* and *E. coli* enzymes where the hydride-transfer step at pH 7 was more than one order of magnitude faster than the steady-state rate,(179, 193) and the *T. maritima* enzyme where the hydride-transfer step was predominantly rate-limiting across the temperature range.(202) From the BsDHFR Arrhenius plot, the apparent activation energy and Arrhenius prefactor for the steady-state reaction with NADPH were calculated as $E_a = 51.6 \pm 1.6 \text{ kJ}\cdot\text{mol}^{-1}$ and $A_H = (2.51 \pm 0.06) \times 10^{10} \text{ s}^{-1}$, respectively. The apparent activation energy with NADPD is $39.8 \pm 0.7 \text{ kJ}\cdot\text{mol}^{-1}$ and $A_D = (1.13 \pm 0.02) \times 10^8 \text{ s}^{-1}$ (Table 3.3). However, these are only apparent values as the rate-limiting step changes with temperature, and so activation parameters for a single step cannot be extracted.

Table 3.3 Activation parameters and corresponding k_{cat} for BsDHFR, MpDHFR, EcDHFR and TmDHFR-catalysed steady-state reactions.

Parameter	BsDHFR	MpDHFR	EcDHFR	TmDHFR
$k_{\text{cat}} / \text{s}^{-1}$ (25°C)	21.6 ± 1.6	18.7 ± 0.8	16.4 ± 3.6	0.10 ± 0.01 ^[b]
$E_a^{\text{H}} / \text{kJ}\cdot\text{mol}^{-1}$ ^[a]	51.6 ± 1.6	39.9 ± 0.5	47.7 ± 0.8	51.9 ± 0.6
$A_H / 10^8 \text{ s}^{-1}$ ^[a]	251 ± 6	1.84 ± 0.36	38.4 ± 1.3	0.86 ± 0.02
[a] E_a^{H} is the apparent activation energy, and A_H is the preexponential factors. [b] Data per monomer subunit for TmDHFR.				

The Michaelis constants (K_M) of BsDHFR for NADPH and H₂F at 20 °C are $108 \pm 29 \mu\text{M}$ and $2.4 \pm 0.4 \mu\text{M}$, respectively. The K_M of H₂F is similar to that of psychrophilic MpDHFR and mesophilic EcDHFR at the same temperature ($1.9 \pm 0.3 \mu\text{M}$ for

MpDHFR(211) and $0.7 \pm 0.3 \mu\text{M}$ for EcDHFR(138)), whereas that for NADPH is markedly larger than other homologues ($13.3 \pm 1.2 \mu\text{M}$ for MpDHFR(211), $4.8 \pm 1.0 \mu\text{M}$ for EcDHFR(138) and $<0.5 \mu\text{M}$ for TmDHFR).(202) The K_M for H₂F did not change significantly with temperature. However, the K_M for NADPH greatly decreases at higher temperatures (Table 3.4). At 60 °C and pH 7, which are expected to be the physiological conditions of the bacterium, the K_M for NADPH and H₂F are $30.0 \pm 5.1 \mu\text{M}$ and $3.5 \pm 0.7 \mu\text{M}$, respectively, which compare well with those reported by Kim (10.4 and $3.7 \mu\text{M}$ respectively(120)). In the BsDHFR-catalysed reaction, H₂F displayed a higher k_{cat}/K_M than NADPH across the entire temperature range studied (Table 3.4). The change of K_M value of BsDHFR results in a great increase in k_{cat}/K_M for both H₂F and NADPH with temperature, which is different to many other enzymes(235-238) (including MpDHFR(211)) whose K_M values usually increase with rising temperature.

Table 3.4 Effect of temperature on the K_M and second-order rate constant k_{cat}/K_M for NADPH and H₂F for the BsDHFR-catalysed reaction at pH 7.

t / °C	$K_M(\text{NADPH})$ / μM	$k_{\text{cat}}/K_M(\text{NADPH})$ / $\mu\text{M}^{-1} \cdot \text{s}^{-1}$	$K_M(\text{H}_2\text{F})$ / μM	$k_{\text{cat}}/K_M(\text{H}_2\text{F})$ / $\mu\text{M}^{-1} \cdot \text{s}^{-1}$
20	108 ± 29	0.13 ± 0.04	2.4 ± 0.4	5.9 ± 0.9
40	76.3 ± 17.2	0.87 ± 0.20	4.2 ± 0.8	15.9 ± 3.2
60	30.0 ± 5.1	6.1 ± 1.1	3.5 ± 0.7	52.1 ± 10.0

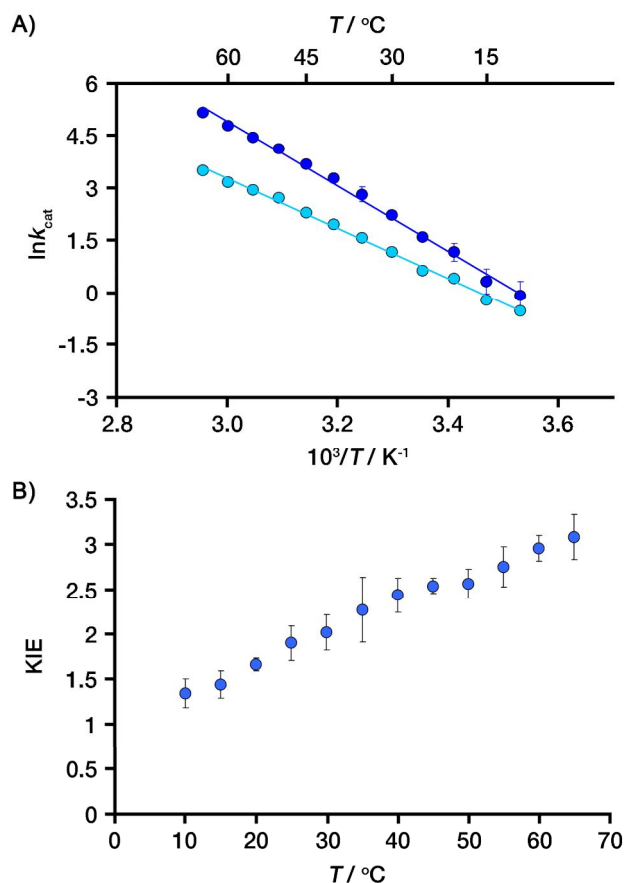


Figure 3.8 A) Arrhenius plots for the steady-state BsDHFR reaction with NADPH (dark blue), and NADPD (light blue) at pH 7; and B) the corresponding KIEs of BsDHFR.

3.2.9 Influence of pH on the steady state kinetics of BsDHFR

The pH dependence of the steady-state rate for BsDHFR has been characterised previously.⁽¹²⁰⁾ This study showed a sigmoidal trend between pH 6 and 10 at 40 °C. However, the behaviour of the BsDHFR-catalysed reaction under pH 6 is still unclear. In this thesis, a wider range of pH was chosen (pH 4-10) for the pH studies of BsDHFR.

It has been shown that the steady-state rate constant for the BsDHFR-catalysed reaction was found to depend on the pH of the solution in a bell shaped trend at 20 °C (Figure 3.9A). k_{cat} is low at high pH and rises to a maximum at $\text{pH } 6.2 \pm 0.1$, with an

apparent pK_a of 7.6 ± 0.2 . The decrease in rate above pH 6.2 is probably a consequence of the influence of pH on protonation of the substrate (protonation of the N^5 atom of H_2F is required for the DHFR catalysed reaction(98)) leading to a greatly reduced rate of hydride transfer and a change in the rate-limiting step as seen for EcDHFR.(138) k_{cat} also decreases from this maximal rate when the pH is lowered, with an apparent pK_a of 5.0 ± 0.1 . Changing the pH therefore led to a more than 150-fold variation in rate. The pH profile of the BsDHFR steady-state reaction is similar to that of MpDHFR (maximal rate is at pH 6.8 ± 0.1 with inversion points at pH 8.1 and 5.7, respectively(211)). EcDHFR and TmDHFR give sigmoidal curves for k_{cat} with inversion points at pH 8.4(239) and pH 6.0 (40 °C),(202) respectively, and no decrease at low pH. The pH dependence of the primary hydrogen KIE on the steady-state reaction was also determined at 20 °C (Figure 3.9B). The primary KIE is maximal at high pH and is reduced as the pH is lowered, showing that the hydride transfer is at least partially rate limiting above pH 8, whereas the steady-state rate constant is limited by a physical step at pH 7 and below. The conclusion agrees with previous results,(120) and is also seen for MpDHFR(212) and EcDHFR.(138, 154) TmDHFR shows a different trend, with the steady state rate constant being at least partially limited by hydride transfer at all values of pH.(202)

Table 3.5 Effect of pH on the steady-state rate constant of the BsDHFR-catalysed reaction and its primary KIE in MTEN buffer at 20 °C.

pH	$k_{\text{cat}} / \text{s}^{-1}$	KIE
4	7.35 ± 0.24	1.15 ± 0.11
4.5	8.99 ± 1.03	1.11 ± 0.15
5	12.1 ± 1.5	1.36 ± 0.26
5.5	14.6 ± 0.3	1.34 ± 0.05
6	16.9 ± 0.4	1.33 ± 0.08
6.5	17.0 ± 0.4	1.44 ± 0.07
7	15.8 ± 1.0	1.80 ± 0.07
7.5	12.2 ± 1.0	2.57 ± 0.50
8	8.36 ± 0.13	2.77 ± 0.44
8.5	3.99 ± 0.32	3.40 ± 0.34
9	1.90 ± 0.03	3.50 ± 0.08
9.5	0.46 ± 0.04	3.59 ± 0.64
10	0.12 ± 0.01	3.36 ± 0.48

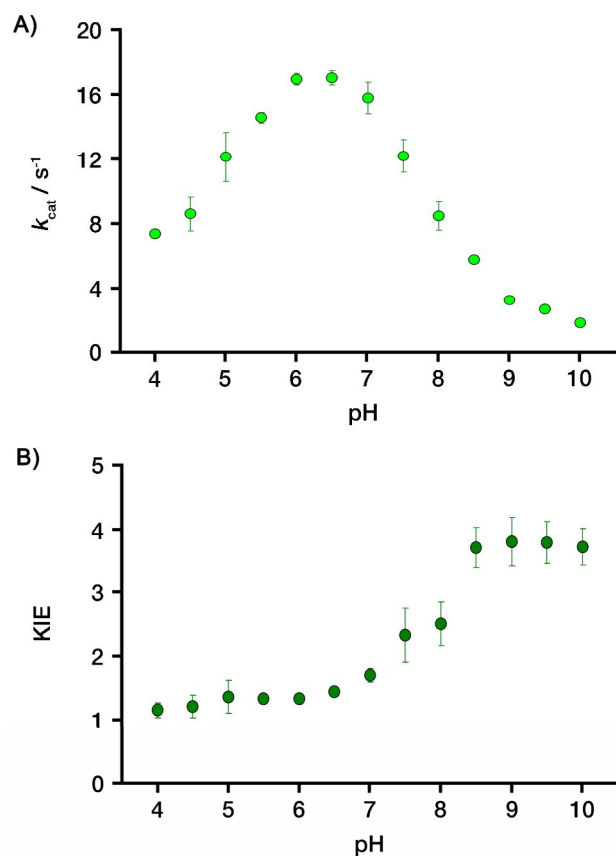


Figure 3.9 A) Effect of pH on the steady-state rate constant k_{cat} of the BsDHFR-catalysed reaction at 20 °C; and B) the corresponding primary KIEs.

3.2.10 Influence of solvents on the steady state kinetics of BsDHFR

The k_{cat} at 20 °C for the BsDHFR-catalysed reaction was measured in the presence of organic cosolvents and compared with the results of MpDHFR, EcDHFR and TmDHFR. CD spectroscopy was used to investigate the effect of cosolvent on the secondary structure of BsDHFR (Figure 3.10). Like TmDHFR,⁽¹⁹²⁾ the thermophilic BsDHFR can conserve its secondary structure in most organic cosolvents, except in 50% tetrahydrofuran (THF). It is therefore likely that the reduction of the rate constants did not relate to solvent-induced structural changes. For MpDHFR and EcDHFR, a certain degree of structural loss was observed in the presence of ethanol, isopropanol, ethylene glycol and THF.^(191, 193)

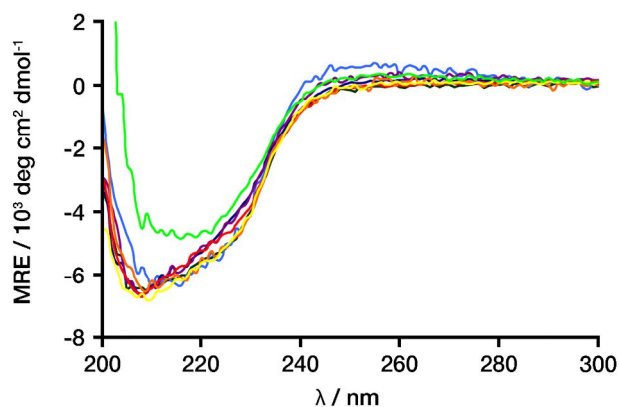


Figure 3.10 CD spectra of BsDHFR (10 μ M) at 20 $^{\circ}$ C in the presence of 50% organic cosolvent, where dark green = no cosolvent, blue = methanol, dark blue = ethanol, purple = isopropanol, red = ethylene glycol, orange = glycerol, yellow = sucrose, and light green = THF.

Organic solvents can influence the enzyme-catalysed reaction mainly in two ways. Firstly, the viscosity might perturb the network of long-range promoting motions, which has been proposed to drive enzyme catalysis.⁽²⁴⁰⁾ Secondly, the effect of the dielectric constant might influence hydride transfer by affecting the shielding of stabilising electrostatic effects within the active site.⁽¹⁸⁸⁾

Increasing concentrations of cosolvents led to a general reduction of steady state rate constant (Figure 3.11). The value of k_{cat} was not reduced in a manner directly proportional to the medium viscosity, but was decreased proportional to the dielectric constant. This is similar to the effect that has previously been observed for MpDHFR,⁽¹⁹³⁾ EcDHFR⁽¹⁹¹⁾ and TmDHFR.⁽¹⁹²⁾ The k_{cat} value dropped to zero when the dielectric constants of the solvents were less than 50 (in the presence of 50% THF). This may in part be caused by enzyme denaturation, as indicated in CD spectroscopic analysis. The KIE on k_{cat} did not alter proportionally to the solvent properties, which is the same as that of TmDHFR.⁽¹⁹²⁾ At non-physiological pH (9 for MpDHFR, 9.5 for EcDHFR) the KIE on k_{cat} decreased proportionally to the dielectric constant, most likely due to a solvent-induced change in rate-limiting step

from the chemical step to the physical step.(191, 193)

Table 3.6 Kinetic parameters for the steady-state reaction of NADPH and H₂F catalysed by BsDFHR in the presence of cosolvents at 20 °C.

Solvent composition	Viscosity / mPa.s ^[a]	Dielectric constant ^[a]	$k_{\text{cat}} / \text{s}^{-1}$	KIE
no cosolvent	1	79	14.3 ± 1.4	1.37 ± 0.18
17 % methanol	1.25	75	14.7 ± 1.3	1.36 ± 0.15
33 % methanol	1.5	65	10.2 ± 0.4	1.26 ± 0.12
50 % methanol	1.6	58	8.38 ± 0.30	1.29 ± 0.09
17 % ethanol	1.45	71	5.50 ± 0.58	1.02 ± 0.17
33 % ethanol	2	60.7	4.62 ± 0.55	1.15 ± 0.14
50 % ethanol	2.3	52	2.55 ± 0.31	1.18 ± 0.15
17 % isopropanol	1.5	59.8	5.22 ± 0.17	1.12 ± 0.04
33 % isopropanol	2.1	59.4	2.06 ± 0.11	0.93 ± 0.08
50 % isopropanol	2.6	50	0.96 ± 0.04	1.16 ± 0.08
17 % ethylene glycol	1.6	76	10.4 ± 0.5	0.98 ± 0.07
33 % ethylene glycol	2.4	70	15.4 ± 1.1	0.98 ± 0.09
50 % ethylene glycol	3.4	65	5.91 ± 0.21	1.01 ± 0.05
17 % glycerol	1.8	74.4	8.53 ± 0.65	1.05 ± 0.14
33 % glycerol	3.4	67.7	8.24 ± 0.33	1.63 ± 0.11
50 % glycerol	8	62	3.28 ± 0.41	1.29 ± 0.29
17 % sucrose	1.8	76.5	13.9 ± 0.3	0.96 ± 0.06
33 % sucrose	3.4	72.6	10.1 ± 0.3	1.43 ± 0.08
17 % THF	1	66.7	3.80 ± 0.21	0.98 ± 0.12
33 % THF	1.2	54.1	0	nd
50 % THF	1.4	40	0	nd
[a] Values were obtained from ref. (192).				

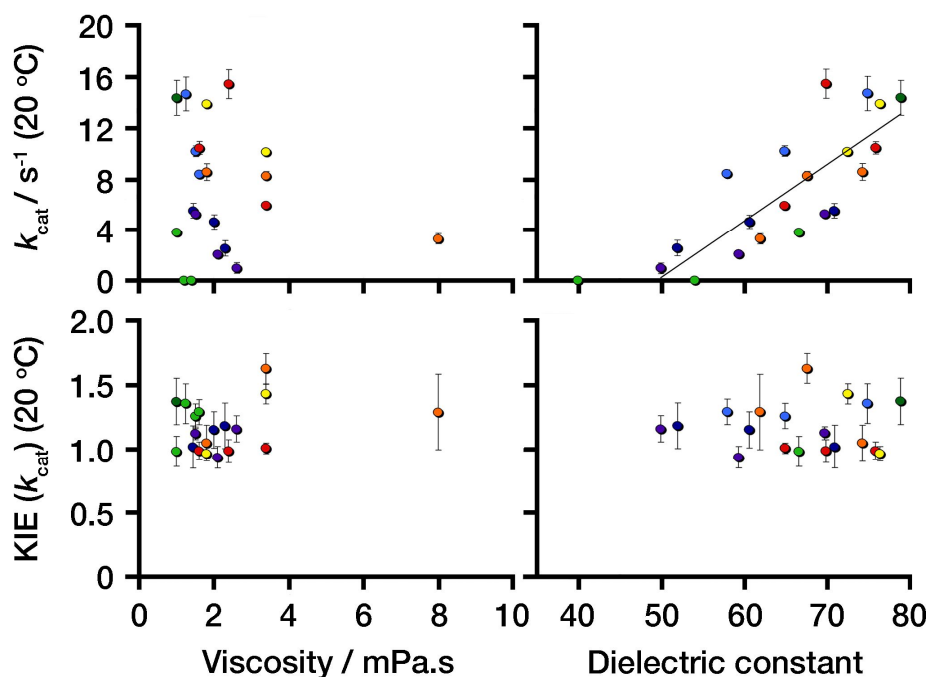


Figure 3.11 Plots of k_{cat} and KIE against solution viscosity (left) and dielectric constant (right). Symbols represent the different cosolvents, where dark green denotes no cosolvent, light blue = methanol, dark blue = ethanol, purple = isopropanol, red = ethylene glycol, orange = glycerol, yellow = sucrose, and light green = THF. In the case of dielectric constant data, lines of best fit are shown.

3.3 Summary and conclusions

The gene encoding DHFR from *G. stearothermophilus* was cloned into a suitable expression vector, pJGetit, and has been successfully purified to yield pure BsDHFR when compared to protocols previously reported.

Sequence alignment indicated that the moderate thermophilic BsDHFR showed the highest sequence identity to psychrophilic MpDHFR. Analysis of the amino acid composition of BsDHFR and MpDHFR revealed more features of thermal adaptation. More prolines are present in the loop regions, which increased the structural rigidity, and fewer thermolabile residues are used to avoid thermal denaturation. The quaternary structure of BsDHFR was determined to be monomer. No obvious oligomerisation has been observed at high concentration.

BsDHFR evolved to maintain a functional three-dimensional structure at relatively high temperature. The melting temperature of BsDHFR was determined to be 66.2 ± 0.4 °C, which lies between those of mesophilic EcDHFR and thermophilic TmDHFR. The temperature unfolding of BsDHFR was irreversible, and incubation of the protein at high temperature resulted in complete precipitation. The melting temperature of BsDHFR measured experimentally is about 9 °C lower than the maximum growth temperature of *G. stearothermophilus*. The analysis of the melting temperature in the presence of salts and ligands suggests that the extra thermostability of BsDHFR should result from the binding of substrate and cofactor and the presence of low concentrations of salts and organic cryoprotectants such as glycerol and sucrose.

Thermophilic BsDHFR maintained an optimal structure-function relationship which allowed it to function at rates comparable to psychrophilic MpDHFR and mesophilic EcDHFR and much higher than hyperthermophilic TmDHFR at room temperature. The steady-state rate constant of BsDHFR reached maximal around its physiological temperature. At their respective physiological temperatures, the steady-state rate constant of BsDHFR was highest among the four DHFRs. Like other DHFRs, the catalytic properties of BsDHFR depended strongly on the physical conditions of the reaction. The KIE at pH 7.0 for the steady state BsDHFR reaction showed that the overall rate of BsDHFR catalysis was not determined by hydride transfer at lower temperatures and it is plausible that product release may be the slow step in the catalytic cycle as seen for EcDHFR. As the temperature was increased, the hydride transfer step became gradually more rate limiting, as was seen for TmDHFR.(202)

The BsDHFR steady state rate is optimal at $\text{pH } 6.2 \pm 0.1$, falling greatly at lower or higher pH. This behaviour is similar to that of MpDHFR which may relate to the change of the rate limiting step at high pH and the acidic denaturation at low pH. The primary KIE is maximal at high pH (above pH 8) and is reduced to unity at low pH, showing a change of the rate-limiting step with the decrease of pH. All the monomeric DHFRs (EcDHFR and MpDHFR) show the same behaviour, whereas TmDHFR is

different. Here hydride transfer is always the rate-limiting step at all values of pH.

CD spectroscopy showed that BsDHFR is relatively stable in the presence of various solvents. Although BsDHFR has previously been shown to have larger amplitude motions than EcDHFR, the value of k_{cat} was not reduced in a manner directly proportional to the medium viscosity, but was decreased proportional to the medium viscosity and the KIE on k_{cat} did not alter proportionally to the solvent properties. The behaviour of BsDHFR in cosolvent was essentially the same as other DHFRs.

4 EXPLORING THE HYDRIDE TRANSFER STEP OF BsDHFR

4.1 Introduction

The complete catalytic cycle of an enzymatic reaction usually consists of more than one stage. The measurement of the steady-state kinetics does not normally indicate which microscopic step is being measured. Under pre-steady-state conditions, the rate of the chemical step can be measured. The chemical step (hydride transfer) is a fast step and not rate limiting at neutral pH for EcDHFR and MpDHFR, but partially rate limiting for TmDHFR.(193, 202) Many events must take place prior to hydride transfer.

The aim of this chapter was to investigate BsDHFR in terms of its hydride transfer step to analyse the contribution of protein motions to the reaction. Measurement of the temperature dependence of the KIE would provide information on quantum-mechanical tunnelling under physiological conditions.

4.2 Results and discussion

4.2.1 Temperature dependence of the hydride transfer of BsDHFR

Stopped-flow fluorescence could be used to measure the hydride-transfer rate constants (k_H) due to the overlap of the emission spectrum of BsDHFR at 340 nm with the excitation maximum of the reduced cofactor NADPH. The change in fluorescence was followed as a function of time and fit to a single exponential expression. The reaction catalysed by BsDHFR occurred with a rate constant of $131 \pm 2 \text{ s}^{-1}$ at pH 7 and 25 °C, which was about a quarter of that of MpDHFR, half of that of EcDHFR and three orders of magnitude greater than that of TmDHFR at the same temperature (Table 4.2). k_H for the BsDHFR-catalysed reaction increased exponentially with temperature up to 50 °C, and was maximal at 60 °C ($308 \pm 5 \text{ s}^{-1}$), which is slightly lower than the thermal melting temperature of the enzyme as measured by CD spectroscopy (*vide supra*), but agrees with the optimal growth

temperature for *G. stearothermophilus*. At higher temperatures, a sharp decrease in k_H was observed as a consequence of the denaturation of the protein. At their respective physiological temperatures, MpDHFR, EcDHFR and BsDHFR showed similar hydride transfer rate constants (258 s^{-1} for MpDHFR,(193) $\sim 300 \text{ s}^{-1}$ for EcDHFR(154) and BsDHFR), about 20 times higher than that of TmDHFR (15.5 s^{-1}).(202) The rate constant for hydride transfer in the BsDHFR catalysed reaction showed typical Arrhenius behaviour (Figure 4.1A), giving an activation energy of $28.1 \pm 0.8 \text{ kJ}\cdot\text{mol}^{-1}$ and Arrhenius prefactor of $(1.02 \pm 0.02) \times 10^7 \text{ s}^{-1}$ at pH 7. The activation energy for hydride transfer within the active site of BsDHFR was slightly higher than the value for MpDHFR ($21.6 \pm 2.2 \text{ kJ}\cdot\text{mol}^{-1}$)(193) and close to that of EcDHFR ($29.9 \pm 0.6 \text{ kJ}\cdot\text{mol}^{-1}$), (154) but was about half of that of the catalytically less efficient TmDHFR ($53.5 \pm 0.4 \text{ kJ}\cdot\text{mol}^{-1}$ above $25 \text{ }^\circ\text{C}$ and $49.9 \pm 1.7 \text{ kJ}\cdot\text{mol}^{-1}$ below it).(155)

Table 4.1 Effect of temperature on the pre-state-state rate constant (k_H) at pH 7 and pH 9 and the corresponding KIEs.

t / $^\circ\text{C}$	$k_H(\text{pH } 7) / \text{s}^{-1}$	KIE (pH 7)	2° KIE (pH 7) ^[a]	$k_H(\text{pH } 9) / \text{s}^{-1}$	KIE (pH 9)
10	68.3 ± 8.3	3.70 ± 0.46	1.16 ± 0.22	2.64 ± 0.11	4.09 ± 0.19
15	79.2 ± 3.7	3.54 ± 0.18	1.05 ± 0.09	3.08 ± 0.10	4.02 ± 0.13
20	102 ± 5	3.44 ± 0.17	1.08 ± 0.13	3.62 ± 0.07	4.04 ± 0.07
25	131 ± 2	3.33 ± 0.07	1.12 ± 0.06	4.39 ± 0.04	3.92 ± 0.14
30	160 ± 8	3.38 ± 0.20	1.13 ± 0.08	5.70 ± 0.10	3.99 ± 0.08
35	184 ± 6	3.27 ± 0.13	1.06 ± 0.06	6.72 ± 0.33	3.86 ± 0.19
40	218 ± 7	3.21 ± 0.20	1.04 ± 0.08	7.83 ± 0.17	3.71 ± 0.17
45	249 ± 12	3.10 ± 0.22	1.03 ± 0.07	9.54 ± 0.53	3.67 ± 0.21
50	297 ± 10	2.83 ± 0.15	1.03 ± 0.04	10.9 ± 0.52	3.61 ± 0.19
[a] Data was measured by William M. Dawson					

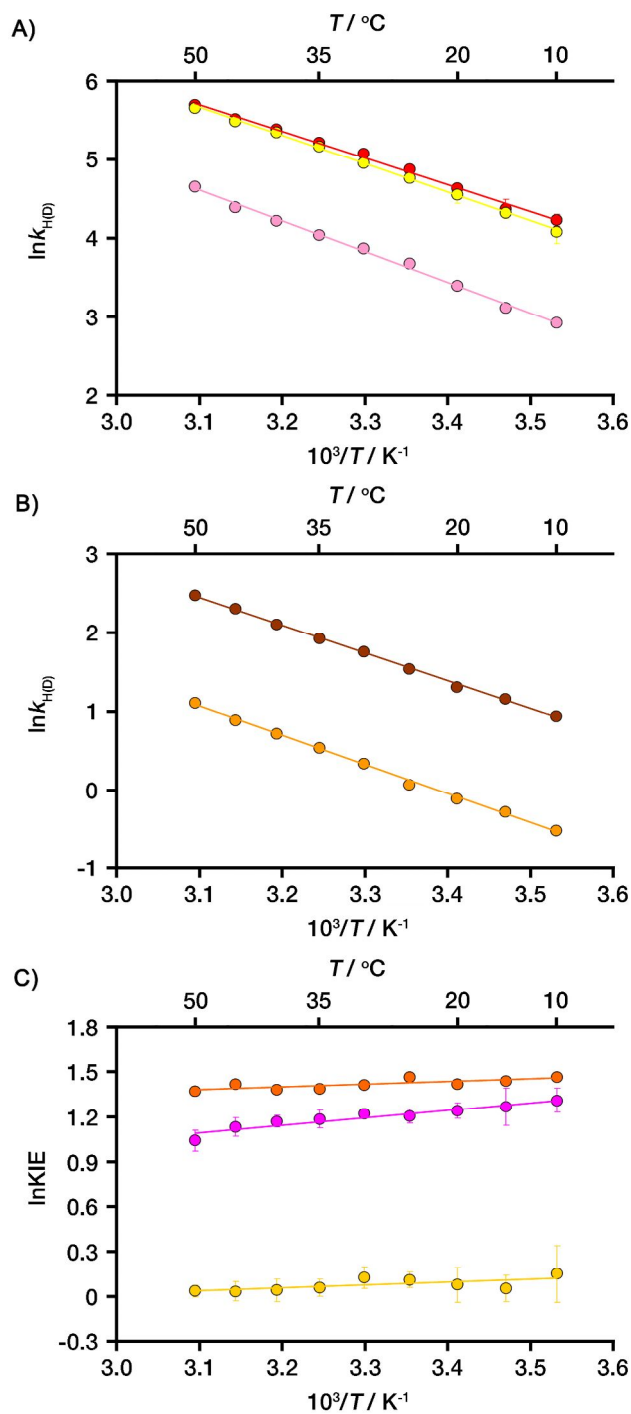


Figure 4.1 A) Arrhenius plots for the hydride transfer and deuteride transfer rate constants at pH 7 (red = hydride transfer, pink = deuteride transfer and yellow = the rate constant for hydride transfer with deuterium in the α -secondary position) and B) pH 9 (brown = hydride transfer and orange = deuteride transfer); and C) Arrhenius plots of the primary KIE at pH 7 (pink) and 9 (orange), and the α -secondary KIE at pH 7 (yellow).

Table 4.2 k_H , KIE at pH 7, 25 °C and corresponding activation parameters for hydride transfer catalysed by BsDHFR, MpDHFR, EcDHFR and TmDHFR.

Parameter	BsDHFR	MpDHFR(193)	EcDHFR(154)	TmDHFR(155)
k_H / s^{-1} (25 °C)	131 ± 2	527 ± 23	204 ± 7	0.169 ± 0.002
KIE	3.33 ± 0.07	1.83 ± 0.10	2.71 ± 0.22	4.02 ± 0.29
$E_a^H / kJ \cdot mol^{-1}$	28.1 ± 0.8	21.6 ± 2.2	29.9 ± 0.6	$53.5 \pm 0.4^{[a]}$
$\Delta E_a / kJ \cdot mol^{-1}$	3.3 ± 1.0	6.6 ± 3.4	7.9 ± 0.9	$2.5 \pm 1.0^{[a]}$
$A_H / 10^7 s^{-1}$	1.02 ± 0.02	0.32 ± 0.02	3.3 ± 0.8	$41.1 \pm 6.8^{[a]}$
A_H/A_D	0.87 ± 0.02	0.13 ± 0.09	0.11 ± 0.04	$1.54 \pm 0.36^{[a]}$
[a] Above 25 °C.				

The primary KIE on hydride transfer in the BsDHFR-catalysed reaction was determined by using deuterium-labelled cofactor 4-(*R*)-NADPD. At 25 °C, the KIE of the BsDHFR-catalysed reaction was 3.33 ± 0.07 . The KIE increases with higher thermostability. This trend can also be observed in alcohol dehydrogenase (ADH). The KIE of thermophilic ADH is higher than that of mesophilic ADH.(158, 241, 242) The activation energy when deuterium was transferred was $31.4 \pm 0.6 kJ \cdot mol^{-1}$ (Arrhenius prefactor was $(1.17 \pm 0.02) \times 10^7 s^{-1}$), which is $3.3 \pm 1.0 kJ \cdot mol^{-1}$ higher than for hydride transfer, while A_H/A_D was within the semiclassical range ($A_H/A_D = 0.87 \pm 0.02$).(243) The weakly temperature-dependent KIE of BsDHFR (Figure 4.1 C) is similar to that of TmDHFR above the breakpoint of 25 °C,(155) but different from the temperature-dependent KIE that was observed in MpDHFR(193) and EcDHFR.(154) The temperature (in)dependence of the KIE of TmDHFR is influenced by intersubunit interactions.(191) However, BsDHFR is monomeric in solution. It has been observed that mutations in the dimer interface of TmDHFR can lead to entirely temperature-independent KIE, suggesting that the temperature dependence of the KIE might be affected by relatively minor structural alterations remote from the active site.(191) The weakly temperature-dependent KIE of BsDHFR may be caused by subtle structural differences relative to EcDHFR and MpDHFR.

An obvious change in the temperature dependence of KIE at non-physiological pH was observed in MpDHFR(193) and EcDHFR,(244) which has been interpreted as a result of a conformational change in the enzyme brought about by deprotonation of key residues.(198) The change of temperature dependence of KIE with pH in BsDHFR, however, is minor. A temperature-independent KIE of 3.88 ± 0.18 was observed on the BsDHFR-catalysed reaction at pH 9 (Figure 4.1C). Values of $28.0 \pm 0.7 \text{ kJ}\cdot\text{mol}^{-1}$ and $(3.68 \pm 0.07) \times 10^5 \text{ s}^{-1}$ were obtained for the activation energy and the pre-exponential factor for hydride transfer, and values $30.4 \pm 0.7 \text{ kJ}\cdot\text{mol}^{-1}$ and $(2.50 \pm 0.06) \times 10^5$ for deuterium transfer, leading to an activation energy difference of $2.4 \pm 1.0 \text{ kJ}\cdot\text{mol}^{-1}$ and a semiclassical $A_{\text{H}}/A_{\text{D}}$ of 1.47 ± 0.04 .(243) The activation energy of BsDHFR-catalysed hydride transfer did not change significantly at elevated pH, and hence the decrease in the Arrhenius prefactors with increased pH was mostly responsible for the change in the hydride-transfer rate constant as was seen for EcDHFR.(198) The temperature dependence of KIE at pH 9 in our result is essentially the same as that seen by Kim *et al.*, who measured an activation energy difference of $4.6 \pm 0.6 \text{ kJ}\cdot\text{mol}^{-1}$.(120) Their published $A_{\text{H}}/A_{\text{D}}$ (0.57 ± 0.15) value lies just outside the lower limit for semiclassical behaviour.(120) The value for EcDHFR was calculated to be 2.71 ± 0.06 which exceeds semiclassical limits.(198) They proposed that the kinetic differences between BsDHFR and EcDHFR can be ascribed to subtle differences in protein dynamics.(219)

The secondary KIE was measured by changing the cofactor NADPH to the deuterium-labelled alternative 4-(*S*)-NADPD. The labelled deuterium was not directly involved in the reduction reaction. Our result showed that the secondary KIE was temperature-independent at pH 7, and was found to be 1.08 ± 0.05 which is similar to those of other DHFRs. The values are 1.04 ± 0.01 for MpDHFR,(193) 1.07 ± 0.02 for EcDHFR(193) and 1.08 ± 0.05 for TmDHFR,(245) respectively.

4.2.2 pH dependence of the hydride transfer of BsDHFR

The hydride transfer rate constant for the BsDHFR catalysed reaction was measured between pH 4.0 and 10.0 at 20 °C. The hydride-transfer rate constant decreased sigmoidally with increasing pH (Figure 4.2). This is different to the bell shaped pH profile seen for the steady-state rate constant, but similar to the sigmoidal pH dependence of k_H seen for MpDHFR,(193) EcDHFR(138) and TmDHFR.(202) The maximal rate at low pH was $280 \pm 15 \text{ s}^{-1}$. The apparent pK_a of the BsDHFR-catalysed hydride transfer rate constant is 6.4 ± 0.1 , compared to 6.5 for MpDHFR(193) and EcDHFR(138) and 6.0 for TmDHFR,(202) and was well described by a single pH-dependent step.

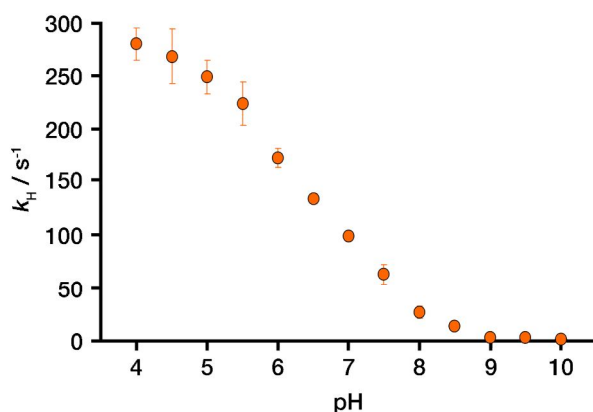


Figure 4.2 pH dependence of the hydride-transfer rate constant at 20 °C for the BsDHFR-catalysed reaction.

Table 4.3 Effect of pH on the pre-steady-state and steady-state rate constants of the BsDHFR-catalysed reaction in MTEN buffer at 20 °C.

pH	k_H / s^{-1}	k_{cat} / s^{-1}
4	280 ± 15	7.35 ± 0.24
4.5	269 ± 26	8.99 ± 1.03
5	249 ± 16	12.1 ± 1.5
5.5	224 ± 20	14.6 ± 0.3
6	173 ± 9	16.9 ± 0.4
6.5	134 ± 5	17.0 ± 0.4
7	99.1 ± 3.2	15.8 ± 1.0
7.5	63.0 ± 9.5	12.2 ± 1.0
8	26.6 ± 5.7	8.36 ± 0.13
8.5	7.60 ± 1.43	3.99 ± 0.32
9	3.10 ± 0.35	1.90 ± 0.03
9.5	0.70 ± 0.14	0.46 ± 0.04
10	0.13 ± 0.03	0.12 ± 0.01

4.2.3 Influence of salt on the hydride transfer of BsDHFR

The effect of various salts (NaCl, KCl, and KF) and their concentrations (0-2 M) on the pre-steady-state rate constant of BsDHFR at 20 and 40 °C was investigated (Figure 4.3). The hydride-transfer rate constant of BsDHFR was increased significantly with NaCl across the concentration range studied. At 2 M NaCl, there were 267% and 99% increases in the hydride transfer rate constant at 20 and 40 °C, respectively, compared to ~0 M NaCl. Similarly, KCl promoted the hydride transfer at all the concentrations tested. There was up to 119% and 50% increase at 20 and 40 °C respectively compared to initial activities. The effect of KF on the hydride transfer was different to that of NaCl and KCl, which slightly increased the pre-steady-state rate of BsDHFR up to ~1.0 M, but at concentrations above 1.5 M the rate constant decreased to 98 % (20 °C) and 88 % (40 °C) of the highest rate at lower ionic strength.

The KIEs at different concentrations of salt was also measured. At both 20 and 40 °C, the KIE remained constant in as much as 1 M salt, but decreased slightly at salt concentrations above 1.5 M. However, hydride transfer is always a fast step in the reaction.

Table 4.4 The effect of salts on the pre-steady-state rate constants of BsDHFR-catalysed reaction in 100 mM potassium phosphate buffer at 20 °C.

[Salt] / M	k_H (NaCl) / s ⁻¹	KIE (NaCl)	k_H (KCl) / s ⁻¹	KIE (KCl)	k_H (KF) / s ⁻¹	KIE (KF)
0	88.7 ± 1.4	3.49 ± 0.06	/	/	/	/
0.1	94.6 ± 1.6	3.39 ± 0.24	99.0 ± 3.5	3.41 ± 0.19	99.3 ± 3.5	3.55 ± 0.15
0.2	104 ± 2	3.25 ± 0.36	106 ± 5	3.26 ± 0.15	99.9 ± 4.4	3.44 ± 0.22
0.5	127 ± 4	3.17 ± 0.44	120 ± 4	3.30 ± 0.14	100 ± 3	3.31 ± 0.32
1.0	169 ± 8	3.10 ± 0.17	147 ± 5	3.13 ± 0.25	104 ± 1	3.28 ± 0.19
1.5	238 ± 16	3.13 ± 0.41	166 ± 1	3.15 ± 0.17	104 ± 1	2.87 ± 0.19
2.0	325 ± 17	2.98 ± 0.24	194 ± 13	2.96 ± 0.25	102 ± 3	2.76 ± 0.11

Table 4.5 The effect of salts on the pre-steady-state rate constants of BsDHFR-catalysed reaction in 100 mM potassium phosphate buffer at 40 °C.

[Salt] / M	k_H (NaCl) / s ⁻¹	KIE (NaCl)	k_H (KCl) / s ⁻¹	KIE (KCl)	k_H (KF) / s ⁻¹	KIE (KF)
0	198 ± 4	2.95 ± 0.07	/	/	/	/
0.1	217 ± 3	3.09 ± 0.08	208 ± 8	2.92 ± 0.15	211 ± 3	2.92 ± 0.18
0.2	231 ± 6	2.94 ± 0.09	214 ± 8	2.79 ± 0.33	218 ± 12	3.01 ± 0.32
0.5	268 ± 4	2.95 ± 0.17	238 ± 13	2.69 ± 0.37	219 ± 10	3.01 ± 0.26
1.0	316 ± 7	2.87 ± 0.08	271 ± 16	2.58 ± 0.17	221 ± 7	3.01 ± 0.26
1.5	375 ± 11	2.83 ± 0.35	278 ± 14	2.31 ± 0.15	221 ± 7	2.81 ± 0.27
2.0	393 ± 20	2.59 ± 0.16	297 ± 15	2.27 ± 0.15	194 ± 9	2.66 ± 0.22

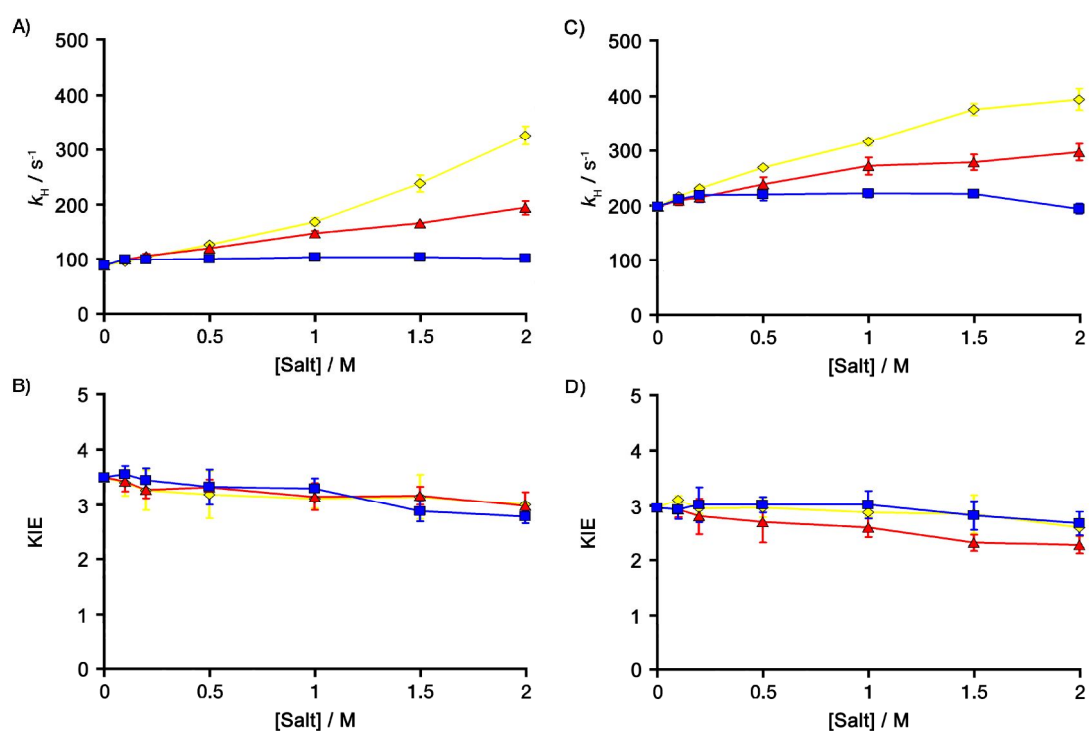


Figure 4.3 The effect of salts on the pre-steady-state rate constant of BsDHFR at 20 °C (A) and 40 °C (C) and their KIEs (B, D). The buffer was 100 mM K_iPO₄, pH 7 in the presence of NaCl (yellow), KCl (red) and KF (blue).

4.2.4 Influence of solvents on the hydride transfer of BsDHFR

The k_H at 20 and 40 °C for the BsDHFR-catalysed reaction was measured in the presence of organic cosolvent and compared with the results of MpDHFR, EcDHFR and TmDHFR. Increasing concentrations of cosolvents led to a general reduction of hydride transfer rates (Figure 4.4). This was also seen for MpDHFR,⁽¹⁹³⁾ EcDHFR⁽¹⁹¹⁾ and TmDHFR.⁽¹⁹²⁾ However, in the case of TmDHFR, glycerol and to a lesser extent sucrose led to an increased rate constant for hydride transfer which is a direct consequence of a pKa shift which is not seen in the other three DHFRs.⁽¹⁹¹⁾

Similar to that observed with the k_{cat} measurement, the value of k_H was not reduced in a manner directly proportional to the medium viscosity, but was decreased in a manner proportional to the dielectric constant. This is similar to the effect that has previously been observed for MpDHFR,⁽¹⁹³⁾ EcDHFR⁽¹⁹¹⁾ and TmDHFR.⁽¹⁹²⁾ The k_H values dropped to zero when the dielectric constants of the solvent were less than 45. The KIE on k_H did not alter proportionally to the solvent properties, which is the same as that of MpDHFR,⁽¹⁹³⁾ EcDHFR⁽¹⁹¹⁾ and TmDHFR.⁽¹⁹²⁾

Table 4.6 Kinetic parameters for the reaction of NADPH and H₂F catalysed by BsDFHR in the presence of cosolvents at 20 °C.

Solvent composition	Viscosity / mPa.s ^[a]	Dielectric constant ^[a]	k_H (20 °C) / s ⁻¹	KIE (20 °C)
No cosolvent	1	79	109 ± 3	3.44 ± 0.23
17 % methanol	1.25	75	91.3 ± 4.0	3.26 ± 0.18
33 % methanol	1.5	65	79.3 ± 2.7	3.44 ± 0.18
50 % methanol	1.6	58	57.7 ± 3.1	3.54 ± 0.27
17 % ethanol	1.45	71	97.9 ± 3.6	3.47 ± 0.20
33 % ethanol	2	60.7	75.8 ± 3.1	3.36 ± 0.30
50 % ethanol	2.3	52	10.5 ± 0.4	1.27 ± 0.14
17 % isopropanol	1.5	59.8	91.2 ± 1.6	1.71 ± 0.08
33 % isopropanol	2.1	59.4	33.3 ± 5.1	2.34 ± 0.36
50 % isopropanol	2.6	50	12.5 ± 3.9	1.40 ± 0.44
17 % ethylene glycol	1.6	76	114 ± 3	3.48 ± 0.38
33 % ethylene glycol	2.4	70	114 ± 2	3.02 ± 0.18
50 % ethylene glycol	3.4	65	73.2 ± 7.7	1.96 ± 0.28
17 % glycerol	1.8	74.4	117 ± 7	3.50 ± 0.26
33 % glycerol	3.4	67.7	139 ± 7	3.18 ± 0.20
50 % glycerol	8	62	60.8 ± 6.4	1.25 ± 0.15
17 % sucrose	1.8	76.5	99.0 ± 6.4	3.46 ± 0.25
33 % sucrose	3.4	72.6	128 ± 1	2.30 ± 0.09
17 % THF	1	66.7	46.2 ± 3.8	2.35 ± 0.22
33 % THF	1.2	54.1	11.0 ± 2.1	1.34 ± 0.37
50 % THF	1.4	40	0	nd
[a] Values were obtained from reference (192).				

Table 4.7 Kinetic parameters for the reaction of NADPH and H₂F catalysed by BsDFHR in the presence of cosolvents at 40 °C.

Solvent composition	Viscosity / mPa.s ^[a]	Dielectric constant ^[a]	k_H (40 °C) / s ⁻¹	KIE (40 °C)
No cosolvent	0.66	73.1	197 ± 8	3.50 ± 0.16
17 % methanol	0.8	69.3	199 ± 3	4.10 ± 0.07
33 % methanol	1	60	137 ± 8	3.33 ± 0.19
50 % methanol	1.1	53.6	57.6 ± 6.0	3.15 ± 0.34
17 % ethanol	1	65	184 ± 9	3.60 ± 0.19
33 % ethanol	1.5	56	60.5 ± 6.2	2.28 ± 0.27
50 % ethanol	1.8	48	0	nd
17 % isopropanol	1	64	165 ± 2	3.54 ± 0.11
33 % isopropanol	1.6	55	35.4 ± 2.1	1.56 ± 0.09
50 % isopropanol	1.9	47	0	nd
17 % ethylene glycol	1	66	212 ± 14	2.96 ± 0.20
33 % ethylene glycol	1.6	60	218 ± 10	2.75 ± 0.14
50 % ethylene glycol	2.4	54	121 ± 11	1.99 ± 0.18
17 % glycerol	1.1	67.5	208 ± 10	2.85 ± 0.16
33 % glycerol	2	62.7	230 ± 11	2.73 ± 0.15
50 % glycerol	4	57.3	123 ± 12	1.31 ± 0.13
17 % sucrose	1.1	68.5	204 ± 10	3.58 ± 0.19
33 % sucrose	1.9	65.6	217 ± 2	3.25 ± 0.03
17 % THF	0.7	60	101 ± 8	3.38 ± 0.27
33 % THF	0.85	47	0	nd
50 % THF	1	37	0	nd
[a] Values were obtained from reference (192).				

Although enzymes with different thermophilicity showed different flexibility and structural stability in cosolvents, their behaviour in organic cosolvents is essentially the same. The absence of a viscosity effect for TmDHFR, EcDHFR and MpDHFR suggests that the long-range network of motions that are affected by the viscosity do not directly drive hydride transfer.⁽¹⁹¹⁾ The absence of a viscosity effect in BsDHFR may have the same cause, although BsDHFR has been shown to have larger amplitude sub-nanosecond motions than EcDHFR.⁽²²⁰⁾ The reduction of k_{cat} and k_{H} as the dielectric constant decreases can be interpreted as the dielectric constant affecting the shielding of stabilising electrostatic effects within the active site.^(191, 192) BsDHFR and TmDHFR maintained the hydride transfer rates better as the dielectric constant decreases, whereas the steady-state rates reduced faster than those of EcDHFR and MpDHFR under the same conditions. This suggests different electrostatic environments among those enzymes. Although the KIE on k_{H} at pH 7 was largely independent of either viscosity or dielectric constant of the cosolvents for all the DHFRs, the ranges of KIE shift were quite different. With the increase of viscosity or dielectric constant, the KIE of EcDHFR and MpDHFR fluctuated within a relatively small range (2.4 to 3.2 for EcDHFR⁽¹⁹¹⁾ and 1.7 to 2.4 for MpDHFR in most of cosolvents⁽¹⁹³⁾), but the KIE of BsDHFR and TmDHFR varied significantly (1.2 to 3.5 for BsDHFR and 2.4 to 5.4 for TmDHFR⁽¹⁹²⁾), which means the influence of solvent composition on the nature of the chemical step of BsDHFR and TmDHFR is much greater than that of EcDHFR and MpDHFR. Interestingly, BsDHFR and TmDHFR appear to have a more stable secondary structure in cosolvents. The conservation of secondary structure, therefore, has no contribution to the nature of the chemical step.

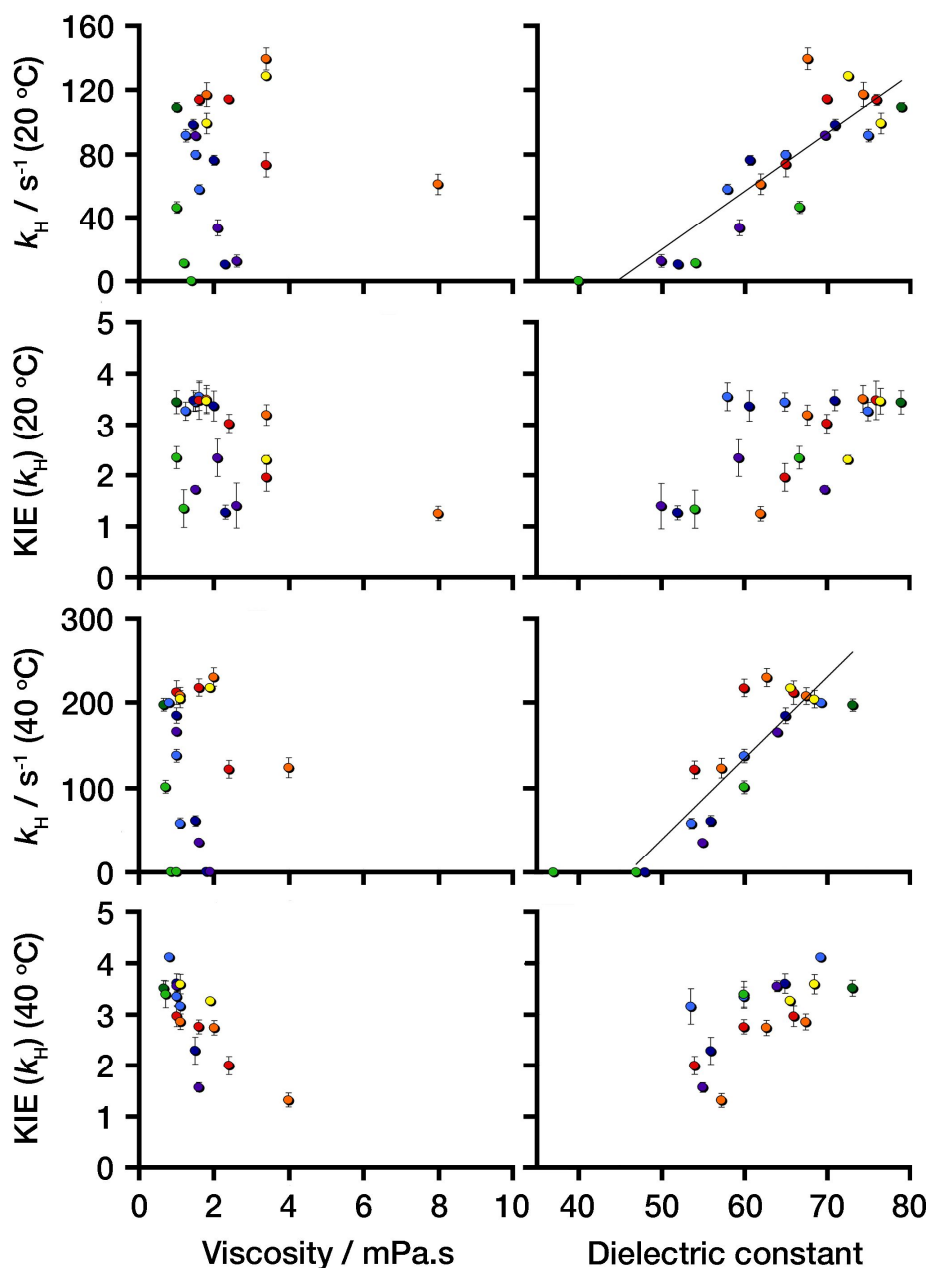


Figure 4.4 Plots of k_H , and KIEs against solution viscosity (left) and dielectric constant (right). Symbols represent the different cosolvent, where dark green denotes no cosolvent, light blue = methanol, dark blue = ethanol, purple = isopropanol, red = ethylene glycol, orange = glycerol, yellow = sucrose, and light green = THF. In the case of dielectric constant data, lines of best fit are shown.

4.3 Conclusions

The hydride transfer rate of thermophilic BsDHFR was measured at different

temperature and pH and compared with those of MpDHFR, EcDHFR and TmDHFR. At room temperature and physiological temperature, the hydride transfer rates of monomeric DHFRs are similar to one another and considerably higher than that of dimeric TmDHFR. At physiological pH (7), the KIE on the chemical step is weakly temperature dependent in BsDHFR, contradicting what has been observed in other monomeric DHFRs (EcDHFR and MpDHFR); this might relate to subtle conformational differences in the active site. At elevated pH (pH 9), the KIE became completely temperature independent. The change in temperature dependence with pH has also observed in MpDHFR and EcDHFR, and has been explained as the change of the conformational ensemble of the enzyme prior to the reaction induced by the change of pH. The hydride transfer rate constant decreases with increasing pH; its sigmoidal-shaped pH profile is similar to other DHFRs. Different from the salt effect on the steady-state rate, the presence of KF did not significantly influence the pre-steady-state rate constant. Furthermore, the presence of NaCl and KCl even increases the hydride transfer rate constant at all measured temperatures. Similar to the effect of cosolvent on the steady-state rate constant, the behaviour of the pre-steady-state rate constant also was not reduced in a manner directly proportional to the medium viscosity, but was decreased in a manner proportional to the dielectric constant.

Combining the data measured with BsDHFR and other homologs MpDHFR, EcDHFR and TmDHFR, one can conclude that thermophilicity does not have a direct correlation with the enzyme catalysis. While monomeric DHFRs have similar kinetic behavior, the catalytic nature of the dimeric TmDHFR is apparently different. Like other monomeric DHFRs, BsDHFR can adopt a closed conformation for the active site, which makes a better electrostatic environment for the reaction to occur. The ability to close the active site gives a comparable activity to its mesophilic and psychrophilic counterparts. The dimer interface of TmDHFR constrains the movement of the loops that are crucial for the catalysis in EcDHFR, and therefore prevents proper closure of the active site, as seen in the crystal structure of TmDHFR.

The more solvent-exposed active site of TmDHFR is most likely the reason for its poor catalytic activity.

5 ANALYSIS OF BsDHFR VARIANT PROTEINS

5.1 Introduction

The above results showed that the K_M for NADPH of BsDHFR is much higher than that of MpDHFR, EcDHFR and TmDHFR (Section 3.2.8). The high K_M value relates to the poor NADPH binding ability of BsDHFR. The residues that are involved in the binding of NADPH are shown in Figure 5.1 and compared with those of EcDHFR, MpDHFR and TmDHFR. This figure shows that the NADPH binding residues are highly conserved. When comparing the NADPH binding sites of BsDHFR and EcDHFR, most of the residues are either the same or exhibit similar chemical properties. There are two thermally labile residues, Met20 and Gln102, (especially Gln102 which is exposed to the surface and can be hydrolysed at high temperature) in EcDHFR. The corresponding residues in BsDHFR, Leu20 and Ala104, are more thermostable but might contribute to the poor cofactor binding. Therefore, the corresponding BsDHFR mutants, L20M and A104Q, were prepared to investigate the influence of NADPH binding residues on the thermostability of BsDHFR.

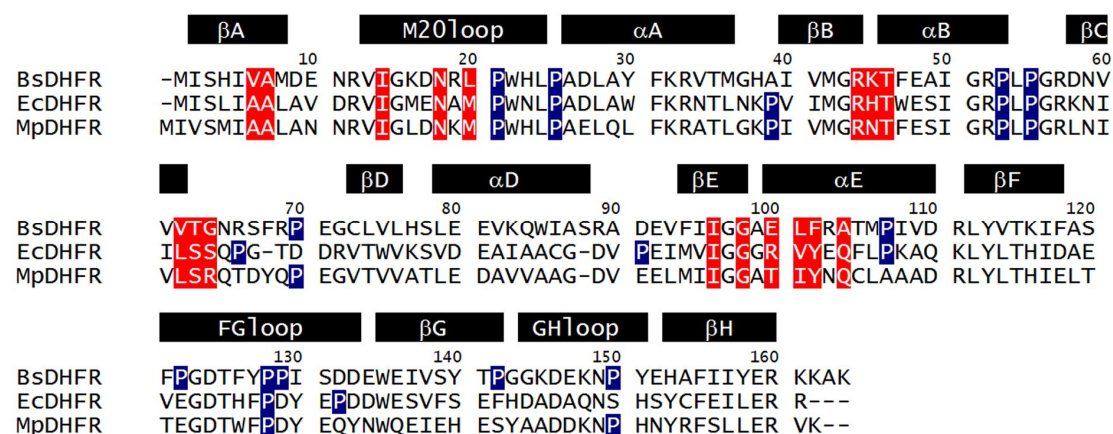


Figure 5.1 Sequence alignment (created using ClustalW) of BsDHFR, EcDHFR and MpDHFR. Residues that contact NADPH in *E. coli* (1RX2) are indicated by red boxes. Proline residues are indicated by dark blue boxes. Tertiary structure is also indicated.

There are 11 proline residues in BsDHFR, compared to 10 in EcDHFR and 8 in MpDHFR (Figure 5.1). While 5 of them are conserved, BsDHFR possesses extra

proline residues in loop regions, which may contribute to the increased thermal stabilisation.⁽¹²⁰⁾ Specifically, Pro122 and Pro129 in the FG loop of BsDHFR correspond to Glu and Asp, respectively, in both MpDHFR and EcDHFR. Therefore, the site-directed mutants P122E and P129D were made to investigate the influence of proline residues on the thermostability and catalysis of BsDHFR.

The aim of this chapter is to assess the contribution of specific residues on the thermostability of BsDHFR by analysing the biophysical properties of various BsDHFR mutants. Each variant was made by site-directed mutagenesis, and the resulting enzymes were expressed and purified. The steady state and pre-steady state rates of each variant were measured, along with the K_M for NADPH. The time dependence of the loss of catalytic activity of BsDHFR at pH 7.0 and 60 °C was also measured.

5.2 Results and discussion

5.2.1 Circular dichroism analysis of BsDHFR variants

Structural properties for each of the BsDHFR variants were investigated by CD spectroscopy. The CD spectra of all site-directed mutants show characteristics of folded BsDHFR structure with secondary structure elements. These spectra were similar, with mild variations in MRE measured at 208 and 222 nm (Figure 5.2). This suggests that the secondary structures of the variants are similar to that of wild type enzyme. Nevertheless, the packing might be different.

Melting points of the BsDHFR variants are approximately 1 to 5 °C lower than that of the wild type enzyme (Table 5.1). Mutants with thermally labile residues incorporated (L20M, A104Q, L20M/A104Q) are more sensitive to thermal destabilisation, showing a 3 to 5 °C drop in melting temperatures. On the other hand, melting temperatures of the proline mutants, P122E, P129D, P122E/P129D, merely drop 1 to 2 °C. Therefore,

the residues Leu20, Ala104, Pro122 and Pro129 contribute to the thermostability of BsDHFR to different extents.

Table 5.1 The melting temperature of BsDHFR and its variants in 10 mM potassium phosphate buffer at pH 7.

Enzyme	$T_m / ^\circ\text{C}$	$\Delta T_m / ^\circ\text{C}$
BsDHFR	66.2 ± 0.4	/
L20M	61.4 ± 0.1	-4.8 ± 0.4
A104Q	62.6 ± 0.1	-3.6 ± 0.4
L20M/A104Q	61.1 ± 0.1	-5.1 ± 0.4
P122E	65.3 ± 0.1	-0.9 ± 0.4
P129D	64.6 ± 0.1	-1.6 ± 0.4
P122E/P129D	65.0 ± 0.1	-1.2 ± 0.4

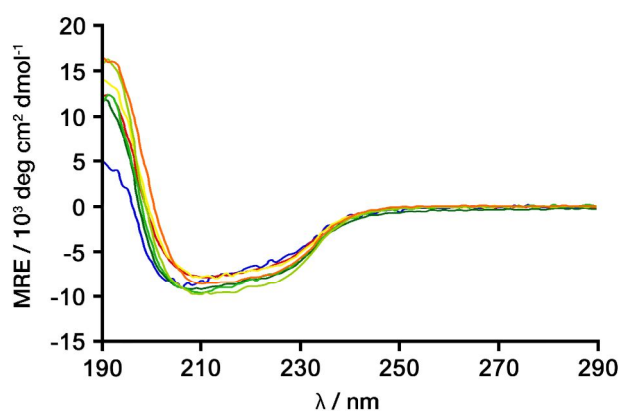


Figure 5.2 CD spectra of BsDHFR and its variants (red = L20M, yellow = A104Q, orange = L20M/A104Q, dark green = P122E, green = P129D and yellow green = P122E/P129D) at 20 °C in 10 mM potassium phosphate buffer at pH 7.

5.2.3 Steady-state kinetics of BsDHFR variants

To understand how the 'thermostabilising' residues Leu20, Ala104, Pro122 and Pro129 affect BsDHFR catalysis, various kinetic experiments, including steady-state

turnover, hydride transfer rate and Michaelis constant measurements, were performed with the corresponding site-direct mutants. The steady-state rate constants (k_{cat}) for the reduction of H_2F by NADPH were measured spectrophotometrically in the presence of excess substrate and cofactor (Chapter 3.2.8). The k_{cat} for all variants at pH 7 increased exponentially up to 55 °C but dropped significantly at higher temperatures (Figure 5.2). This suggests that all of the mutants are less stable than the wild type enzyme, which can function at 65 °C. The k_{cat} values of A104Q, P122E, P129D, and P122E/P129D variants are similar to that of wild type BsDHFR. However, the Leu 20 mutants, L20M and L20M/A104Q, show a noticeable decrease in steady-state turnover, which were nearly halved at all temperature range measured. A likely explanation is that Leu20 is located in the center of the ligand binding sites and slight changes in residue size (*e.g.* replacement of a slightly longer residue Met) might lead to significant changes in the rate of steady-state turnover. All the mutations change the activation energy of BsDHFR moderately (Table 5.3), suggesting the catalytic cycles are not significantly affected by the mutations.

The mutants were characterised by measuring the Michaelis constants (K_{M}) for both NADPH and H_2F . The measured K_{M} values of the mutants are not markedly different from that of the wild type, except in the mutant A104Q and L20M/A104Q, which show greatly improved NADPH binding and provide K_{M} values 5-fold lower than that of the wild type. It has been hypothesised that the relatively high K_{M} value for NADPH is likely due to the nature of poor cofactor binding. Thus, this result suggests that introducing glutamine at position 104 adds favorable binding interactions between the enzyme and NADPH.

Table 5.2 Temperature dependence of the steady-state reaction catalysed by BsDHFR and its variants at pH 7.

t / °C	BsDHFR / s ⁻¹	L20M / s ⁻¹	A104Q / s ⁻¹	L20M/A104Q / s ⁻¹	P122E / s ⁻¹	P129D / s ⁻¹	P122E/P129D / s ⁻¹
10	7.02 ± 1.95	3.05 ± 0.62	4.10 ± 0.14	3.76 ± 1.01	4.32 ± 0.48	5.91 ± 0.56	1.32 ± 0.23
15	9.29 ± 2.23	5.61 ± 1.16	9.77 ± 1.13	6.03 ± 0.48	8.43 ± 0.42	7.18 ± 0.42	5.80 ± 0.76
20	16.2 ± 2.8	9.03 ± 1.31	15.2 ± 1.5	8.69 ± 0.74	13.0 ± 0.2	14.5 ± 1.2	10.6 ± 0.4
25	21.6 ± 1.6	11.6 ± 1.3	26.6 ± 0.9	13.0 ± 1.5	24.8 ± 1.0	25.2 ± 1.4	17.8 ± 0.4
30	32.7 ± 1.4	17.3 ± 2.4	35.3 ± 2.0	18.1 ± 1.1	37.4 ± 1.5	35.5 ± 1.2	26.0 ± 0.4
35	48.6 ± 6.8	23.4 ± 3.9	54.4 ± 5.4	23.9 ± 1.5	53.9 ± 1.4	55.8 ± 3.3	36.2 ± 1.8
40	66.7 ± 3.9	30.6 ± 2.8	83.6 ± 3.7	29.0 ± 0.7	80.0 ± 2.7	102 ± 2	52.3 ± 3.1
45	87.3 ± 2.3	42.2 ± 2.5	105 ± 5	37.3 ± 1.0	99.6 ± 6.6	118 ± 4	71.6 ± 2.3
50	116 ± 5	59.1 ± 7.1	132 ± 11	45.4 ± 2.6	116 ± 4	118 ± 4	90.7 ± 4.4
55	145 ± 8	77.3 ± 5.1	156 ± 7	57.2 ± 0.8	144 ± 4	143 ± 4	117 ± 8
60	183 ± 8	115 ± 4	nd	nd	nd	nd	nd
65	236 ± 18	nd	nd	nd	nd	nd	nd
nd: not determined.							

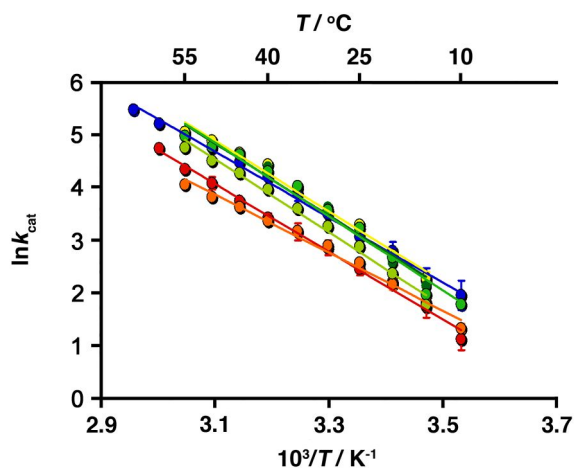


Figure 5.3 The Arrhenius plots of steady-state rate constant for the reaction catalysed by BsDHFR and its variants (red = L20M, yellow = A104Q, orange = L20M/A104Q, dark green = P122E, green = P129D and yellow green = P122E/P129D) at pH 7.

Table 5.3 Activation parameters of BsDHFR and its variants, and their K_M values at 20 °C, pH 7.

Enzyme	$E_a^H / \text{kJ mol}^{-1}$	$A_H / 10^{10} \text{ s}^{-1}$	$K_M(\text{NH}) / \mu\text{M}$	$K_M(\text{H}_2\text{F}) / \mu\text{M}$
BsDHFR	51.6 ± 1.6	2.51 ± 0.06	108 ± 28	2.4 ± 0.4
L20M	52.9 ± 1.3	2.70 ± 0.06	114 ± 29	2.6 ± 0.5
A104Q	55.1 ± 2.5	14.4 ± 0.5	21.6 ± 2.4	2.1 ± 0.3
L20M/ A104Q	45.2 ± 1.7	0.12 ± 0.01	15.3 ± 1.6	3.2 ± 0.7
P122E	56.0 ± 3.5	18.7 ± 0.10	105 ± 20	1.6 ± 0.4
P129D	57.5 ± 3.0	33.3 ± 1.5	107 ± 22	2.5 ± 0.3
P122E/ P129D	57.1 ± 2.4	20.8 ± 0.8	126 ± 21	3.1 ± 0.9

5.2.4 Pre-steady-state kinetics of BsDHFR variants

The chemical step in each of the BsDHFR variants was inspected using a stopped-flow experimental setup, which was used to measure the rate of hydride

transfer by FRET (Chapter 4.2.1) with results for signals measured fitted to a single exponential decay. In general, the rate of hydride transfer k_H in these BsDHFR variants increased exponentially to about 35 °C, and began to drop at higher temperatures (Figure 5.4A). The wild type enzyme, in contrast, remained highly active up to 50 °C, thus suggesting that the mutants are relatively less thermostable. Similar to the k_{cat} observations, the rates of hydride transfer in A104Q, P122E, P129D and P122E/P129D variants were close to that of wild type BsDHFR, but are much lower in the Leu20 mutants, L20M and L20M/A104Q, likely due to distortion(s) in the active site. The measured hydride transfer rates in A104Q, P122E, P129D and P122E/P129D variants are at least one order of magnitude greater than the steady-state turnover rates at low temperature (<25 °C), implying that a physical step of catalysis is rate limiting. As temperature increases, the chemical step becomes partially rate-limiting, providing hydride transfer rates that are only 3-4 times higher than the turnover reaction rates. In contrast, the chemical steps in both L20M and L20M/A104Q variants are partially rate-limiting step across the temperature range; the hydride transfer rates are 2-3 times higher than the turnover reaction rates. Additionally, the mutation of Leu20 to methionine leads to a remarkable increase in activation energy. The KIEs for k_H of all the BsDHFR variants-catalysed reaction were also measured. While the KIEs for all the BsDHFR variants decreased slightly, these mutations did not affect the temperature dependence of the KIE (Figure 5.4B).

Table 5.4 Temperature dependence of the rate constant for hydride transfer (k_H) during catalysis by BsDHFR and its variants at pH 7.

t / °C	BsDHFR / s ⁻¹	L20M / s ⁻¹	A104Q / s ⁻¹	L20M/A104Q / s ⁻¹	P122E / s ⁻¹	P129D / s ⁻¹	P122E/P129D / s ⁻¹
5	nd	6.90 ± 0.17	63.5 ± 2.9	8.02 ± 0.28	47.5 ± 1.2	46.6 ± 0.5	50.8 ± 1.0
10	68.3 ± 8.3	8.73 ± 0.32	80.6 ± 3.9	10.2 ± 0.2	58.2 ± 0.6	58.2 ± 1.7	65.0 ± 0.8
15	79.2 ± 3.4	12.4 ± 0.29	99.5 ± 6.4	14.1 ± 0.1	68.3 ± 0.9	67.7 ± 1.5	75.5 ± 3.2
20	102 ± 5	16.7 ± 0.1	125 ± 8	19.0 ± 0.1	84.8 ± 3.7	86.4 ± 3.8	92.2 ± 3.3
25	131 ± 2	20.4 ± 0.1	156 ± 7	25.5 ± 0.3	109 ± 5	108 ± 5	117 ± 8
30	160 ± 8	25.7 ± 0.36	181 ± 17	33.6 ± 0.1	139 ± 8	147 ± 6	139 ± 6
35	184 ± 6	33.2 ± 0.6	216 ± 13	41.0 ± 0.7	183 ± 6	181 ± 3	nd
40	218 ± 7	nd	nd	49.6 ± 0.5	nd	nd	nd
45	249 ± 12	nd	nd	nd	nd	nd	nd
50	297 ± 10	nd	nd	nd	nd	nd	nd
nd: not determined.							

Table 5.5 Temperature dependence of the rate constant for deuteride transfer (k_D) during catalysis by BsDHFR and its variants at pH 7.

t / °C	BsDHFR / s ⁻¹	L20M / s ⁻¹	A104Q / s ⁻¹	L20M/A104Q / s ⁻¹	P122E / s ⁻¹	P129D / s ⁻¹	P122E/P129D / s ⁻¹
5	nd	2.20 ± 0.03	27.2 ± 2.8	4.01 ± 0.18	21.1 ± 0.5	20.6 ± 0.6	23.5 ± 0.6
10	18.4 ± 0.5	2.90 ± 0.07	37.2 ± 2.3	5.37 ± 0.12	27.7 ± 0.3	27.6 ± 0.7	29.6 ± 0.4
15	22.3 ± 0.5	4.27 ± 0.08	47.4 ± 6.4	7.16 ± 0.06	34.0 ± 0.8	33.1 ± 0.4	37.2 ± 1.1
20	29.6 ± 6	5.97 ± 0.33	62.7 ± 4.5	9.98 ± 0.44	41.9 ± 1.7	42.2 ± 1.0	48.7 ± 1.1
25	39.2 ± 0.5	7.14 ± 0.06	77.8 ± 2.5	13.7 ± 0.1	55.0 ± 4.2	57.1 ± 1.9	60.1 ± 1.1
30	47.5 ± 1.5	9.29 ± 0.07	101 ± 9	18.1 ± 0.3	72.9 ± 2.1	77.3 ± 5.3	75.1 ± 2.3
35	56.4 ± 1.3	11.7 ± 0.4	118 ± 7	24.2 ± 0.7	93.5 ± 1.6	94.7 ± 9.7	nd
40	68.0 ± 3.7	nd	nd	30.7 ± 0.4	nd	nd	nd
45	80.2 ± 4.0	nd	nd	nd	nd	nd	nd
50	105 ± 4	nd	nd	nd	nd	nd	nd
nd: not determined.							

Table 5.6 Temperature dependence of the kinetic isotope effect (KIE) on hydride transfer during catalysis by BsDHFR and its variants at pH 7.

t / °C	BsDHFR	L20M	A104Q	L20M/ A104Q	P122E	P129D	P122E/ P129D
5	nd	3.13 ± 0.09	2.34 ± 0.26	2.00 ± 0.11	2.25 ± 0.08	2.26 ± 0.07	2.16 ± 0.07
10	3.70 ± 0.46	3.01 ± 0.13	2.17 ± 0.17	1.89 ± 0.06	2.10 ± 0.03	2.11 ± 0.08	2.19 ± 0.04
15	3.54 ± 0.18	2.84 ± 0.08	2.10 ± 0.31	1.96 ± 0.02	2.01 ± 0.05	2.05 ± 0.05	2.03 ± 0.10
20	3.44 ± 0.17	2.80 ± 0.16	2.00 ± 0.19	1.90 ± 0.08	2.02 ± 0.12	2.05 ± 0.10	1.89 ± 0.08
25	3.33 ± 0.07	2.86 ± 0.03	2.00 ± 0.11	1.86 ± 0.03	1.98 ± 0.18	1.89 ± 0.10	1.94 ± 0.14
30	3.38 ± 0.20	2.77 ± 0.04	1.80 ± 0.23	1.85 ± 0.03	1.90 ± 0.13	1.91 ± 0.15	1.84 ± 0.09
35	3.27 ± 0.13	2.84 ± 0.12	1.84 ± 0.15	1.69 ± 0.06	1.95 ± 0.07	1.91 ± 0.20	nd
40	3.21 ± 0.20	nd	nd	1.61 ± 0.03	nd	nd	nd
45	3.10 ± 0.22	nd	nd	nd	nd	nd	nd
50	2.83 ± 0.15	nd	nd	nd	nd	nd	nd
nd: not determined.							

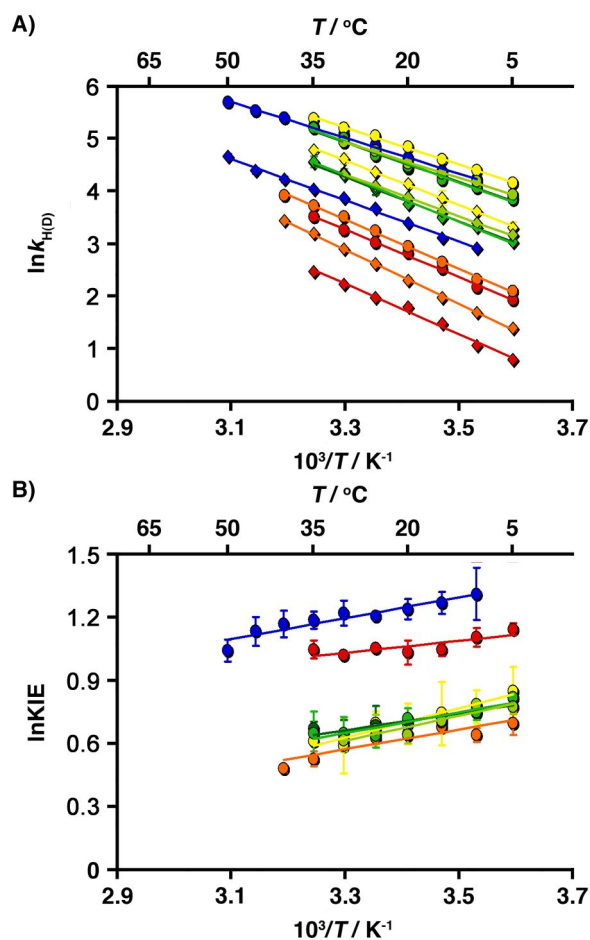


Figure 5.4 A) Arrhenius plots of the pre-steady-state rate constant of the BsDHFR (blue) catalysed reaction and its variants (red = L20M, yellow = A104Q, orange = L20M/A104Q, dark green = P122E, green = P129D and yellow green = P122E/P129D) catalysed reaction at pH 7; B) plots of the KIEs on a logarithmic scale against the inverse temperature.

Table 5.7 The activation parameters for hydride transfer catalysed by BsDHFR and its mutants.

Enzyme	$E_a^H / \text{kJ mol}^{-1}$	$\Delta E_a / \text{kJ mol}^{-1}$	$A_H / 10^7 \text{ s}^{-1}$	A_H/A_D
BsDHFR	28.1 ± 0.8	3.3 ± 1.0	1.02 ± 0.02	0.87 ± 0.02
L20M	37.5 ± 1.0	2.3 ± 1.8	7.80 ± 0.18	1.10 ± 0.05
A104Q	29.3 ± 0.5	5.8 ± 1.0	2.05 ± 0.03	0.18 ± 0.01
L20M/ A104Q	39.1 ± 0.9	3.9 ± 1.0	17.2 ± 0.3	0.38 ± 0.01
P122E	31.7 ± 1.6	3.3 ± 1.9	4.01 ± 0.15	0.52 ± 0.02
P129D	32.4 ± 1.5	4.1 ± 2.0	5.48 ± 0.19	0.38 ± 0.02
P122E/ P129D	27.9 ± 0.9	4.9 ± 1.0	0.90 ± 0.02	0.26 ± 0.01

5.2.5 Thermostability of BsDHFR variants

The effect of temperature on the steady-state activity of BsDHFR and its variants at pH 7 was evaluated as a function of time (Figure 5.5). Wild type BsDHFR retains almost its full catalytic rate for at least half an hour at 60 °C, but all of the site-directed mutants could only maintain 70 to 78 % of their initial activities. Specifically, mutants with thermally labile residues are slightly more stable over time than the mutants with the proline site-directed mutants, being able to maintain >75% of activity after the heat incubation. Interestingly, proline residue variants showed higher melting temperatures, showing that the thermostability does not directly relate to the melting temperature (see above). It is hard to quantify the relative contribution of the thermostable residues and proline residues. The reduced presence of thermolabile residues on the protein surface is also a contributor to the thermostability of BsDHFR. However, it is never mentioned in the previous work.(120)

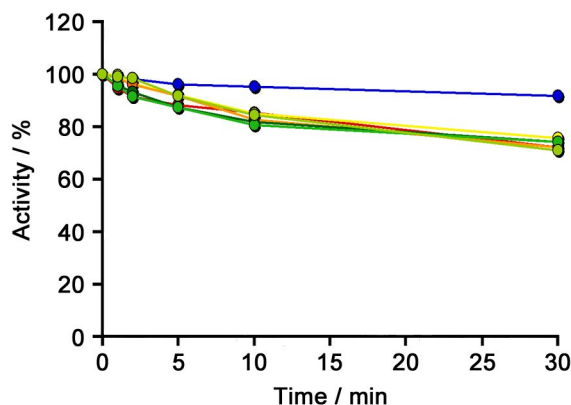


Figure 5.5 The time dependence of the loss the catalytic activity of BsDHFR (blue) and its variants (red = L20M, yellow = A104Q, orange = L20M/A104Q, dark green = P122E, green = P129D and yellow green = P122E/P129D) at pH 7 and 60 °C.

5.3 Conclusions

Thermostability of BsDHFR was analysed by a series of site-directed mutagenesis studies. To analyse the reason for the relatively poor cofactor binding, Leu20 and Ala104 in BsDHFR were mutated to methionine and glutamine, respectively. Proline mutants, P122E and P129D, were made to study their effects on thermostability and the functional roles of the FG loop in BsDHFR. CD spectroscopic studies indicated that all of the mutations have no effect on the secondary structure, but cause a drop in thermal melting temperatures. The overall kinetic behaviour of the A104Q variant is similar to that of wild type BsDHFR. However, the steady-state and pre-steady-state rate constants of L20M and L20M/A104Q variants are much lower than wild type BsDHFR and the other variants, suggesting a distortion in the geometrical setup of the active site. This conformational change also led to a great increase in the hydride transfer activation energy.

Although the substitution of Ala104 to glutamine causes a drop in thermal melting point, it also greatly improves the efficiency of cofactor binding, decreasing the K_M for NADPH 5-fold. This mutation likely introduces favorable hydrogen bonding

interactions between the purine ring of NADPH and the glutamine residue. However the functional group of glutamine is thermally labile when exposed to solvent and becomes easily hydrolysed at high temperature. Hence, poor binding of NADPH of BsDHFR is probably a trade-off for thermal adaptation.

Mutations of the proline residues should increase the relative flexibility of the FG loop, whose loop movements are crucial for catalysis in EcDHFR. The flexibility increase in the loop region decreased thermostability of BsDHFR. However, the mutants P122E, P129D and P112E/P129D do not influence the overall kinetic behaviour of BsDHFR.

6 CREATION AND ANALYSIS OF HYBRID ENZYMES

The work described in this chapter has been published as: Jiannan Guo, E. Joel Loveridge, Louis Y. P. Luk, and Rudolf K. Allemann, Effect of dimerization on dihydrofolate reductase catalysis, *Biochemistry* 2013, **52**(22), 3881-3887.

6.1 Introduction

Several characterised thermophilic enzymes, such as exopolygalacturonase (246) and DHFR isolated from *Thermotoga maritima* (TmDHFR) are oligomeric, whereas their mesophilic homologues are monomeric. Indeed, TmDHFR is the only chromosomally encoded DHFR known to form a stable homodimer (it is likely that DHFRs from other *Thermotoga* species also form dimers, but none has yet been characterised (208)). It has been well documented that the dimeric nature of TmDHFR contributes significantly to the enhanced thermal stability,(118, 206, 209) and similar conclusions have been made in the studies of other oligomeric thermophilic enzymes.(52) However, the effect of dimerisation on catalysis has not been systematically elucidated. For the mesophilic EcDHFR, catalytic efficiency depends on movement of the M20 and FG loops.(153, 183, 247) In contrast, the corresponding loops of TmDHFR are buried into the dimer interface, forming a tightly packed hydrophobic core (Ile15, Val19, Trp22, Tyr125, Phe127 in one subunit and Tyr140 in the other) and a key intermolecular ion pair (Lys129 of one subunit with Glu136 and Glu138 of the other).(118) These intersubunit interactions constrain free movement of the loops corresponding to the M20 and FG loops of EcDHFR.(215)

This chapter presents the preparation of EcDHFR/TmDHFR and BsDHFR/TmDHFR hybrid enzymes, which were used to investigate the functional role(s) of the dimer interface in the catalysis of TmDHFR and also its thermostability. By introducing residues of the TmDHFR dimeric interface, a stable dimeric EcDHFR variant, namely Xet-3, was created. Quaternary structural properties of this variant was assessed by size exclusion chromatographic studies. Also, temperature and pH profiles of steady-state and pre-steady-state kinetics of Xet-3 were measured, as well as KIEs at pH 7.0 as a function of temperature. All the data were summarised and compared to the parental enzymes EcDHFR and TmDHFR and the site-directed mutant TmDHFR-V11D, which functions as a monomer in the presence of CHAPS,

6.2 Results and discussion

6.2.1 Strategies of hybrid enzyme preparation

The tertiary structures of EcDHFR and TmDHFR are relatively similar, despite their low sequence identity (24%). Our initial approach to hybrid enzyme preparation involved swapping the C-terminal fragments between TmDHFR and EcDHFR or BsDHFR. Unfortunately, the hybrid enzymes, Xet-1, Xte-1, Xet-2, Xte-2, Xbt-1, and Xtb-1 (X = cross, e = EcDHFR, t = TmDHFR, b = BsDHFR, et = parent enzyme comes from EcDHFR and dimer interface comes from TmDHFR, and so on) were expressed as inclusion bodies in *E. coli* and remained as aggregates even after multiple attempts of refolding. A plausible explanation is that the swapped peptide fragments are incapable of forming a thermodynamically stable folded structure.

6.2.2 Preparation of worked hybrid enzyme Xet-3

To circumvent this problem, we employed another method, by which residues involved in the formation of the dimer interface of TmDHFR were introduced into EcDHFR by site-directed mutagenesis (Figure 6.1A). This method does not perturb the overall structural organisation of EcDHFR, thus the resulting hybrid enzyme could likely adopt a stable folded structure (Figure 6.1B). Hybrid mutants Xte-3, Xbt-3 and Xet-3 were generated accordingly. Both Xte-3 and Xbt-3 could not be used in the studies, because they could not be folded properly into a functioning dimeric enzyme. Fortunately, Xet-3 was found to be stable and its biophysical characterisations are elaborated below.

SDS-PAGE analysis (Figure 6.2), hybrid Xet-3 runs at approximately 14.4 kDa, slightly lower than the calculated molecular mass from the primary sequence (17.8 kDa).

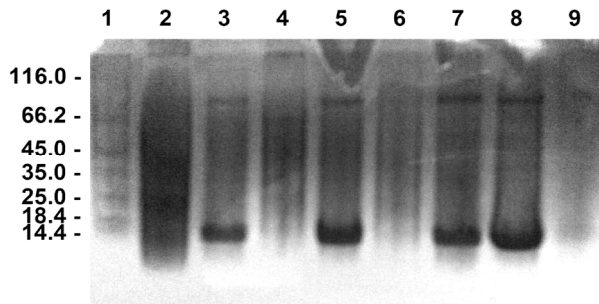


Figure 6.2 SDS-PAGE gel of Xet-3 purification: 1) protein marker in kilodaltons; 2) soluble protein in 50 mM Tris (pH 8.0); 3) insoluble protein in 50 mM Tris (pH 8.0); 4) soluble protein in 1% Triton; 5) insoluble protein in 1% Triton; 6) soluble proteins in 2 M urea; 7) insoluble protein in 2 M urea; 8) soluble proteins in 8 M urea; 9) insoluble protein in 8 M urea.

The refolded protein was loaded onto a DEAE anion exchange column pre-equilibrated with 50 mM Tris (pH 8.0) and eluted with a 0 to 1 M NaCl gradient. One main peak was obtained (Figure 6.3A) which was mostly the target protein.

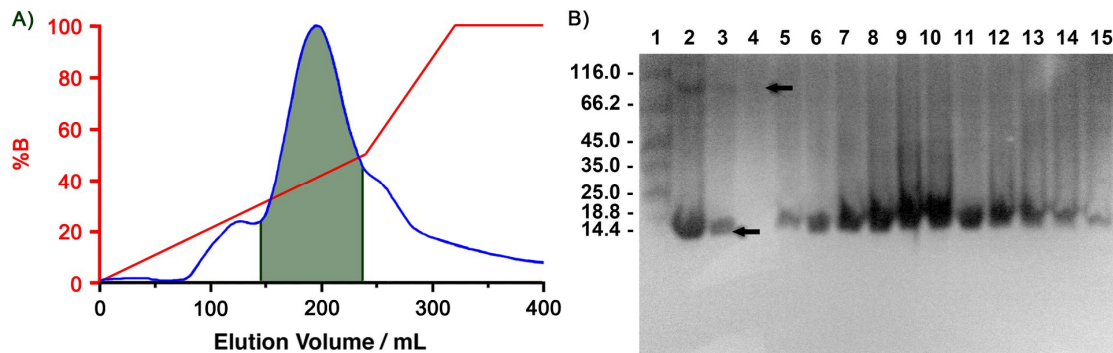


Figure 6.3 A) Chromatogram of DEAE anion exchange chromatography of Xet-3 (blue trace) with increasing NaCl gradient (red). Active fractions are highlighted. B) SDS-PAGE gel following Xet-3 purification: 1) protein marker in kilodaltons; 2) total proteins in 8 M urea; 3) after refolding step; 4) flow through; 5-15) active fractions.

SDS-PAGE of the crude refolded protein (Figure 6.3B) showed an impurity protein at ~80 kDa, and was removed after DEAE chromatography. The active fractions were pooled, concentrated, and further purified using Superdex 75 size exclusion column chromatography (Figure 6.4A).

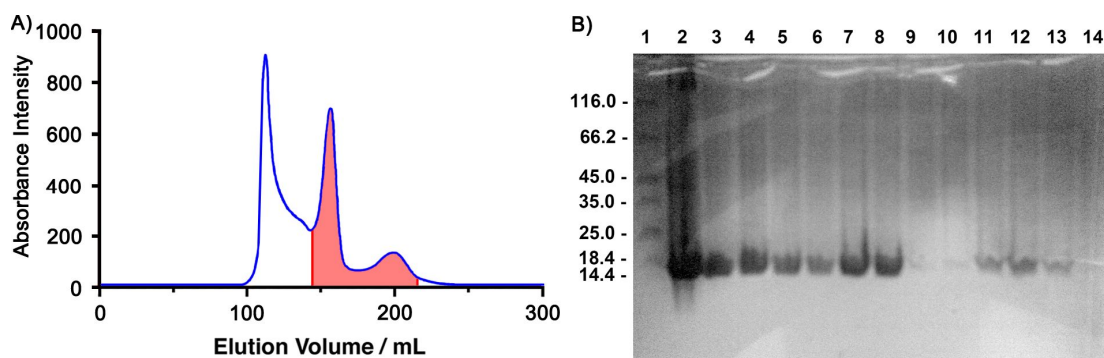


Figure 6.4 A) Chromatogram of size exclusion chromatography of Xet-3 (blue trace). Active peaks are highlighted. B) SDS-PAGE gel following size exclusion chromatography purification: 1) protein marker in kilodaltons; 2) total proteins; 3-6) aggregated proteins, first peak; 7-9) dimeric form of Xet-3, second peak; 10-14) monomeric form of Xet-3, third peak.

Three main peaks were observed (Figure 6.4A) in the Superdex 75 size exclusion chromatographic trace. The size of the hybrid protein and its oligomeric state were evaluated by comparing the retention volume of the dimeric TmDHFR and the monomeric EcDHFR. The retention volume of the first peak (~110 mL) was much lower than that of the dimeric TmDHFR (160 mL) and showed no sign of activity, thus it was believed to be inactive aggregates. In turn, the retention volumes of the second (155 mL) and the third (197 mL) peaks are similar to those of TmDHFR (160 mL) and EcDHFR (189 mL), thus they likely represent the dimeric and monomeric forms of the hybrid DHFR, respectively. This therefore implies that the folded hybrid enzyme Xet-3 is in an equilibrium between monomer and dimer, in contrast to TmDHFR, which appears only as a dimer in solution. A possible explanation for the observed difference is that the dimer interface of the hybrid variant contains two negatively charged residues, Asp134 of one monomer and Asp142 of another monomer, which are in proximity based on modelling studies and likely result in

unfavorable interactions upon dimerisation.

6.2.3 Size exclusion chromatography analysis of Xet-3

To further analyse the oligomeric state of the recombinant protein under neutral conditions, EcDHFR, TmDHFR and Xet-3 were subjected to size exclusion chromatography (Figure 6.5A). The elution profile of 20 μM solution of Xet-3 shows two peaks at 10.0 and 12.5 mL, whereas monomeric EcDHFR and dimeric TmDHFR show only one peak with elution volumes of 12.2 and 10.2 mL, respectively, indicating that Xet-3 is a mixture of monomer and dimer. The relative peak areas, moreover, change with the concentration of Xet-3 (1, 5, 20 μM) suggesting a slow equilibrium between these two states with an equilibrium constant of $\sim 1 \mu\text{M}$ at 20 $^{\circ}\text{C}$ (Figure 6.5B). The Xet-3 dimer and monomer are relatively stable, as immediate reinjection of either isolated peak fraction onto the column gave a single peak only (Figure 6.5A). The elution profiles remain unchanged after incubation at 4 $^{\circ}\text{C}$ for nearly one week. On the other hand, this equilibrium was re-established at elevated temperatures, with a half-life of ~ 5 hours at 40 $^{\circ}\text{C}$.

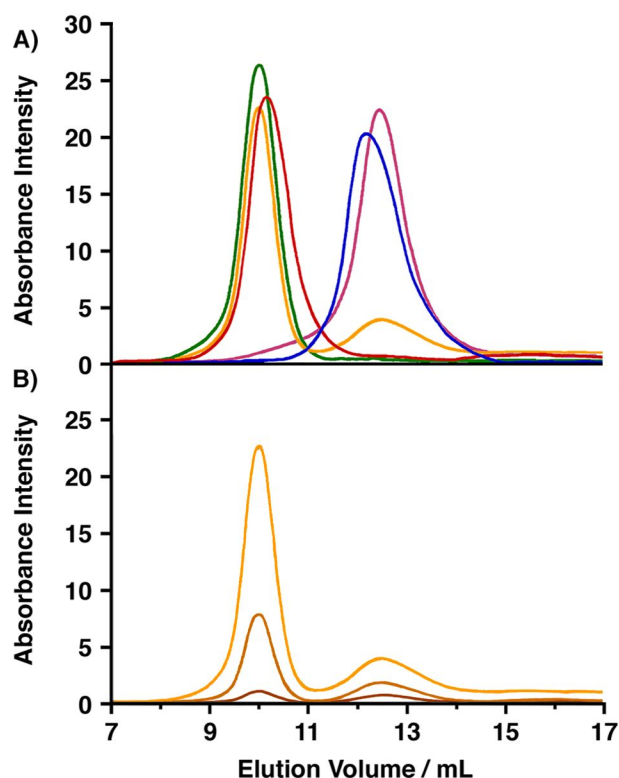


Figure 6.5 A) Size exclusion chromatography of 20 μM Xet-3 (orange) and immediate reinjection of both peaks of Xet-3 (green and purple) in 100 mM potassium phosphate (pH 7) containing 100 mM NaCl at 20 $^{\circ}\text{C}$. EcDHFR (blue) and TmDHFR (red) serve as monomer and dimer markers, respectively. B) Size exclusion chromatography of Xet-3 at 20 (orange), 5 (dark orange) and 1 (brown) μM under the same conditions.

6.2.4 Circular dichroism analysis and thermal unfolding of Xet-3

Far-UV circular dichroism (CD) spectra of the dimeric and monomeric fractions of Xet-3 were both characteristic of folded proteins (Figure 6.6A). There is a broad negative peak between 208 and 222 nm for both oligomeric states of Xet-3. The peak for the monomer is slightly wider and more intense than that of the dimer. At 20 $^{\circ}\text{C}$, there is a minimum mean residue ellipticity (MRE) of $-7,485 \text{ deg}\cdot\text{cm}^2\cdot\text{dmol}^{-1}$ at 219 nm for the dimer and $-6,495 \text{ deg}\cdot\text{cm}^2\cdot\text{dmol}^{-1}$ at 222 nm for the monomer.

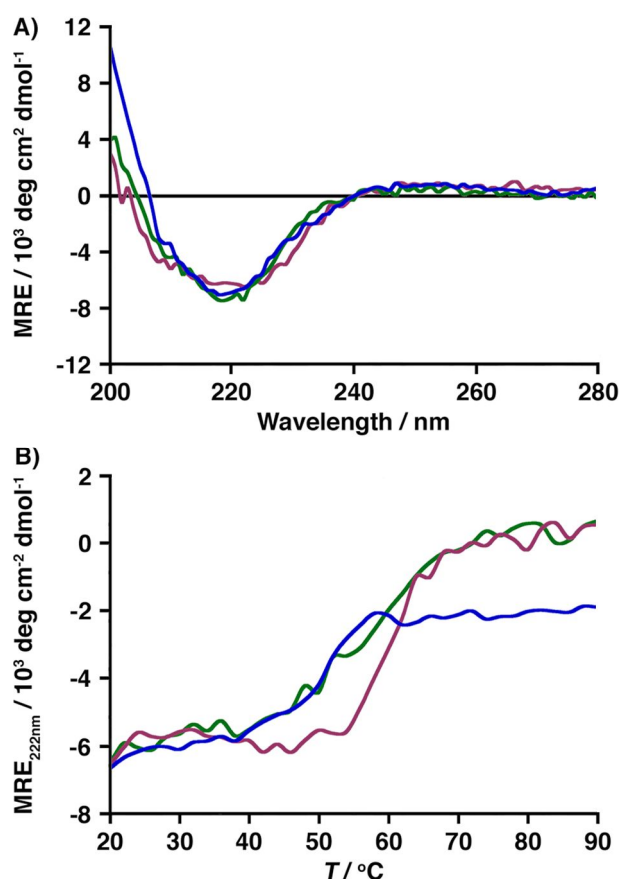


Figure 6.6 A) CD spectra at 20 °C in 10 mM potassium phosphate buffer at pH 7 and B) temperature dependence of the mean residue ellipticity at 222 nm of EcDHFR (blue), dimeric Xet-3 (green) and monomeric Xet-3 (purple).

The thermal melting temperature (T_m) was measured by monitoring the change in MRE at 222 nm with increasing temperature (Figure 6.6B). Thermal denaturation of both monomeric and dimeric forms of Xet-3 is not reversible due to aggregation of the denatured proteins (not shown). Apparent T_m values were 57.2 ± 0.4 and 60.6 ± 0.3 °C for the dimeric and monomeric forms of Xet-3, respectively. Given the acceleration of the return to equilibrium at higher temperature (*vide supra*), it is likely that equilibrium is at least partly re-established during measurement of T_m . The monomer/dimer ratio is probably therefore similar once higher temperatures are reached regardless of the starting populations. In any case, the T_m of Xet-3 is significantly higher than that of EcDHFR (51.2 ± 0.3 °C).⁽¹⁷⁹⁾

Molecular modeling studies have shown that the ‘hinge’ region of EcDHFR around Asp87, far removed from the dimer interface of Xet-3, unfolds early in the denaturation process, while the β -sheet regions which in TmDHFR are in the dimer interface, unfold relatively late.(179, 206, 248, 249) Glycosylation at position 87 of EcDHFR is known to increase thermal stability,(250) whereas glycosylation on the FG loop does not.(251) Therefore, the thermostability of Xet-3 may be limited by the unfolding of other regions of the enzyme that are afforded no additional protection by dimerisation.

6.2.5 The steady-state kinetics of Xet-3

The steady-state rate constants (k_{cat}) for the NADPH-dependent reduction of H₂F catalysed by monomeric and dimeric Xet-3 at pH 7 increase in an exponential fashion up to 40 °C, but decrease markedly at higher temperatures (Figure 6.7A). K_M values for the two forms are ~4-fold higher than those of EcDHFR (Table 6.1), implying that the mutations have a relatively small effect on ligand binding. The affinity of Xet-3 for its ligands is more similar to that of EcDHFR than TmDHFR, as would be expected given that no active-site mutations were introduced. In contrast, dimerisation leads to a great decrease in the rate of turnover (Table 6.1). At 20 °C, the turnover number k_{cat} for the monomer of Xet-3 is 9-fold lower than that of EcDHFR, whereas the k_{cat} for the dimer of Xet-3 is almost 270-fold lower and comparable to that of TmDHFR. Monomerisation of TmDHFR-V11D with CHAPS has previously been reported and leads to a ~20-fold reduction in k_{cat} , whereas CHAPS had no effect on wild type TmDHFR.(209)

Table 6.1 Temperature dependence of the rate constant for steady-state turnover with NADPH (k_{cat}) during catalysis by EcDHFR, TmDHFR and their variants at pH 7.

t / °C	EcDHFR / s ⁻¹ (202)	Xet-3 dimer / s ⁻¹	Xet-3 monomer / s ⁻¹	TmDHFR / s ⁻¹ (209)	TmDHFR-V11D + CHAPS / s ⁻¹ (209)
5	nd	nd	nd	0.010 ± 0.006	0.0006 ± 0.0002
10	nd	0.023 ± 0.06	0.29 ± 0.07	0.019 ± 0.005	0.001 ± 0.001
15	8.5 ± 1.2	0.038 ± 0.002	0.67 ± 0.11	0.034 ± 0.011	0.002 ± 0.001
20	12.6 ± 1.4	0.046 ± 0.001	1.39 ± 0.09	0.061 ± 0.008	0.003 ± 0.001
25	16.4 ± 3.6	0.068 ± 0.001	2.65 ± 0.40	0.103 ± 0.018	0.006 ± 0.001
30	24.0 ± 3.0	0.115 ± 0.002	5.04 ± 0.20	0.134 ± 0.017	0.011 ± 0.001
35	32.0 ± 5.0	0.194 ± 0.013	8.79 ± 0.67	0.192 ± 0.018	0.018 ± 0.001
40	44.9 ± 6.1	0.287 ± 0.008	13.5 ± 2.40	0.261 ± 0.007	0.036 ± 0.001
45	nd	nd	nd	0.346 ± 0.030	0.057 ± 0.009
50	nd	nd	nd	0.439 ± 0.014	0.089 ± 0.009
55	nd	nd	nd	0.530 ± 0.042	nd
60	nd	nd	nd	0.756 ± 0.034	nd
nd: not determined.					

Table 6.2 k_{cat} , K_M (20 °C), activation energies, and Arrhenius prefactors for steady state turnover at pH 7 by wild type EcDHFR, TmDHFR and their variants.

Enzymes	$k_{\text{cat}} / \text{s}^{-1}$ (20 °C)	E_a^{H} / kJ mol^{-1}	$A_{\text{H}} / \text{s}^{-1}$	$K_M(\text{NADPH})$ / μM	$K_M(\text{H}_2\text{F})$ / μM
EcDHFR	12.6 ± 1.4	47.7 ± 0.8	$(3.84 \pm 0.13) \times 10^9$	4.8 ± 1.0	0.7 ± 0.3
Xet-3 dimer	0.046 ± 0.001	61.4 ± 3.5	$(4.58 \pm 0.29) \times 10^9$	19.9 ± 3.9	7.7 ± 1.4
Xet-3 monomer	1.39 ± 0.09	94.6 ± 2.8	$(9.47 \pm 0.27) \times 10^{16}$	19.5 ± 3.5	2.7 ± 0.7
TmDHFR	0.061 ± 0.008	80.5 ± 0.5 ^[a] 46.5 ± 1.1 ^[b]	$(1.33 \pm 0.01) \times 10^{13}$ ^[a] $(1.43 \pm 0.04) \times 10^7$ ^[b]	< 0.5	< 0.5
TmDHFR -V11D + CHAPS	0.003 ± 0.001	89.0 ± 2.1	$(2.26 \pm 0.06) \times 10^{13}$	< 1	< 1
[a] below 25 °C. [b] above 25 °C.					

6.2.7 The pre-steady-state kinetics of Xet-3

Similar to the behaviour of wild type EcDHFR, the hydride-transfer rate constants (k_{H}) for both oligomeric forms of Xet-3 (Figure 6.7B) are 5- to 30-fold higher than the k_{cat} values over the whole temperature range examined at neutral pH,⁽¹⁵⁴⁾ indicating that the chemical step is always a fast step in the catalytic cycle. As was seen for k_{cat} , dimerisation causes a decrease in the k_{H} of Xet-3. At 20 °C, k_{H} for the monomer ($17.4 \pm 0.6 \text{ s}^{-1}$) is 9-fold lower than that of wild type EcDHFR ($159.8 \pm 7.9 \text{ s}^{-1}$),⁽²⁰⁷⁾ whereas k_{H} for the dimer is almost 400-fold lower ($0.44 \pm 0.02 \text{ s}^{-1}$) and is comparable to that of TmDHFR ($0.122 \pm 0.003 \text{ s}^{-1}$).⁽²⁰⁹⁾ In contrast, monomerisation of TmDHFR-V11D led to only a four-fold reduction of k_{H} ($0.029 \pm 0.004 \text{ s}^{-1}$).

Table 6.3 Temperature dependence of the rate constant for hydride transfer (k_H) during catalysis by EcDHFR, TmDHFR and their variants at pH 7.

t / °C	EcDHFR / s ⁻¹ (207)	Xet-3 dimer / s ⁻¹	Xet-3 monomer / s ⁻¹	TmDHFR / s ⁻¹ (209)	TmDHFR-V11D + CHAPS / s ⁻¹ (209)
5	81.9 ± 1.7	0.09 ± 0.01	7.68 ± 0.17	0.044 ± 0.001	0.0120 ± 0.0028
10	106 ± 3	0.15 ± 0.01	9.72 ± 0.37	0.060 ± 0.003	0.0173 ± 0.0041
15	135 ± 6	0.26 ± 0.02	13.7 ± 0.6	0.087 ± 0.002	0.0212 ± 0.0038
20	160 ± 8	0.44 ± 0.02	17.4 ± 0.6	0.122 ± 0.003	0.0292 ± 0.0042
25	204 ± 7	0.68 ± 0.05	20.7 ± 0.4	0.169 ± 0.002	0.0473 ± 0.0054
30	235 ± 14	1.05 ± 0.09	26.5 ± 0.2	0.242 ± 0.005	0.0687 ± 0.0114
35	288 ± 12	nd	nd	0.341 ± 0.006	0.0960 ± 0.0138
40	nd	nd	nd	0.488 ± 0.010	0.132 ± 0.013
45	nd	nd	nd	0.668 ± 0.015	0.193 ± 0.024
50	nd	nd	nd	0.932 ± 0.036	0.231 ± 0.019
55	nd	nd	nd	1.25 ± 0.06	nd
60	nd	nd	nd	1.65 ± 0.09	nd
65	nd	nd	nd	2.12 ± 0.16	nd

nd: not determined.

Table 6.4 Temperature dependence of the rate constant for deuteride transfer (k_D) during catalysis by wild type EcDHFR, TmDHFR and their variants at pH 7.

t / °C	EcDHFR / s ⁻¹ (207)	Xet-3 dimer / s ⁻¹	Xet-3 monomer / s ⁻¹	TmDHFR / s ⁻¹ (209)	TmDHFR-V11D + CHAPS / s ⁻¹ (209)
5	26.9 ± 1.9	0.03 ± 0.01	2.90 ± 0.20	0.0066 ± 0.0002	0.0051 ± 0.0007
10	34.1 ± 3.4	0.06 ± 0.01	3.96 ± 0.12	0.010 ± 0.001	0.0072 ± 0.0010
15	44.6 ± 3.7	0.09 ± 0.01	5.63 ± 0.05	0.016 ± 0.001	0.0091 ± 0.0010
20	60.2 ± 4.1	0.17 ± 0.01	7.42 ± 0.26	0.027 ± 0.001	0.0148 ± 0.0009
25	75.1 ± 5.4	0.27 ± 0.01	9.21 ± 0.31	0.042 ± 0.003	0.0233 ± 0.0019
30	98.5 ± 2.8	0.42 ± 0.01	12.53 ± 0.25	0.060 ± 0.002	0.0370 ± 0.0042
35	125.9 ± 3.5	nd	nd	0.082 ± 0.005	0.0585 ± 0.0055
40	nd	nd	nd	0.116 ± 0.007	0.0850 ± 0.0094
45	nd	nd	nd	0.161 ± 0.003	0.1120 ± 0.0155
50	nd	nd	nd	0.245 ± 0.011	0.1610 ± 0.0134
55	nd	nd	nd	0.336 ± 0.015	nd
60	nd	nd	nd	0.444 ± 0.019	nd
65	nd	nd	nd	0.575 ± 0.013	nd

nd: not determined.

Table 6.5 Temperature dependence of the kinetic isotope effect (KIE) on hydride transfer during catalysis by wild type EcDHFR, TmDHFR and their variants at pH 7.

t / °C	EcDHFR(207)	Xet-3 dimer	Xet-3 monomer	TmDHFR(209)	TmDHFR-V11D + CHAPS(209)
5	3.04 ± 0.22	2.87 ± 0.15	2.65 ± 0.19	6.67 ± 0.25	2.35 ± 0.27
10	3.12 ± 0.32	2.75 ± 0.19	2.45 ± 0.12	6.19 ± 0.71	2.40 ± 0.27
15	3.03 ± 0.28	2.71 ± 0.08	2.44 ± 0.11	5.44 ± 0.36	2.33 ± 0.21
20	2.65 ± 0.22	2.50 ± 0.09	2.34 ± 0.12	4.52 ± 0.20	1.97 ± 0.16
25	2.71 ± 0.22	2.54 ± 0.07	2.25 ± 0.09	4.02 ± 0.29	2.03 ± 0.14
30	2.39 ± 0.16	2.50 ± 0.09	2.11 ± 0.04	4.03 ± 0.16	1.86 ± 0.20
35	2.29 ± 0.11	nd	nd	4.16 ± 0.26	1.64 ± 0.17
40	nd	nd	nd	4.21 ± 0.27	1.56 ± 0.15
45	nd	nd	nd	4.15 ± 0.12	1.72 ± 0.19
50	nd	nd	nd	3.80 ± 0.23	1.43 ± 0.12
55	nd	nd	nd	3.73 ± 0.24	nd
60	nd	nd	nd	3.73 ± 0.26	nd
65	nd	nd	nd	3.69 ± 0.29	nd

nd: not determined.

Table 6.6 k_H (20 °C), Activation energies and Arrhenius prefactors for hydride and deuteride transfer by wild type EcDHFR, TmDHFR and their variants.

Enzymes	k_H / s^{-1} (20 °C)	E_a^H / kJ mol ⁻¹	ΔE_a / kJ mol ⁻¹	A_H / s^{-1}	A_H/A_D
EcDHFR	159.8 ± 7.9	29.9 ± 0.6	7.9 ± 0.9	(3.4 ± 0.5) × 10 ⁷	0.11 ± 0.02
Xet-3 dimer	0.44 ± 0.02	69.9 ± 0.8	4.0 ± 1.8	(1.20 ± 0.02) × 10 ¹²	0.50 ± 0.01
Xet-3 monomer	17.4 ± 0.6	34.9 ± 1.3	5.7 ± 1.7	(2.74 ± 0.09) × 10 ⁷	0.22 ± 0.01
TmDHFR	0.122 ± 0.003	49.9 ± 1.7 ^[a] 53.5 ± 0.4 ^[b]	19.3 ± 4.1 ^[a] 2.5 ± 0.9 ^[b]	(9.47 ± 0.36) × 10 ⁷ ^[a] (4.11 ± 0.03) × 10 ⁸ ^[b]	0.002 ± 0.001 ^[a] 1.56 ± 0.47 ^[b]
TmDHFR -V11D + CHAPS	0.0292 ± 0.0042	51.3 ± 1.4	8.5 ± 2.2	(4.64 ± 0.15) × 10 ⁷	0.060 ± 0.003
[a] below 25 °C. [b] above 25 °C.					

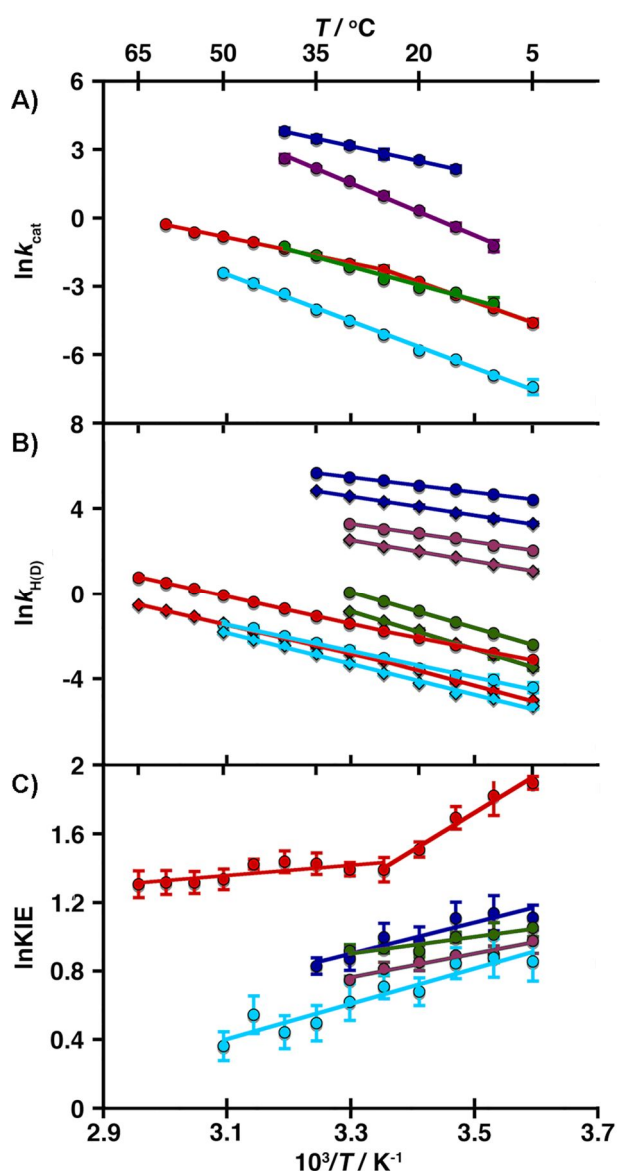


Figure 6.7 A) Arrhenius plots of the steady-state rate constants, B) Arrhenius plots for hydride (circles) and deuteride (diamond) transfer rate constants, and C) the corresponding KIEs on hydride transfer plotted on a logarithmic abscissa against the inverse temperature, for EcDHFR (blue), Xet-3 dimer (green), Xet-3 monomer (purple), TmDHFR (red), and TmDHFR-V11D+CHAPS (cyan) at pH 7.

The primary KIE on hydride transfer was determined by replacing the cofactor NADPH with the deuterium-labelled alternative (NADPD) (Figure 6.7C). At 20 °C, the KIEs of the dimeric and monomeric Xet-3-catalysed reactions are 2.50 ± 0.09 and 2.34 ± 0.12 , respectively. Unlike TmDHFR-V11D, where the temperature dependence

of the KIE changes upon monomerisation, it is not significantly affected by the quaternary structure of Xet-3.

Xet-3 appears to also have different active site electrostatic properties to Ec- and TmDHFR. The apparent pK_a of the catalysed reaction (Figure 6.8B) was found to be 7.48 ± 0.04 for monomeric Xet-3 and 8.05 ± 0.01 for dimeric Xet-3. In EcDHFR and TmDHFR the apparent pK_a arises from protonation of N5 of the substrate dihydrofolate in the Michaelis complex,(202, 252) and the same is likely to be true in Xet-3. Therefore, protonation of dihydrofolate is more favourable in Xet-3 than in its parent enzymes; the apparent pK_a of the reaction catalysed by EcDHFR is 6.48 ± 0.03 ,(191) while that of TmDHFR is 5.83 ± 0.06 .(209) Protonation of H_2F may be favored in Xet-3 relative to EcDHFR due to a more tightly closed active site. This has been seen in computational studies of EcDHFR, where a ‘tightly closed’ conformation of the Michaelis complex led to an increase to almost 9 of the pK_a of dihydrofolate.(253) The situation in TmDHFR is again different; its active site is more open than in EcDHFR (118) and hence the pK_a is lower(202, 209) and monomerisation does not decrease the pK_a .(209)

Table 6.7 pH dependence of the hydride transfer rates (k_H , s^{-1}) at 20 °C for the reaction of NADPH and H₂F catalysed by wild type EcDHFR, TmDHFR and their variants.

pH	EcDHFR / s^{-1} (191)	Xet-3 dimer / s^{-1}	Xet-3 monomer / s^{-1}	TmDHFR / s^{-1} (209)	TmDHFR-V11D + CHAPS / s^{-1} (209)
4	737 ± 56	0.57 ± 0.02	15.4 ± 0.8	1.05 ± 0.01	0.412 ± 0.001
4.5	698 ± 11	0.60 ± 0.01	15.4 ± 0.7	0.912 ± 0.045	0.416 ± 0.001
5	688 ± 25	0.57 ± 0.02	16.0 ± 0.3	0.847 ± 0.028	0.385 ± 0.023
5.5	623 ± 29	0.59 ± 0.01	15.0 ± 0.6	0.667 ± 0.032	0.368 ± 0.028
6	533 ± 47	0.60 ± 0.02	15.3 ± 0.4	0.474 ± 0.017	0.206 ± 0.066
6.5	368 ± 34	0.57 ± 0.01	15.0 ± 0.5	0.224 ± 0.05	0.072 ± 0.016
7	171 ± 6	0.56 ± 0.01	12.9 ± 0.3	0.105 ± 0.01	0.022 ± 0.003
7.5	71.3 ± 11.9	0.48 ± 0.01	7.3 ± 0.7	0.039 ± 0.0002	0.012 ± 0.001
8	34.2 ± 1.7	0.31 ± 0.02	3.5 ± 0.3	0.017 ± 0.0001	0.0050 ± 0.0006
8.5	22.2 ± 1.0	0.13 ± 0.01	1.8 ± 0.2	0.007 ± 0.0001	0.0029 ± 0.0001
9	11.9 ± 0.8	0.024 ± 0.001	0.79 ± 0.07	0.004 ± 0.0004	0.0031 ± 0.0007
9.5	nd	0.010 ± 0.001	0.31 ± 0.04	nd	nd
10	nd	0.0033 ± 0.0003	0.10 ± 0.01	nd	nd
nd: not determined.					

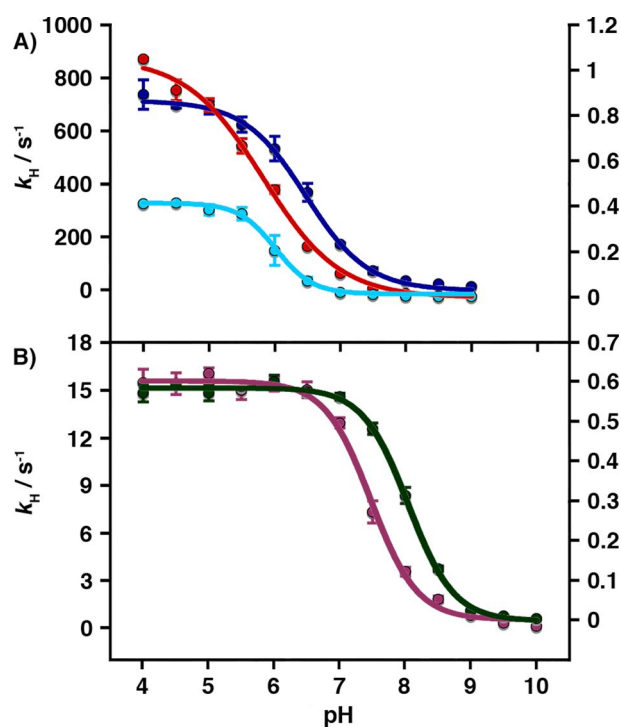


Figure 6.8 pH dependence of the hydride transfer rate constants for the reactions catalysed by A) EcDHFR (blue, left axis), TmDHFR (red, right axis) and TmDHFR-V11D (cyan, right axis), and B) Xet-3 in its monomeric (purple, left axis) and dimeric (green, right axis) forms.

The results presented here showed that the effects of subunit interactions on catalysis are totally different in Xet-3 and in TmDHFR. Dimerisation in Xet-3 makes protonation of the substrate more favorable and reduces the rate constants for both hydride transfer and overall catalytic turnover. It has no effect on the temperature dependence of the observed kinetic isotope effects on hydride transfer. In TmDHFR-V11D, monomerisation reduces the rate constant for overall turnover and changes the temperature dependence of the observed kinetic isotope effects on hydride transfer, but has no significant effect on the rate constants for hydride transfer or the protonation state of the substrate. Since Xet-3 originates predominantly from EcDHFR, the data presented here demonstrate that the catalytic cycles of EcDHFR and TmDHFR, and the roles of their respective loop regions, are markedly different. Release of the constrained loops around the interface region in TmDHFR does not simply have the opposite effect to applying such a constraint in EcDHFR.

Dimerisation of EcDHFR likely restrains or otherwise alters the behaviour of the M20, FG and GH loops, which are crucial in adopting the correct conformations for efficient progression through the catalytic cycle,(125) and therefore decreases the rate of catalytic turnover. As conformational motions do not drive the chemical step of DHFR catalysis, (189, 191, 193, 198, 208) the decrease in the hydride transfer rate constant on dimerisation of Xet-3 is likely due to subtle changes to the geometry and electrostatics of the active site, although these changes also facilitate the favorable protonation of the substrate. In contrast, the loss of intersubunit interactions in TmDHFR and likely increase in the flexibility of the loop regions normally involved in dimerisation, is detrimental to catalytic turnover but not to hydride transfer. Since *T. maritima* has a ThyX-type thymidylate synthase,(254) which regenerates tetrahydrofolate rather than oxidizing it to dihydrofolate, and since tetrahydrofolate is particularly unstable at higher temperatures, only very low DHFR activity is required.(207) The predominant evolutionary pressure on TmDHFR is therefore for thermostability rather than for rapid turnover of substrate. Lastly, while the positive effect of oligomerisation on the thermostability of enzymes has been well documented,(255, 256) its effect on catalysis greatly depends on the interactions between the oligomer interface and the active site. In a similar study of tetrameric ADH from *Thermoanaerobacter brockii*, monomerisation upon engineering results in no detectable enzyme activity because part of the active site is located at the interface between subunits.(257) Conversely, there is essentially no effect on activity when phosphoribosylanthranilate isomerase from *T. maritima* is monomerised, since the dimer interface is fairly distant from the active site.(258)

6.3 Conclusions

EcDHFR has been dimerised by mimicking the interface region of TmDHFR. The resulting EcDHFR/TmDHFR hybrid, Xet-3, exists as a mixture of dimer and monomer, which interconvert only slowly even at elevated temperature. CD spectroscopy shows that the dimeric and monomeric forms of Xet-3 shared similar

secondary structure with EcDHFR. The apparent T_m of Xet-3 is ~6 to 9 °C higher than that of wild type EcDHFR, demonstrating some protection from thermal denaturation. Monomerisation of TmDHFR (as in TmDHFR-V11D) leads to a ~20 °C decrease in the T_m .(209) Additional changes to EcDHFR are therefore required to attain similar thermostability to TmDHFR.

The monomeric form of Xet-3 shows similar steady-state and pre-steady-state rate constants to wild type EcDHFR. However, both kinetic parameters of the dimeric form are much lower than those of the monomeric form and are highly similar to the corresponding values for TmDHFR. In the case of the monomeric TmDHFR-V11D, k_H remains similar to the dimeric wild type counterpart but k_{cat} is reduced dramatically. The results presented here demonstrate that the effect of dimerisation/monomerisation on catalysis is significantly different for EcDHFR and TmDHFR. In EcDHFR, the physical steps of the catalytic cycle are promoted by movement of flexible loop regions, so restricting their movement in Xet-3 leads to lower values of k_{cat} . k_H is also reduced, most likely due to subtle structural changes which propagate to the active site.(179) In TmDHFR, on the other hand, monomerisation is detrimental to catalysis, demonstrating that loop flexibility is not an important factor in TmDHFR catalysis.

This work demonstrates that TmDHFR cannot simply be thought of in the same way as monomeric DHFRs. Possibly as a result of differing selective pressures on TmDHFR compared to monomeric DHFRs, the effect of monomerisation on TmDHFR catalysis is very different to that predicted from EcDHFR catalysis. Interpreting the effects of oligomerisation on the catalytic efficiency of thermophilic enzymes in terms of their mesophilic counterparts is therefore not appropriate. Broad conclusions on the effect of oligomerisation on the catalytic efficiency of thermophilic enzymes in general are therefore difficult. Our results therefore suggest that while EcDHFR may serve as a paradigmatic system for the study of enzyme catalysis in general, it is not a good model for the details of catalysis by other DHFRs.

7 GENERAL SUMMARY AND CONCLUSIONS

The moderately thermophilic DHFR from *Geobacillus stearothermophilus* (BsDHFR) and the artificial hybrid derived from the mesophilic EcDHFR and the hyperthermophilic TmDHFR, Xet-3, were characterised in this thesis. This work has given us a better understanding of the relationship between thermophilicity and enzyme catalysis. Although the temperatures for optimal activity differ greatly among them, MpDHFR (psychrophilic DHFR), EcDHFR and BsDHFR are all monomeric and exhibit similar catalytic activity. In contrast, the most thermophilic homologue, TmDHFR, is dimeric and shows greatly reduced catalytic activity. Similarly, dimerising EcDHFR by introducing residues located at the dimer interface of TmDHFR greatly decreases the catalytic activity, but also enhances the thermal melting temperature of the hybrid enzyme.

7.1 The thermoadaptation of BsDHFR

BsDHFR is a moderately thermophilic DHFR. Its melting temperature was determined to be 66.2 ± 0.4 °C, located in between those of mesophilic EcDHFR and hyperthermophilic TmDHFR. Its steady-state and pre-steady-state rate constants reach maxima around this temperature. The extra thermostability of BsDHFR can be obtained in the presence of salt or by ligand binding. Interestingly, sequence alignment indicated that BsDHFR showed the highest sequence identity to the psychrophilic MpDHFR whose melting temperature is about 30 °C lower. Although the three-dimensional structures of BsDHFR and MpDHFR, determined by X-ray crystallography, are highly conserved, the overall structure of BsDHFR is much more rigid, especially the loop region and protein core.(193, 219)

Amino acid composition revealed that the thermostability of BsDHFR might be enhanced by the extra proline residues located at the loop regions. Substitution of two proline residues in the FG loop (Pro122 and 129) with acidic residues slightly lowered the melting temperature. Moreover, there are fewer thermolabile residues, such as methionine, asparagine and glutamine, in BsDHFR. Gln104 in MpDHFR or Gln102

in EcDHFR play a key role in binding by forming hydrogen bonds with the adenine moiety of NADPH. However, glutamine residues are prone to deamidation and induce cleavage of the peptide backbone at elevated temperature, thus this residue is substituted by alanine in BsDHFR, weakening the enzyme's affinity for NADPH as a trade-off for improved thermal stability. BsDHFR has evolved to choose the more thermostable residues at the NADPH binding site in order to keep its activity at high temperature. Site-directed mutation of Ala104 to Gln improves the binding of NADPH but reduces its thermostability.

The strategy for thermal adaptation is considerably different in TmDHFR; the K_M of NADPH of TmDHFR is much lower than other DHFRs, indicating a very strong NADPH binding ability. Since NADPH is quite unstable at the optimal working temperature of TmDHFR (80 °C), the tight binding of NADPH in the active site can stabilise both the enzyme and the cofactor. This feature of tight ligand binding has been observed in various hyperthermophilic enzymes, whose optimal working temperature is above 80 °C.(231-233) Nevertheless, the optimal working temperature of BsDHFR is lower (60 °C), at which NADPH is relatively stable, thus BsDHFR can adopt an alternative method to retain its tertiary structure at high temperature.

7.2 The contribution of protein dynamics to catalysis

Hydrogen transfer reactions have been proposed to be driven by quantum-mechanical tunnelling and are expected to sensitively link to the relative molecular motions of the surrounding environment. The measurements of solvent effects and the temperature dependence of the KIE of BsDHFR at different pH aim to gain clues to the relationship between protein dynamics and catalysis. Our results suggested that the protein dynamics does not directly contribute to the catalysis.

Changing the solvent viscosity by changing the composition of the reaction medium can perturb the network of long-range promoting motions of an enzyme, which has

been proposed to drive catalysis.(190) However, neither the steady-state and pre-steady-state rate constants of the BsDHFR-catalysed reaction nor their KIEs appear to be sensitive to the medium viscosity. Similar results have been observed in the studies of MpDHFR, EcDHFR and TmDHFR. Furthermore, these results are also analogous to the study on a catalytically compromised variant, EcDHFR-N23PP/S148A performed in our group.(189) The magnitude of KIEs is not affected by these mutations, implying that electrostatic preorganisation and reorganisation,(188) rather than the hypothetical microsecond to millisecond promoting motions, are hampered. These results together argue strongly against a direct coupling of large-scale millisecond protein motions to the chemical step of catalysis. Another recent study of heavy isotope-labelled EcDHFR in our group further showed that mass-dependent vibration frequencies perturb the fast protein vibrations on femtosecond timescale, and we discovered a small measurable decrease in the hydride transfer rate. Although it appears that fast protein motions might promote hydride transfer by dynamical coupling, computer simulations showed that enzymatic isotope substitution has no effect on modulating the barrier or driving the tunnelling. Instead, the slow reaction rate in the heavy enzyme is related to the differences in protein environment of the hydride transfer step.(197) In other words, EcDHFR lowers the recrossing events of hydride transfer. While this microscopic interaction has been elucidated, additional studies are needed to see if fast protein vibrational coupling is common among enzymatic systems.

The KIE on hydride transfer was weakly temperature dependent in BsDHFR at pH 7, but became completely temperature independent at pH 9. This type of pH dependence has been observed in MpDHFR and EcDHFR. Indeed, our group has observed that, in EcDHFR catalysis, the KIE switches sharply from temperature-dependent to temperature-independent, when the pH of the buffer switches from 7.5 to 8.0.(198) The pK_a of the reactions of BsDHFR, EcDHFR and MpDHFR is between 6.4 and 6.5, corresponding to the pK_a of protonated H_2F in the Michaelis complex. Therefore, the sharp change in temperature dependence in KIE during the switch from pH 7.5 to 8 is

unlikely to be due to protonation of substrate, but rather due to changes in protonation state of the protein. Together with the previous results obtained in the studies of solvent effect and heavy isotope labelling of enzyme, these observations suggest that protein motions or conformational changes do not have a direct influence on hydride tunneling. In turn, the factor that influences the rate of hydride transfer is the conformational ensemble of the enzyme prior to reaction, which in turn is sensitive to temperature- and pH-dependent changes.

7.3 The effect of thermophilicity on catalysis

BsDHFR is a relatively 'smart' enzyme. It just rigidifies only certain parts of the protein for thermostability. Flexibility for the rest region is still retained or even enhanced for conformational sampling, thus the enzyme reaction maintains a low reorganisation energy. Therefore, the kinetic behaviour of BsDHFR is generally similar to those of monomeric EcDHFR and MpDHFR. This contradicts the hypothesis that extra stabilising interactions found in thermophilic enzymes enhance rigidity of an enzyme but reduce the activity at low temperature. Accordingly, thermophilicity does not appear to have a direct correlation with the enzyme catalysis. The activity of TmDHFR is much lower and is most likely relates to its dimeric structure.

7.4 The effect of dimerisation on catalysis

Dimerisation changes the biophysical properties of EcDHFR dramatically. While it appears to enhance the enzyme's thermostability by increasing the thermal melting temperature, the kinetic activity of the dimerised enzyme is much lower than that of the wild type EcDHFR and is comparable to the corresponding values of TmDHFR. In the case of the monomeric variant of TmDHFR-V11D, k_H remains similar to the dimeric wild type counterpart but k_{cat} is greatly reduced. This result demonstrates that the effect of dimerisation/monomerisation on catalysis is significantly different for EcDHFR and TmDHFR. In EcDHFR, the physical steps of the catalytic cycle are

promoted by movements of the flexible loops, so restricting their movement by dimerisation leads to lower values of k_{cat} . k_{H} is also reduced, most likely due to subtle structural changes which propagate to the active site.⁽¹⁷⁹⁾ In TmDHFR, on the other hand, monomerisation is detrimental to catalysis, indicating that the reduced catalytic ability of TmDHFR relative to EcDHFR is not simply a consequence of reduced loop flexibility in the dimeric enzyme.

Crystal structures of apo-TmDHFR and its ternary complex with bound cofactor and inhibitor all showed open conformations.⁽¹¹⁸⁾ The proper closure of the active site is therefore prevented by the intersubunit interaction of TmDHFR. The more solvent-exposed active site of TmDHFR is most likely the reason for its poor catalytic activity. However, EcDHFR can adopt a closed conformation for the active site which makes a better electrostatic environment for the reaction to occur. Like EcDHFR, BsDHFR can also form the closed conformation. The ability to form the closed conformation of the active site gives BsDHFR a comparable activity to its mesophilic and psychrophilic counterparts.

In conclusion, this work shows that thermophilic BsDHFR has evolved to maintain an optimal structure-function relationship which allows it to function at rates comparable to psychrophilic MpDHFR and mesophilic EcDHFR and much higher than hyperthermophilic TmDHFR at room temperature. The difference between TmDHFR and other monomeric DHFR catalysis seems to be mainly due to its dimeric structure, which prohibit the enzyme from optimising its conformational sampling. The presence of the dimer interface constrains the movements of catalytically important loops and therefore prevents the proper closure of the active site of TmDHFR. However, the relatively poor activity of TmDHFR is not simply a consequence of reduced loop flexibility. The full catalytic function of TmDHFR appears to rely significantly on intersubunit interactions. This work suggests that TmDHFR cannot simply be considered in the same way as monomeric DHFRs.

8 REFERENCES

1. Johnson, D. L., Ambrose, S. H., Bassett, T. J., Bowen, M. L., Crummey, D. E., Isaacson, J. S., Johnson, D. N., Lamb, P., M.Saul, and E.Winter-Nelson, A. (1997) Meanings of environmental terms, *J. Environ. Qual.* 26, 581-589.
2. Saenphet, K., and Hofer, R. (2009) Solar ultraviolet radiation and fish, *Trends Res. Sci. Technol.* 1, 55-63.
3. Rothschild, L. J., and Mancinelli, R. L. (2001) Life in extreme environments, *Nature* 409, 1092-1101.
4. Guyer, R. L., and Koshland, D. E. J. (1989) The molecule of the year, *Science* 246, 1543-1546.
5. Higashibata, A., Fujiwara, T., and Fukumori, Y. (1998) Studies on the respiratory system in alkaliphilic *Bacillus*; a proposed new respiratory mechanism, *Extremophiles* 2, 83-92.
6. Hirabayashi, T., Goto, T., Morimoto, H., Yoshimune, K., Matsuyama, H., and Yumoto, I. (2012) Relationship between rates of respiratory proton extrusion and ATP synthesis in obligately alkaliphilic *Bacillus clarkii* DSM 8720(T), *J. Bioenerg. Biomembr.* 44, 265-272.
7. Cooper, J. B., Khan, G., Taylor, G., Tickle, I. J., and Blundell, T. L. (1990) X-ray analyses of aspartic proteinases: II. Three-dimensional structure of the hexagonal crystal form of porcine pepsin at 2.3Å resolution, *J. Mol. Biol.* 214, 199-222.
8. Bönisch, H., Schmidt, C. L., Schäfer, G., and Ladenstein, R. (2002) The structure of the soluble domain of an archaeal Rieske iron-sulfur protein at 1.1Å resolution, *J. Mol. Biol.* 319, 791-805.
9. Kastiris, P. L., Papandreou, N. C., and Hamdrakas, S. J. (2007) Haloadaptation: Insights from comparative modeling studies of halophilic archaeal DHFRs, *Int. J. Biol. Mac.* 41, 447-453.
10. Paul, S., Bag, S. K., Das, S., Harvill, E. T., and Dutta, C. (2008) Molecular signature of hypersaline adaptation: Insights from genome and proteome composition of halophilic prokaryotes, *Genome Bio.* 9, R70.
11. MSNBC. (2011) Giant amoebas discovered in deepest ocean trench, *MSNBC*.
12. Murata, Y., Homma, T., Kitagawa, E., Momose, Y., Sato, M. S., Odani, M., Shimizu, H., Hasegawa-Mizusawa, M., Matsumoto, R., Mizhkami, S., Fujita, K., Parveen, M., Komatsu, Y., and Iwahashi, H. (2006) Genome-wide expression analysis of yeast response during exposure to 4 °C, *Extremophiles* 10, 117-128.
13. Mikucki, J. A., Pearson, A., Johnston, D. T., Turchyn, A. V., Farquhar, J., Schrag, D. P., Anbar, A. D., Priscu, J. C., and Lee, P. A. (2009) A contemporary microbially maintained subglacial ferrous "ocean", *Science* 324, 397-400.
14. Takai, K., Nakamura, K., Toki, T., Tsunogai, U., Miyazaki, M., Miyazaki, J., Hirayama, H., Nakagawa, S., Nunoura, T., and Horikoshi, K. (2008) Cell

- proliferation at 122°C and isotopically heavy CH₄ production by a hyperthermophilic methanogen under high pressure cultivation, *Proc. Natl. Acad. Sci. USA* 105, 10949-10954.
15. Blöchl, E., Rachel, R., Burggraf, S., Hafenbradl, D., Jannasch, H. W., and Stetter, K. O. (1997) *Pyrolobus fumarii*, gen. and as. nov., represents a novel group of archaea, extending the upper temperature limit for life to 113°C, *Extremophiles* 1, 14-21.
 16. Kashefi, K., and Lovley, D. R. (2003) Extending the upper temperature limit for life, *Science* 310, 934.
 17. Menzel, U., and Gottschalk, G. (1985) The internal pH of *Acetobacterium wieringae* and *Acetobacter aceti* during growth and production of acetic acid, *Arch. Microbiol.* 143, 47-51.
 18. Anton, J., Rossello-Mora, R., Rodriguez-Valera, F., and Amann, R. (2000) Extremely halophilic bacteria in crystallizer ponds from solar salterns, *Appl. Environ. Microbiol.* 66, 3052-3057.
 19. Sharma, A., Scott, J. H., Cody, G. D., Fogel, M. L., Hazen, R. M., Hemley, R. J., and Huntress, W. T. (2002) Microbial activity at gigapascal pressures, *Science* 295, 1514-1516.
 20. Stetter, K. O. (1984) Anaerobic life at extremely high temperature, *Origins Life Evol. B.* 14, 809-815.
 21. Woese, C. R. (1987) Bacterial evolution, *Bacteriol. Rev.* 51, 221-271.
 22. Woese, C. R., Kandler, O., and Wheelis, M. L. (1990) Towards a natural system of organisms: Proposal for the domains archaea, bacteria, and eucarya, *Proc. Natl. Acad. Sci. USA* 87, 4576-4579.
 23. Kandler, O. (1992) Where next with the archaeobacteria?, *Biochem. Soc. Symp.* 58, 195-207.
 24. Zillig, W. (1991) Comparative biochemistry of archaea and bacteria, *Curr. Opin. Genet. Dev.* 1, 544-551.
 25. Bergey, D. H. (1919) Thermophilic bacteria, *J. Bacteriol.* 4, 301-306.
 26. Campbell, L. L., and Williams, O. B. (1953) The effect of temperature on the nutritional requirements of facultative and obligate thermophilic bacteria, *J. Bacteriol.* 65, 141-145.
 27. Stetter, K. O., Fiala, G., Huber, G., and Segerer, A. (1990) Hyperthermophilic microorganisms, *FEMS Microbiol. Rev.* 75, 117-124.
 28. Stetter, K. O., Huber, R., Blöchl, E., Kurr, M., Eden, R. D., Fielder, M., Cash, H., and Vance, I. (1993) Hyperthermophilic archaea are thriving in deep north sea and Alaskan oil reservoirs, *Nature* 365, 743-745.
 29. Blöchl, E., Burggraf, S., Fiala, G., Lauerer, G., Huber, G., Huber, R., Rachel, R., Segerer, A., Stetter, K. O., and Völkl, P. (1995) Isolation, taxonomy and phylogeny of hyperthermophilic microorganisms, *World J. Microbiol. Biotechnol.* 11, 26-56.
 30. Fliermans, C. B., and Brock, T. D. (1972) Ecology of sulfur-oxidizing bacteria in hot acid soils, *J. Bacteriol.* 111, 343-350.
 31. Schönheit, P., and Schäfer, T. (1995) Metabolism of hyperthermophiles, *World*

- J. Microbiol. Biotechnol.* 11, 26-57.
32. Walsh, K. A. J., Daniel, R. M., and Morgan, H. W. (1983) A soluble NADH dehydrogenase (NADH: Ferricyanide oxidoreductase) from *Thermus aquaticus* strain T351, *Biochem. J.* 209, 427-433.
 33. Schäfer, T., Selig, M., and Schönheit, P. (1993) Acetyl-CoA synthetase (ADP forming) in archaea, a novel enzyme involved in acetate formation and ATP synthesis, *Arch. Microbiol.* 159, 72-83.
 34. Daniel, R. M., and Danson, M. J. (1995) Did primitive microorganisms use nonhem iron proteins in place of NAD/P, *J. Mol. Evol.* 40, 559-563.
 35. Iwasaki, T., Wakagi, T., Isogai, Y., Tanaka, K., Iizuka, T., and Oshima, T. (1994) Functional and evolutionary implications of a [3Fe-4S] cluster of the dicluster-type ferredoxin from the thermoacidophilic archaon, *Sulfolobus* sp. strain 7, *J. Biol. Chem.* 269, 2944-2945.
 36. Grogan, D. W. (1998) Hyperthermophiles and the problem of DNA stability, *Mol. Microbiol.* 28, 1043-1049.
 37. Spothem-Maurizot, M., Garnier, F., Sabattier, R., and Charlier, M. (1992) Metal ions protect DNA against strand breakage induced by fast neutrons, *Int. J. Radiat. Biol.* 62, 659-666.
 38. Scholz, S. J., Sonnenbichler, W., Schäfer, W., and Hensel, R. (1992) Di-myo-inositol-1,1'-phosphate: A new inositol phosphate isolated from *Pyrococcus woesei*, *FEBS Lett.* 306, 239-242.
 39. Hensel, R., and König, H. (1988) Thermoadaptation of methanogenic bacteria by intracellular ion concentration, *FEMS Microbiol. Lett.* 49, 75-79.
 40. Sandman, K., Krzycki, J. A., Dobrinski, B., Lurz, R., and Reeve, J. N. (1990) HMf, a DNA binding protein isolated from the hyperthermophilic archaea *Methanothermus fervidus*, is most closely related to histones, *Proc. Natl. Acad. Sci. USA* 87, 5788-5791.
 41. de la Tour, C. B., Protomer, C., Nadal, M., Stetter, K. O., Forterre, P., and Duguet, M. (1990) Reverse gyrase, a hallmark of the hyperthermophilic archaeobacteria, *J. Bacteriol.* 172, 6803-6308.
 42. Hopfner, K., Eichinger, A., Engh, R. A., Laue, F., Ankenbauer, W., Huber, R., and Angerer, B. (1999) Crystal structure of a thermostable type B DNA polymerase from *Thermococcus gorgonarius*, *Proc. Natl. Acad. Sci. USA* 96, 3600-3605.
 43. Choquet, C. G., Patel, G. B., Beveridge, T. J., and Sprott, G. D. (1994) Stability of pressure-extruded liposomes made from archaeobacterial ether lipids, *Appl. Microbiol. Biotechnol.* 42, 375-384.
 44. De Rosa, M., Morana, A., Riccio, A., Gambacorta, A., Trincone, A., and Incani, O. (1994) Lipids of the archaea: A new tool for bioelectronics, *Biosens. Bioelectron.* 9, 669-675.
 45. Dill, K. A. (1990) Dominant forces in protein folding, *Biochemistry* 29, 7133-7155.
 46. Russell, R. J. M., Ferguson, J. M. C., Hough, D. W., Danson, M. J., and Taylor, G. L. (1997) The crystal structure of citrate synthase from the

- hyperthermophilic *Archaeon pyrococcus furiosus* at 1.9 Å resolution, *Biochemistry* 36, 9983-9994.
47. Haney, P., Konisky, J., Koretke, K. K., Luthey-Schulten, Z., and Wolynes, P. G. (1997) Structural basis for thermostability and identification of potential active site residues for adenylate kinases from the archaeal genus *Methanococcus*, *Proteins* 28, 117-130.
 48. Zuber, H. (1988) Temperature adaptation of lactate dehydrogenase structure, functional and genetic aspects, *Biophys. Chem.* 29, 171-179.
 49. Russell, R. J. M., Gerike, U., Danson, M. J., Hough, D. W., and Taylor, G. L. (1998) Structural adaptations of the cold-active citrate synthase from an antarctic bacterium, *Structure* 6, 351-361.
 50. Vogt, G., and Argos, P. (1997) Protein thermal stability: Hydrogen bonds or internal packing?, *Fold. Des.* 2, S40-S46.
 51. Vogt, G., Woell, S., and Argos, P. (1997) Protein thermal stability, hydrogen bonds, and ion pairs, *J. Mol. Biol.* 269, 631-643.
 52. Salminen, T., Teplyakov, A., Kankare, J., Cooperman, B. S., Lahti, R., and Goldman, A. (1996) An unusual route to thermostability disclosed by the comparison of *Thermus thermophilus* and *Escherichia coli* inorganic pyrophosphatases, *Protein Sci.* 5, 1014-1025.
 53. Ermler, U., Merckel, M. C., Thauer, R. K., and Shima, S. (1997) Formylmethanofuran: Tetrahydromethanopterin formyltransferase from *Methanopyrus kandleri* - new insights into salt-dependence and thermostability, *Structure* 5, 635-646.
 54. Watanabe, K., Hata, Y., Kizaki, H., Katsube, Y., and Suzuki, Y. (1997) The refined crystal structure of *Bacillus cereus* oligo-1,6-glucosidase at 2.0 Å resolution: Structural characterization of proline-substitution sites for protein thermostabilization, *J. Mol. Biol.* 269, 142-153.
 55. Bogin, O., Peretz, M., Hacham, Y., Korkhin, Y., Frolow, F., Kalb, A. J., and Burstein, Y. (1998) Enhanced thermal stability of *Clostridium beijerinckii* alcohol dehydrogenase after strategic substitution of amino acid residues with prolines from the homologous thermophilic *Thermoanaerobacter brockii* alcohol dehydrogenase, *Protein Sci.* 7, 1156-1163.
 56. Yip, K. S. P., Britton, K. L., Stillman, T. J., Lebbink, J., De Vos, W. M., Robb, F. T., Vetriani, C., Maeder, D., and Rice, D. W. (1998) Insights into the molecular basis of thermal stability from the analysis of ion-pair networks in the glutamate dehydrogenase family *Eur. J. Biochem.* 255, 336-346.
 57. Yip, K. S. P., Stillman, T. J., Britton, K. L., Artymiuk, P. J., Baker, P. J., Sedelnikova, S. E., Engel, P. C., Pasquo, A., Chiaraluce, R., Consalvi, V., Scandurra, R., and Rice, D. W. (1995) The structure of *Pyrococcus-furiosus* glutamate-dehydrogenase reveals a key role for ion-pair networks in maintaining enzyme stability at extreme temperatures, *Structure* 3, 1147-1158.
 58. Elcock, A. H. (1998) The stability of salt bridges at high temperatures: Implications for hyperthermophilic proteins *J. Mol. Biol.* 284, 489-502.
 59. Xiao, L., and Honig, B. (1999) Electrostatic contributions to the stability of

- hyperthermophilic proteins *J. Mol. Biol.* 289, 1435-1444.
60. Kumar, S., Ma, B. Y., Tsai, C. J., and Nussinov, R. (2000) Electrostatic strengths of salt bridges in thermophilic and mesophilic glutamate dehydrogenase monomers, *Proteins* 38, 368-383.
 61. Lam, S. Y., Yeung, R. C. Y., Yu, T. H., Sze, K. H., and Wong, K. B. (2011) A rigidifying salt-bridge favors the activity of thermophilic enzyme at high temperatures at the expense of low temperature activity, *PLoS Biol.* 9, e1001027.
 62. Szilágyi, A., and Závodszy, P. (2000) Structural differences between mesophilic, moderately thermophilic and extremely thermophilic protein subunits: Results of a comprehensive survey, *Structure* 8, 493-504.
 63. Cambillau, C., and Claverie, J. M. (2000) Structural and genomic correlates of hyperthermostability, *J. Biol. Chem.* 275, 32383-32386.
 64. Daniel, R. M., Cowan, D. A., Morgan, H. W., and Curran, M. P. (1982) A correlation between protein thermostability and resistance to proteolysis, *Biochem. J.* 207.
 65. Vieille, C., and Zeikus, G. J. (2001) Hyperthermophilic enzymes: Sources, uses, and molecular mechanism for thermostability, *Microbiol. Mol. Biol. Rev.* 65, 1-43.
 66. Adams, M. W. W., and Kelly, R. M. (1995) Enzymes from microorganisms in extreme environments, *Chem. Eng. News* 73, 32-42.
 67. Bauer, M. W., Driskill, L. E., and Kelly, R. M. (1998) Glycosyl hydrolases from hyperthermophilic microorganisms, *Curr. Opin. Biotechnol.* 9, 141-145.
 68. Kim, M. S., Park, J. T., Kim, Y. W., Lee, H. S., Nyawira, R., Shin, H. S., Park, C. S., Yoo, S. H., Kim, Y. R., Moon, T. V., and Park, K. H. (2004) Properties of a novel thermostable glucoamylase from the hyperthermophilic archaeon *Sulfolobus solfataricus* in relation to starch processing, *Appl. Environ. Microbiol.* 70, 3933-3940.
 69. Rao, M., Tankasale, A., Ghatge, M., and Desphande, V. (1998) Molecular and biotechnological aspects of microbial proteases, *Microbiol. Mol. Biol. Rev.* 62, 597-634.
 70. Haki, G. D., and Rakshit, S. K. (2003) Developments in industrially important thermostable enzymes: A review, *Bioresour. Technol.* 89, 17-34.
 71. Eichler, J. (2001) Biotechnological uses of archaeal extremozymes, *Biotechnol. Adv.* 19, 261-278.
 72. Klingenberg, M., Hashwa, F., and Antrakikian, G. (1991) Properties of extremely thermostable proteases from anaerobic hyperthermophilic bacteria, *Appl. Microbiol. Biotechnol.* 34, 715-719.
 73. Niehaus, F., Bertoldo, C., Käler, M., and Antranikian, G. (1999) Extremophiles as a source of novel enzymes for industrial application, *Appl. Microbiol. Biotechnol.* 51, 711-729.
 74. Bauer, M. W., Driskill, L. E., Callen, W., Snead, M. A., Mathur, E. J., and Kelly, R. M. (1999) An endoglucanase, eglA, from the hyperthermophilic archaeon *Pyrococcus furiosus* hydrolyzes β -1,4 bonds in mixed-linkage

- (1→3),(1→4)- β -D-glucans and cellulose, *J. Bacteriol.* *181*, 284-290.
75. Morris, D. D., Gibbs, M. D., Chin, C. W. J., Koh, M.-H., Wong, K. K. Y., Allison, R. W., Nelson, P. J., and Bergquist, P. L. (1998) Cloning of the *xynB* gene from *Dictyoglomus thermophilum* Rt46B.1 and action of the gene product on kraft pulp, *Appl. Environ. Microbiol.* *64*, 1759-1765.
76. Saul, D. J., Williams, L. C., Reeves, R. A., Gibbs, M. D., and Bergquist, P. L. (1995) Sequence and expression of a xylanase gene from the hyperthermophile *Thermotoga* sp. strain FjSS3-B.1 and characterization of the recombinant enzyme and its activity on kraft pulp, *Appl. Environ. Microbiol.* *61*, 4110-4113.
77. Jaeger, K.-E., and Reetz, M. T. (1998) Microbial lipases from versatile tools for biotechnology, *Trends Biotechnol.* *16*, 396-403.
78. Hotta, Y., Ezaki, S., Atomi, H., and Imanaka, T. (2002) Extremely stable and versatile carboxylesterase from a hyperthermophilic archaeon, *Appl. Environ. Microbiol.* *68*, 3925-3931.
79. Ikeda, M., and Clark, D. S. (2000) Molecular cloning of extremely thermostable esterase gene from hyperthermophilic archaeon *Pyrococcus furiosus* in *Escherichia coli*, *Biotechnol. Bioeng.* *57*, 624-629.
80. Ando, S., Ishida, H., Kosugi, Y., and Ishikawa, K. (2002) Hyperthermostable endoglucanase from *Pyrococcus horikoshii*, *Appl. Environ. Microbiol.* *68*, 430-433.
81. Mullis, K., Faloona, F., Scarf, S., Saiki, R., Horn, G., and Erlich, H. (1986) Specific enzymatic amplification of DNA *in vitro* - the polymerase chain reaction, *Cold Spring Harbor Symposia on Quantitative Biology* *51*, 263-273.
82. Takagi, M., Nishioka, M., Kakihara, H., Kitabayashi, M., Inoue, H., Kawakami, B., Oka, M., and Imanaka, T. (1997) Characterization of DNA polymerase from *Pyrococcus* sp. strain KOD1 and its application to PCR, *Appl. Environ. Microbiol.* *63*, 4504-4510.
83. Kletzin, A. (1992) Molecular characterisation of a DNA ligase gene of the extremely thermophilic archaeon *Desulfurolobus ambivalens* shows close phylogenetic relationship to eukaryotic ligases, *Nucleic Acids Res.* *20*, 5389-5396.
84. Cheung, Y. Y., Lam, S. Y., Allen, M. D., Bycroft, M., and Wong, K. B. (2005) Crystal structure of a hyperthermophilic archaeal acylphosphatase from *Pyrococcus horikoshii* structural insights into enzymatic catalysis, thermostability, and dimerization, *Biochemistry* *44*, 4601-4611.
85. Georgette, D., Damien, B., Blaise, V., Depiereux, E., Uversky, V. N., Gerday, C., and Feller, G. (2003) Structural and functional adaptations to extreme temperatures in psychrophilic, mesophilic, and thermophilic DNA ligases, *J. Biol. Chem.* *278*, 37015-37023.
86. Bae, E., and Phillips, G. N. (2004) Structures and analysis of highly homologous psychrophilic, and thermophilic adenylate kinases, *J. Biol. Chem.* *279*, 28202-28208.
87. Collins, T., Meuwis, M. A., Gerday, C., and Feller, G. (2003) Activity, stability

- and flexibility in glycosidases adapted to extreme thermal environments, *J. Mol. Biol.* 328.
88. Olufsen, M., Smalas, A. O., Moe, E., and Brandsdal, B. O. (2005) Increased flexibility as a strategy for cold adaptation: A comparative molecular dynamics study of cold- and warm-active uracil DNA glycosylase, *J. Biol. Chem.* 280, 18042-18048.
 89. D'Amico, S., Sohler, J. S., and Feller, G. (2006) Kinetics and energetics of ligand binding determined by microcalorimetry: Insights into active site mobility in a psychrophilic α -amylase, *J. Mol. Biol.* 358, 1296-1304.
 90. Smalas, A. O., Heimstad, E. S., Hordvik, A., Willassen, N. P., and Male, R. (1994) Cold adaption of enzymes: Structural comparison between salmon and bovine trypsins, *Proteins* 20, 149-166.
 91. Fields, P. A., and Somero, G. N. (1998) Hot spots in cold adaptation: Localized increases in conformational flexibility in lactate dehydrogenase A4 orthologs of Antarctic notothenioid fishes, *Proc. Natl. Acad. Sci. USA* 95, 11476-11481.
 92. Feller, G. (2006) Life at low temperatures: Is disorder the driving force?, *Extremophiles* 11, 211-216.
 93. Siddiqui, K., and Cavicchioli, R. (2006) Cold-adapted enzymes, *Annu. Rev. Biochem.* 75, 211-216.
 94. Zavodszky, P., Kardos, J., Svingor, A., and Petsko, G. A. (1998) Adjustment of conformational flexibility is a key event in the thermal adaptation of proteins, *Proc. Natl. Acad. Sci. USA* 95, 7406-7411.
 95. Fitter, J., and Heberle, J. (2000) Structural equilibrium fluctuations in mesophilic and thermophilic α -amylase, *Biophys. J.* 79, 1629-1636.
 96. Fitter, J., Herrmann, R., Dencher, N. A., Blume, A., and Hauss, T. (2001) Activity and stability of a thermostable α -amylase compared to its mesophilic homologue: Mechanism of thermal adaptation, *Biochemistry* 40, 10723-10731.
 97. Hernandez, G., Jr., J., F. E., Adams, M. W. W., and LeMaster, D. M. (2000) Millisecond time scale conformational flexibility in a hyperthermophile protein at ambient temperature, *Proc. Natl. Acad. Sci. USA* 97, 3166-3170.
 98. Charlton, P. A., Young, D. W., Birdsall, B., Feeney, J., and Roberts, G. C. K. (1979) Stereochemistry of reduction of folic-acid using dihydrofolate-reductase, *J. Chem. Soc., Chem. Commun.*, 922-924.
 99. Charlton, P. A., Young, D. W., Birdsall, B., Feeney, J., and Roberts, G. C. K. (1985) Stereochemistry of reduction of the vitamin folic-acid by dihydrofolate-reductase, *J. Chem. Soc., Perkin Trans. 1*, 1349-1353.
 100. Haslam, N., and Probert, C. S. (1998) An audit of the investigation and treatment of folic acid deficiency, *J. R. Soc. Med.* 91, 72-73.
 101. Roland, S., Ferone, R., Harvey, R. J., Styles, V. L., and Morrison, R. W. (1979) The characteristics and significance of sulfonamides as substrates for *Escherichia coli* dihydrofolate synthase, *J. Biol. Chem.* 254, 10337-10345.
 102. Achari, A., Somers, D. O., Champness, J. N., Bryant, P. K., Rosemond, J., and Stammers, D. K. (1997) Crystal structure of the anti-bacterial sulfonamide drug target dihydropteroate synthase, *Nat. Struct. Biol.* 4, 490-497.

103. Meyer, L. M., Miller, F. R., Rowen, M. J., Bock, G., and Rutzky, J. (1950) Treatment of acute leukemia with amethopterin (4-amino,10-methyl pteroyl glutamic acid), *Acta Haematol.* 4, 157-167.
104. Wright, J. C., Prigot, A., and Wright, B. P. (1951) An evaluation of folic acid antagonists in adults with neoplastic diseases. A study of 93 patients with incurable neoplasms, *J. Nat. Med. Assoc.* 43, 211-240.
105. Li, M. C., Hertz, R., and Spencer, D. B. (1956) Effect of methotrexate upon choriocarcinoma, *Proc. Soc. Exp. Biol. Med.* 93, 361-366.
106. Wright, J. C., Lyons, M., and Walker, D. G. (1964) Observations on the use of cancer chemotherapeutic agents in patients with mycosis fungoides, *Cancer* 17, 1045-1062.
107. Rossi, A., Ricciardi, S., Maione, P., de Marinis, F., and Gridelli, C. (2009) Pemetrexed in the treatment of advanced non-squamous lung cancer, *Lung Cancer* 66, 141-149.
108. Hazarika, M., White, R. M., Johnson, J. R., and Pazdur, R. (2004) FDA drug approval summaries: Pemetrexed (Alimta), *Oncologist* 9, 482-488.
109. Rajagopalan, P. T. R., Zhang, Z., McCourt, L., Dwyer, M., Benkovic, S. J., and Hammes, G. G. (2002) Interaction of dihydrofolate reductase with methotrexate: Ensemble and single-molecule kinetics, *Proc. Natl. Acad. Sci. USA* 99, 13481-13486.
110. Heaslet, H., Harris, M., Fahnoe, K., Sarver, R., Putz, H., Chang, J., Subramanyam, C., Barreiro, G., and Miller, J. R. (2009) Structural comparison of chromosomal and exogenous dihydrofolate reductase from *Staphylococcus aureus* in complex with the potent inhibitor trimethoprim, *Proteins: Struct., Funct., Bioinf.* 76, 706-717.
111. Thomson, C. J. (1993) Trimethoprim and brodimoprim resistance of gram-positive and gram-negative bacteria, *J. Chemother.* 5, 458-464.
112. Aschhoff, H. S., and Vergin, H. (1979) Tetroxoprim - a new inhibitor of bacterial dihydrofolate reductase, *J. Antimicrob. Chemother.* 5, 19-25.
113. Gatton, M. L., Martin, L. B., and Cheng, Q. (2004) Evolution of resistance of sulfadoxine-pyrimethamine in *Plasmodium falciparum*, *Antimicrob. Agents Chemother.* 48, 2116-2123.
114. Carrington, H. C., Crowther, A. F., Davey, D. G., Levi, A. A., and Rose, F. L. (1951) A metabolite of paludrine with high antimalarial activity, *Nature* 168, 1080.
115. Peppard, W. J., and Schuenke, C. D. (2008) Iclaprim, a diaminopyrimidine dihydrofolate reductase inhibitor for the potential treatment of antibiotic-resistant staphylococcal infections, *Curr. Opin. Investig. Drug* 9, 210-225.
116. Mui, E. J., Schiehser, G. A., Milhous, W. K., Hsu, H., Roberts, C. W., Kirisits, M., Muench, S., Rice, D., Dubey, J. P., Fowble, J. W., Rathod, P. K., Queener, S. F., Liu, S. R., Jacobus, D. P., and McLeod, R. (2008) Novel triazine JPC-2067-B inhibits *Toxoplasma gondii* in vitro and in vivo, *PLoS Negl. Trop. Dis.* 2, e190.

117. Matthews, D. A., Alden, R. A., Bolin, J. T., Freer, S. T., Hamlin, R., Xuong, N., Kraut, J., Poe, M., Williams, M., and Hoogsteen, K. (1977) Dihydrofolate reductase: X-ray structure of the binary complex with methotrexate, *Science* 197, 452-455.
118. Dams, T., Auerbach, G., Bader, G., Jacob, U., Ploom, T., Huber, R., and Jaenicke, R. (2000) The crystal structure of dihydrofolate reductase from *Thermotoga maritima*: Molecular features of thermostability, *J. Mol. Biol.* 297, 659-672.
119. Bolin, J. T., Filman, D. J., Matthews, D. A., Hamlin, R. C., and Kraut, J. (1982) Crystal-structures of *Escherichia-coli* and *Lactobacillus-casei* dihydrofolate-reductase refined at 1.7 Å resolution. 1. General features and binding of methotrexate, *J. Biol. Chem.* 257, 3650-3662.
120. Kim, H. S., Damo, S. M., Lee, S. Y., Wemmer, D., and Klinman, J. P. (2005) Structure and hydride transfer mechanism of a moderate thermophilic dihydrofolate reductase from *Bacillus stearothermophilus* and comparison to its mesophilic and hyperthermophilic homologues, *Biochemistry* 44, 11428-11439.
121. Li, R., Sriawaraporn, R., Chitnumsub, P., Sirawaraporn, W., Wooden, J., Athappilly, F., Turley, S., and Hol, W. G. (2000) Three-dimensional structure of *M. tuberculosis* dihydrofolate reductase reveals opportunities for the design of novel tuberculosis drugs., *J. Mol. Biol.* 295, 307-323.
122. Whitlow, M., Howard, A. J., Stewart, D., Hardman, K. D., Kuyper, L. F., Baccanari, D. P., Fling, M. E., and Tansik, R. L. (1997) X-ray crystallographic studies of *Candida albicans* dihydrofolate reductase. High resolution structures of the holoenzyme and an inhibited ternary complex., *J. Mol. Biol.* 272.
123. McTigue, M. A., Davies 2nd, J. F., Kaufman, B. T., and Kraut, J. (1993) Crystal structures of chicken liver dihydrofolate reductase: Binary thioNADP⁺ and ternary thioNADP⁺.biopterin complexes., *Biochemistry* 32, 6855-6862.
124. Cody, V., and Pace, J. (2011) Structural analysis of *Pneumocystis carinii* and human DHFR complexes with NADPH and a series of five potent 6-[5'-(ω-carboxyalkoxy)benzyl]pyrido[2,3-d]pyrimidine derivatives, *Acta Crystallogr., Sect. D* 67, 1-7.
125. Sawaya, M. R., and Kraut, J. (1997) Loop and subdomain movements in the mechanism of *Escherichia coli* dihydrofolate reductase: Crystallographic evidence, *Biochemistry* 36, 586-603.
126. Rod, T. H., and Brooks III, C. L. (2003) How dihydrofolate reductase facilitates protonation of dihydrofolate, *J. Am. Chem. Soc.* 125, 8718-8719.
127. Bystroff, C., Oatley, S. J., and Kraut, J. (1990) Crystal structures of *Escherichia coli* dihydrofolate reductase: The NADP⁺ holoenzyme and the folate-NADP⁺ ternary complex. substrate binding and a model for the transition state, *Biochemistry* 29, 3263-3277.
128. Fierke, C. A., and Benkovic, S. J. (1989) Probing the functional role of threonine-113 of *Escherichia coli* dihydrofolate reductase for its effect on

- turnover efficiency, catalysis and binding, *Biochemistry* 28, 478-486.
129. Warren, M. S., Brown, K. A., Farnum, M. F., Howell, E. E., and Kraut, J. (1991) Investigation of the functional role of tryptophan-22 in *Escherichia coli* dihydrofolate reductase by site-directed mutagenesis, *Biochemistry* 30, 11092-11103.
 130. Villafranca, J. E., Howell, E. E., Voet, D. H., Strobel, M. J., Ogden, R. C., Abelson, J. N., and Kraut, J. (1983) Directed mutagenesis of dihydrofolate reductase, *Science* 222, 782-788.
 131. Howell, E. E., Villafranca, J. E., Warren, M. S., Oatley, S. J., and Kraut, J. (1986) Functional role of aspartic acid-27 in dihydrofolate reductase by mutagenesis, *Science* 231, 1123-1129.
 132. Appleman, J. R., Howell, E. E., Kraut, J., and Blakely, R. L. (1990) Role of aspartate 27 of dihydrofolate reductase from *Escherichia coli* interconversion of active and inactive conformers and binding of NADPH, *J. Biol. Chem.* 265, 5579-5584.
 133. Miller, G. P., and Benkovic, S. J. (1998) Stretching exercises - flexibility in dihydrofolate reductase catalysis, *Chem. Biol.* 5, R105-R113.
 134. Chen, Y.-Q., Kraut, J., and Callender, R. (1997) pH-dependent conformational changes in *Escherichia coli* dihydrofolate reductase revealed by Raman difference spectroscopy, *Biophys. J.* 72, 936-941.
 135. McTigue, M. A., Davies, J. F., Kaufman, B. T., and Kraut, J. (1992) Crystal structure of chicken liver dihydrofolate reductase complexed with NADP⁺ and biopterin, *Biochemistry* 31, 7264-7273.
 136. Deng, H., and Callender, R. (1998) Structure of dihydrofolate when bound to dihydrofolate reductase, *J. Am. Chem. Soc.* 120, 7730-7737.
 137. Shrimpton, P., and Allemann, R. K. (2002) Role of water in the catalytic cycle of *E. coli* dihydrofolate reductase, *Protein Sci.* 11, 1442-1451.
 138. Fierke, C. A., Johnson, K. A., and Benkovic, S. J. (1987) Construction and evaluation of the kinetic scheme associated with dihydrofolate reductase from *Escherichia coli*, *Biochemistry* 26, 4085-4092.
 139. Stone, S. R., and Morrison, J. F. (1982) Kinetic mechanism of the reaction catalyzed by dihydrofolate reductase from *Escherichia coli* *Biochemistry* 21, 3757-3765.
 140. Penner, M. H., and Frieden, C. (1987) Kinetic analysis of the mechanism of *Escherichia coli* dihydrofolate reductase, *J. Biol. Chem.* 262, 15908-15914.
 141. Falzone, C. J., Wright, P. E., and Benkovic, S. J. (1994) Dynamics of a flexible loop in dihydrofolate reductase from *Escherichia coli* and its implication for catalysis, *Biochemistry* 33, 439-442.
 142. Li, L., Falzone, C. J., Wright, P. E., and Benkovic, S. J. (1992) Functional role of mobile loop of *Escherichia coli* dihydrofolate reductase in transition-state stabilization, *Biochemistry* 31, 7826-7833.
 143. Bystroff, C., and Kraut, J. (1991) Crystal structure of unliganded *Escherichia coli* dihydrofolate reductase. Ligand induced conformational changes and cooperativity in binding, *Biochemistry* 30, 2227-2239.

144. Harris, R. J., Meskys, R., Sutcliffe, M. J., and Scrutton, N. S. (2000) Kinetic studies of the mechanism of carbon-hydrogen bond breakage by the heterotetrameric sarcosine oxidase of *Arthrobacter* sp. 1-IN, *Biochemistry* 39, 1189-1198.
145. Basran, J., Sutcliffe, M. J., and Scrutton, N. S. (1999) Enzymatic H-transfer requires vibration-driven extreme tunneling, *Biochemistry* 39, 3218-3222.
146. Bahnson, B. J., Colby, T. D., Chin, J. K., Goldstein, B. M., and Klinman, J. P. (1997) A link between protein structure and enzyme catalyzed hydrogen tunneling, *Proc. Natl. Acad. Sci. USA* 94, 12797-12802.
147. Chin, J. K., and Klinman, J. P. (2000) Probes of a role for remote binding interactions on hydrogen tunneling in the horse liver alcohol dehydrogenase reaction, *Biochemistry* 39, 1278-1284.
148. Roston, D., Islam, Z., and Kohen, A. (2013) Isotope effects as probes for enzyme catalyzed hydrogen-transfer reactions, *Molecules* 18, 5543-5567.
149. Knapp, M. J., and Klinman, J. P. (2002) Environmentally coupled hydrogen tunneling, *Eur. J. Biochem.* 269, 3113-3132.
150. Klinman, J. P. (2009) An integrated model for enzyme catalysis emerges from studies of hydrogen tunneling, *Chem. Phys. Lett.* 471, 179-193.
151. Haslett, J. W. (1973) Translation of phase waves of de Broglie, *Am. J. Phys.* 41, 445.
152. Bell, R. P. (1980) *The tunnel effect in chemistry*, Chapman and Hall, London.
153. Agarwal, P. K., Billeter, S. R., Rajagopalan, P. T. R., Benkovic, S. J., and Hammes-Schiffer, S. (2002) Network of coupled promoting motions in enzyme catalysis, *Proc. Natl. Acad. Sci. USA* 99, 2794-2799.
154. Swanwick, R. S., Maglia, G., Tey, L.-H., and Allemann, R. K. (2006) Coupling of protein motions and hydrogen transfer during catalysis by *Escherichia coli* dihydrofolate reductase, *Biochem. J.* 394, 259-265.
155. Maglia, G., and Allemann, R. K. (2003) Evidence for environmentally coupled hydrogen tunneling during dihydrofolate reductase catalysis, *J. Am. Chem. Soc.* 125, 13372-13373.
156. Rickert, K. W., and Klinman, J. P. (1997) Nature of hydrogen transfer in soybean lipoxygenase 1: Separation of primary and secondary isotope effects, *Biochemistry* 38, 12219-12228.
157. Nesheim, J. C., and Lipscomb, J. D. (1996) Large kinetic isotope effects in methane oxidation catalyzed by methane monooxygenase: Evidence for C-H bond cleavage in a reaction cycle intermediate, *Biochemistry* 35, 10240-10247.
158. Kohen, A., Cannio, R., Bartolucci, S., and Klinman, J. P. (1999) Enzyme dynamics and hydrogen tunnelling in a thermophilic alcohol dehydrogenase, *Nature* 399, 496-499.
159. Antoniou, D., Caratzoulas, S., Kalyanaraman, C., Mincer, J. S., and Schwartz, S. D. (2002) Barrier passage and protein dynamics in enzymatically catalyzed reactions, *Eur. J. Biochem.* 269, 3103-3112.
160. Mincer, J. S., and Schwartz, S. D. (2003) A computational method to identify

- residues important in creating a protein promoting vibration in enzymes, *J. Phys. Chem. B* *107*, 366-371.
161. Mincer, J. S., and Schwartz, S. D. (2004) Rate-promoting vibrations and coupled hydrogen-electron transfer reactions in the condensed phase: a model for enzyme catalysis, *J. Chem. Phys.* *120*, 7755-7760.
 162. Basner, J. E., and Schwartz, S. D. (2004) Donor-acceptor distance and protein promoting vibration coupling hydride transfer: A possible mechanism for kinetic control in isozymes of human lactate dehydrogenase, *J. Phys. Chem. B* *108*, 444-451.
 163. Sutcliffe, M. J., and Scrutton, N. S. (2002) A new conceptual framework for enzyme catalysis: Hydrogen tunneling coupled to enzyme dynamics in flavoprotein and quinoprotein enzymes, *Eur. J. Biochem.* *269*, 3096-3102.
 164. Masgrau, L., Basran, J., Hothi, P., Sutcliffe, M. J., and Scrutton, N. S. (2004) Hydrogen tunneling in quinoproteins, *Arch. Biochem. Biophys.* *428*, 41-51.
 165. Garcia-Viloca, M., Truhlar, D. G., and Gao, J. (2003) Reaction-path energetics and kinetics of the hydride transfer reaction catalysed by dihydrofolate reductase, *Biochemistry* *42*, 13558-13575.
 166. Knapp, M. J., Rickert, K., and Klinman, J. P. (2002) Temperature dependent isotope effects in soybean lipoxygenase-1: Correlating hydrogen tunneling with protein dynamics, *J. Am. Chem. Soc.* *124*, 3865-3874.
 167. Nagel, Z. D., and Klinman, J. P. (2009) A 21st century revisionist's view at a turning point in enzymology, *Nat. Chem. Biol.* *5*, 543-550.
 168. Benkovic, S. J., and Hammes-Schiffer, S. (2006) Enzyme motions inside and out, *Science* *312*, 208-209.
 169. Olsson, M. H. M., Parson, W. W., and Warshel, A. (2006) Dynamical contributions to enzyme catalysis: Critical tests of a popular hypothesis, *Chem. Rev.* *106*, 1737-1756.
 170. Pislakov, A. V., Cao, J., Kamerlin, S. C. L., and Warshel, A. (2009) Enzyme millisecond conformational dynamics do not catalyze the chemical step, *Proc. Natl. Acad. Sci. USA* *106*, 17359-17364.
 171. Antoniou, D., and Schwartz, S. D. (2006) Protein dynamics and enzymatic chemical barrier passage, *Phil. Trans. Roy. Soc. B* *361*, 1433-1438.
 172. Hay, S., Pudney, C. R., and Scrutton, N. S. (2009) Structural and mechanistic aspects of flavoproteins: Probes of hydrogen tunnelling, *FEBS J.* *276*, 3930-3941.
 173. Kuznetsov, A. M., and Ulstrup, J. (1999) Proton and hydrogen atom tunnelling in hydrolytic and redox enzyme reactions, *Can. J. Chem.* *77*, 1085-1096.
 174. Miller, G. P., and Benkovic, S. J. (1998) Strength of an interloop hydrogen bond determines the kinetic pathway in catalysis by *Escherichia coli* dihydrofolate reductase *Biochemistry* *37*, 6336-6342.
 175. Miller, G. P., Wahnon, D. C., and Benkovic, S. J. (2001) Interloop contacts modulate ligand cycling during catalysis by *Escherichia coli* dihydrofolate reductase, *Biochemistry* *40*, 867-875.
 176. Cameron, C. E., and Benkovic, S. J. (1997) Evidence for a functional role of

- the dynamics of Glycine-121 of *Escherichia coli* dihydrofolate reductase obtained from kinetic analysis of a site-directed mutant, *Biochemistry* 36, 15792-15800.
177. Miller, G. P., and Benkovic, S. J. (1998) Deletion of a highly motional residue affects formation of the Michaelis complex for *Escherichia coli* dihydrofolate reductase, *Biochemistry* 37, 6327-6335.
178. Watney, L. B., Agarwal, P. K., and Hammes-Schiffer, S. (2003) Effect of mutation on enzyme motion in dihydrofolate reductase, *J. Am. Chem. Soc.* 125, 3745-3750.
179. Swanwick, R. S., Shrimpton, P. J., and Allemann, R. K. (2004) Pivotal role of Gly 121 in dihydrofolate reductase from *Escherichia coli*: The altered structure of a mutant enzyme may form the basis of its diminished catalytic performance, *Biochemistry* 43, 4119-4127.
180. Rod, T. H., Radkiewicz, J. L., and Brooks III, C. L. (2003) Correlated motions and the effect of distal mutation in dihydrofolate reductase catalysis, *Proc. Natl. Acad. Sci. USA* 100, 6980-6985.
181. Epstein, D. M., Benkovic, S. J., and Wright, P. E. (1995) Dynamics of the dihydrofolate reductase-folate complex: Catalytic sites and regions known to undergo conformational change exhibit diverse dynamical features, *Biochemistry* 34, 11037-11048.
182. Osborne, M. J., Schnell, J., Benkovic, S. J., Dyson, H. J., and Wright, P. E. (2001) Backbone dynamics in dihydrofolate reductase complexes: Role of loop flexibility in the catalytic mechanism, *Biochemistry* 40, 9846-9859.
183. Radkiewicz, J. L., and III, C. L. B. (2000) Protein dynamics in enzymatic catalysis: Exploration of dihydrofolate reductase, *J. Am. Chem. Soc.* 122, 225-231.
184. Agarwal, P. K., Billeter, S. R., and Hammes-Schiffer, S. (2002) Nuclear quantum effects and enzyme dynamics in dihydrofolate reductase catalysis, *J. Phys. Chem. B* 106, 3283-3293.
185. Boehr, D. D., McElheny, D., Dyson, H. J., and Wright, P. E. (2006) The dynamic energy landscape of dihydrofolate reductase catalysis *Science* 313, 1638-1642.
186. Schnell, J. R., Dyson, H. J., and Wright, P. E. (2004) Structure, dynamics, and catalytic function of dihydrofolate reductase, *Annu. Rev. Biophys. Biomol. Struct.* 33, 119-140.
187. Bhabha, G., Lee, J., Ekiert, D. C., Gam, J., Wilson, I. A., Dyson, H. J., Benkovic, S. J., and Wright, P. E. (2011) A dynamic knockout reveals that conformational fluctuation influence the chemical step of enzyme catalysis, *Science* 332, 234-238.
188. Adamczyk, A. J., Cao, J., Kamerlin, S. C. L., and Warshel, A. (2011) Catalysis by dihydrofolate reductase and other enzymes arises from electrostatic preorganization, not conformational motions, *Proc. Natl. Acad. Sci. USA* 108, 14115-14120.
189. Loveridge, E. J., Behiry, E. M., Guo, J., and Allemann, R. K. (2012) Evidence

- that a 'dynamic knockout' in *Escherichia coli* dihydrofolate reductase does not affect the chemical step of catalysis, *Nat. Chem.* *4*, 292-297.
190. Hay, S., Pudney, C. R., Sutcliffe, M. J., and Scrutton, N. S. (2008) Are environmentally coupled enzymatic hydrogen tunneling reactions influenced by changes in solution viscosity?, *Angew. Chem. Int. Ed.* *47*, 537-540.
191. Loveridge, E. J., Tey, L.-H., and Allemann, R. K. (2010) Solvent effects on catalysis by *Escherichia coli* dihydrofolate reductase, *J. Am. Chem. Soc.* *132*, 1137-1143.
192. Loveridge, E. J., Evans, R. M., and Allemann, R. K. (2008) Solvent effects on environmentally coupled hydrogen tunnelling during catalysis by dihydrofolate reductase from *Thermotoga maritima*, *Chem. -Eur. J.* *14*, 10782-10788.
193. Loveridge, E. J., Tey, L.-H., Behiry, E. M., Dawson, W. M., Evans, R. M., Whittaker, S. B.-M., Gunther, U. L., Williams, C., Crump, M. P., and Allemann, R. K. (2011) The role of large-scale motion in catalysis by dihydrofolate reductase, *J. Am. Chem. Soc.* *133*, 20561-20570.
194. van den Bedem, H., Bhabha, G., Yang, K., Wright, P. E., and Fraser, J. S. (2013) Automated identification of functional dynamic contact networks from X-ray crystallography, *Nat. Methods* *10*, 896-902.
195. Silva, R. G., Murkin, A. S., and Schramm, V. L. (2011) Femtosecond dynamics coupled to chemical barrier crossing in a Born-Oppenheimer enzyme, *Proc. Natl. Acad. Sci. USA* *108*.
196. Kipp, D. R., SILVA, R. G., and Schramm, V. L. (2011) Mass-dependent bond vibrational dynamics influence catalysis by HIV-1 protease, *J. Am. Chem. Soc.* *133*, 19358-19361.
197. Luk, L. Y. P., Ruiz-Pernia, J. J., Dawson, W. M., Roca, M., Loveridge, E. J., Glowacki, D. R., Harvey, J. N., Mulholland, A. J., Tuñón, I., Moliner, V., and Allemann, R. K. (2013) Unraveling the role of protein dynamics in dihydrofolate reductase catalysis, *Proc. Natl. Acad. Sci. USA* *110*, 16344-16349.
198. Loveridge, E. J., and Allemann, R. K. (2011) Effect of pH on hydride transfer by *Escherichia coli* dihydrofolate reductase, *ChemBioChem* *12*, 1258-1262.
199. Glowacki, D. R., Harvey, J. N., and Mulholland, A. J. (2012) Taking Ockham's razor to enzyme dynamics and catalysis, *Nat. Chem.* *4*, 169-176.
200. Glowacki, D. R., Harvey, J. N., and Mulholland, A. J. (2012) Protein dynamics and enzyme catalysis: The ghost in the machine?, *Biochem. Soc. Trans.* *40*, 515-521.
201. Huber, R., Langworthy, T. A., König, H., Thomm, M., Woese, C. R., Sleytr, U. B., and Stetter, K. O. (1986) *Thermotoga maritima* sp. nov. represents a new genus of unique extremely thermophilic eubacteria growing up to 90 °C, *Arch. Microbiol.* *144*, 324-333.
202. Maglia, G., Javed, M. H., and Allemann, R. K. (2003) Hydride transfer during catalysis by dihydrofolate reductase from *Thermotoga maritima*, *Biochem. J.* *374*, 529-535.

203. Dams, T., Bohm, G., Auerbach, G., Bader, G., Schuring, H., and Jaenicke, R. (1998) Homo-dimeric recombinant dihydrofolate reductase from *Thermotoga maritima* shows extreme intrinsic stability, *Biol. Chem.* *379*, 367-371.
204. Dams, T., and Jaenicke, R. (1999) Stability and folding of dihydrofolate reductase from the hyperthermophilic bacterium *Thermotoga maritima*, *Biochemistry* *38*, 9169-9178.
205. Wilquet, V., Gaspar, J. A., van de Lande, M., van de Castele, M., Legrain, C., Meiering, E. M., and Glansdorff, N. (1998) Purification and characterization of recombinant *Thermotoga maritima* dihydrofolate reductase, *Eur. J. Biochem.* *255*, 628-637.
206. Pang, J. Y., and Allemann, R. K. (2007) Molecular dynamics simulation of thermal unfolding of *Thermotoga maritima* DHFR, *Phys. Chem. Chem. Phys.* *9*, 711-718.
207. Loveridge, E. J., Maglia, G., and Allemann, R. K. (2009) The role of arginine 28 in catalysis by dihydrofolate reductase from the hyperthermophile *Thermotoga maritima*, *ChemBioChem* *10*, 2624-2627.
208. Loveridge, E. J., and Allemann, R. K. (2010) The temperature dependence of the kinetic isotope effects of dihydrofolate reductase from *Thermotoga maritima* is influenced by intersubunit interactions, *Biochemistry* *49*, 5390-5396.
209. Loveridge, E. J., Rodriguez, R. J., Swanwick, R. S., and Allemann, R. K. (2009) Effect of dimerization on the stability and catalytic activity of dihydrofolate reductase from the hyperthermophile *Thermotoga maritima*, *Biochemistry* *48*, 5922-5933.
210. Allemann, R. K., Evans, R. M., and Loveridge, E. J. (2009) Probing coupled motions in enzymatic hydrogen tunnelling reactions, *Biochem. Soc. Trans.* *37*, 349-353.
211. Evans, R. M., Behiry, E. M., Tey, L.-H., Guo, J., Loveridge, E. J., and Allemann, R. K. (2010) Catalysis by dihydrofolate reductase from the psychropiezophile *Moritella profunda*, *ChemBioChem* *11*, 2010-2017.
212. Hay, S., Evans, R. M., Levy, C., Loveridge, E. J., Wang, X., Leys, D., Allemann, R. K., and Scrutton, N. S. (2009) Are the catalytic properties of enzymes from piezophilic organisms pressure adapted?, *ChemBioChem* *10*, 2348-2353.
213. Cummins, P. L., and Gready, J. E. (2001) Energetically most likely substrate and active-site protonation sites and pathways in the catalytic mechanism of dihydrofolate reductase, *J. Am. Chem. Soc.* *123*, 3418-3428.
214. Loveridge, E. J., Behiry, E. M., Swanwick, R. S., and Allemann, R. K. (2009) Different reaction mechanisms for mesophilic and thermophilic dihydrofolate reductases, *J. Am. Chem. Soc.* *131*, 6926-6927.
215. Pang, J. Y., Pu, J. Z., Gao, J. L., Truhlar, D. G., and Allemann, R. K. (2006) Hydride transfer reaction catalyzed by hyperthermophilic dihydrofolate reductase is dominated by quantum mechanical tunneling and is promoted by both inter- and intramonomeric correlated motions, *J. Am. Chem. Soc.* *128*,

- 8015-8023.
216. Donk, P. J. (1920) A highly resistant thermophilic organism, *J. Bacteriol.* 5, 373-374.
217. Nazina, T. N., Tourova, T. P., Poltarau, A. B., Novikova, E. V., Grigoryan, A. A., Ivanova, A. E., Lysenko, A. M., Petrunyaka, V. V., Osipov, G. A., Belyaev, S. S., and Ivanov, M. V. (2001) Taxonomic study of aerobic thermophilic Bacilli: Descriptions of *Geobacillus subterraneus* gen. nov., sp. nov and *Geobacillus uzenensis* sp. nov from petroleum reservoirs and transfer of *Bacillus stearothermophilus*, *Bacillus thermocatenulatus*, *Bacillus thermoleovorans*, *Bacillus kaustophilus*, *Bacillus thermoglucosidasius* and *Bacillus thermodenitrificans* to *Geobacillus* as the new combinations *G. stearothermophilus*, *G. thermocatenulatus*, *G. thermoleovorans*, *G. kaustophilus*, *G. thermoglucosidasius* and *G. thermodenitrificans*, *Int. J. Syst. Evol. Micr.* 51, 433-446.
218. Hashizume, S., Sekiguchi, T., and Nosoh, Y. (1976) Effect of temperature on viability of *Bacillus-stearothermophilus* *Arch. Microbiol.* 107, 75-80.
219. Oyeyemi, O. A., Sours, K. M., Lee, T., Resing, K. A., Ahn, N. G., and Klinman, J. P. (2010) Temperature dependence of protein motions in a thermophilic dihydrofolate reductase and its relationship to catalytic efficiency, *Proc. Natl. Acad. Sci. USA* 107, 10074-10079.
220. Meinhold, L., Clement, D., Tehei, M., Daniel, R., Finney, J. L., and Smith, J. C. (2008) Protein dynamics and stability: The distribution of atomic fluctuations in thermophilic and mesophilic dihydrofolate reductase derived using elastic incoherent neutron scattering, *Biochem. J.* 94, 4812-4818.
221. Oyeyemi, O. A., Sours, K. M., Lee, T., Kohen, A., Resing, K. A., Ahn, N. G., and Klinman, J. P. (2011) Comparative hydrogen-deuterium exchange for a mesophilic vs thermophilic dihydrofolate reductase at 25 °C: Identification of a single active site region with enhanced flexibility in the mesophilic protein, *Biochemistry* 50, 8251-8260.
222. Brinboim, H. C., and Doly, J. (1979) A rapid alkaline extraction procedure for screening recombinant plasmid DNA, *Nucleic Acids Res.* 7, 1513-1523.
223. Studier, F. W., and Moffatt, B. A. (1986) Use of bacteriophage T7 RNA polymerase to direct selective high-level expression of cloned genes, *J. Mol. Biol.* 189, 113-130.
224. Zakrzewski, S. F. (1966) On mechanism of chemical and enzymatic reduction of folate and dihydrofolate *J. Biol. Chem.* 241, 2962-2967.
225. Jeong, S. S., and Gready, J. E. (1994) A method of preparation and purification of (4R)-deuterated-reduced nicotinamide adenine dinucleotide phosphate, *Anal. Biochem.* 221, 273-277.
226. Orr, G. A., and Blanchard, J. S. (1984) High-performance ion-exchange separation of oxidized and reduced nicotinamide adenine dinucleotide, *Anal. Biochem.* 142, 232-234.
227. Greenfield, N., and Fasman, G. D. (1969) Computed circular dichroism spectra for the evaluation of protein conformation, *Biochemistry* 8, 4108-4116.

228. Kumar, S., Tsai, C. J., and Nussinov, R. (2000) Factors enhancing protein thermostability, *Protein Eng.* 13, 179-191.
229. Manavalan, P., and Johnson, W. C. (1983) Sensitivity of circular dichroism to protein tertiary structure class, *Nature* 305, 831-832.
230. Ng, T. M., and Schaffner, D. W. (1997) Mathematical models for the effects of pH, temperature, and sodium chloride on the growth of *Bacillus stearothermophilus* in salty carrots, *Appl. Environ. Microbiol.* 63, 1237-1243.
231. Koch, R., Canganella, F., Hippe, H., Jahnke, K. D., and Antranikian, G. (1997) Purification and properties of a thermostable pullulanase from a newly isolated thermophilic anaerobic bacterium, *Fervidobacterium pennavorans* Ven5, *Appl. Environ. Microbiol.* 63, 1088-1094.
232. Klingenberg, M., Galunsky, B., Sjolholm, C., Kasche, V., and Antranikian, G. (1995) Purification and properties of a highly thermostable, sodium dodecyl sulfate-resistant and stereospecific proteinase from the extremely thermophilic archaeon *Thermococcus stetteri*, *Appl. Environ. Microbiol.* 61, 3098-3104.
233. Andreotti, G., Cubellis, M. V., Nitti, G., Sannia, G., Mai, X. H., Adams, M. W. W., and Marino, G. (1995) An extremely thermostable aromatic aminotransferase from the hyperthermophilic archaeon *Pyrococcus furiosus*, *Biochim. Biophys. Acta* 1247, 90-96.
234. Hahn, G. M., and Li, G. C. (1982) Thermotolerance and heat shock proteins in mammalian cells, *Radiat. Res.* 92, 452-457.
235. Davidson, D., and Simon, J.-P. (1983) Thermal adaptation and acclimation of ecotypic populations of *Spirodela polyrhiza* (lemnaceae): Thermostability and apparent activation energy of NAD malate dehydrogenase, *J. Therm. Biol.* 8, 289-296.
236. Westermann, P., Ahring, B. K., and Ham, R. A. (1989) Temperature compensation in *Methanosarcina barkeri* by modulation of hydrogen and acetate affinity, *Appl. Environ. Microbiol.* 55, 1262-1266.
237. Londesborough, J., and Lukkari, T.-M. (1980) The pH and temperature dependence of the activity of the high K_m cyclic nucleotide phosphodiesterase of bakers' yeast, *J. Biol. Chem.* 255, 9262-9267.
238. Silvius, J. R., Read, B. D., and McElhaney, R. N. (1978) Membrane enzymes: Artifacts in arrhenius plots due to temperature dependence of substrate-binding affinity, *Science* 199, 902-904.
239. Stone, S. R., and Morrison, J. F. (1984) Catalytic mechanism of the dihydrofolate reductase reaction as determined by pH studies, *Biochemistry* 23, 2753-2758.
240. Hay, S., Pudney, C. R., Sutcliffe, M. J., and Scrutton, N. S. (2008) Are Environmentally Coupled Enzymatic Hydrogen Tunneling Reactions Influenced by Changes in Solution Viscosity?, *Angewandte Chemie-International Edition* 47, 537-540.
241. Cha, Y., Murray, C. J., and Klinman, J. P. (1989) Hydrogen tunneling in enzyme-reactions, *Science* 243, 1325-1330.
242. Bahnson, B. J., Park, D. H., Kim, K., Plapp, B. V., and Klinman, J. P. (1993)

- Unmasking of hydrogen tunneling in the horse liver alcohol dehydrogenase reaction by site-directed mutagenesis, *Biochemistry* 32, 5503-5507.
243. Schneider, M. E., and Stern, M. J. (1972) Arrhenius preexponential factors for primary hydrogen kinetic isotope effects, *J. Am. Chem. Soc.* 94, 1517.
244. Sikorski, R. S., Wang, L., Markham, K. A., Rajagopalan, P. T. R., Benkovic, S. J., and Kohen, A. (2004) Tunneling and coupled motion in the *Escherichia coli* dihydrofolate reductase catalysis, *J. Am. Chem. Soc.* 126, 4778-4779.
245. Hay, S., Pang, J. Y., Monaghan, P. J., Wang, X., Evans, R. M., Sutcliffe, M. J., Allemann, R. K., and Scrutton, N. S. (2008) Secondary kinetic isotope effects as probes of environmentally-coupled enzymatic hydrogen tunneling reactions, *ChemPhysChem* 9, 1536-1539.
246. Pijning, T., van Pouderoyen, G., Kluskens, L., van der Oost, J., and Dijkstra, B. W. (2009) The crystal structure of a hyperthermoactive exopolysaccharuronase from *Thermotoga maritima* reveals a unique tetramer., *FEBS Lett.* 583, 3665-3670.
247. Benkovic, S. J., and Hammes-Schiffer, S. (2003) A perspective on enzyme catalysis, *Science* 301, 1196-1202.
248. Sham, Y. Y., Ma, B. Y., Tsai, C. J., and Nussinov, R. (2002) Thermal unfolding molecular dynamics simulation of *Escherichia coli* dihydrofolate reductase: Thermal stability of protein domains and unfolding pathway, *Proteins* 46, 308-320.
249. Frieden, C. (1990) Refolding of *Escherichia-coli* dihydrofolate reductase - sequential formation of substrate binding sites, *Proc. Natl. Acad. Sci. USA* 87, 4413-4416.
250. Swanwick, R. S., Daines, A. M., Tey, L. H., Flitsch, S. L., and Allemann, R. K. (2005) Increased thermal stability of site-selectively glycosylated dihydrofolate reductase, *ChemBioChem* 6, 1338-1340.
251. Tey, L. H., Loveridge, E. J., Swanwick, R. S., Flitsch, S. L., and Allemann, R. K. (2010) Highly site-selective stability increases by glycosylation of dihydrofolate reductase, *FEBS J.* 277, 2171-2179.
252. Chen, Y.-Q., Kraut, J., Blakely, R. L., and Callender, R. (1994) Determination by raman spectroscopy of the pKa of N5 of dihydrofolate bond to dihydrofolate reductase: Mechanistic implications, *Biochemistry* 33, 7021-7026.
253. Khavrutskii, I. V., Price, D. J., Lee, J., and Brooks III, C. L. (2007) Conformational change of the methionine 20 loop of *Escherichia coli* dihydrofolate reductase modulates pK_a of the bound dihydrofolate, *Protein Sci.* 16, 1087-1100.
254. Kuhn, P., Lesley, S. A., Mathews, I. I., Canaves, J. M., Brinen, L. S., Dai, X. P., Deacon, A. M., Elsliger, M. A., Eshaghi, S., Floyd, R., Godzik, A., Grittini, C., Klock, H. E., Koesema, E., Kovarik, J. M., Kreuzsch, A. T., McMullan, D., McPhillips, T. M., Miller, M. A., Miller, M., Morse, A., Moy, K., Ouyang, J., Robb, A., Rodrigues, K., Selby, T. L., Spraggon, G., Stevens, R. C., Taylor, S. S., van der Bedem, H., Velasquez, J., Vincnet, J., Wang, X. H., West, B., Wolf,

- G., Wooley, J., and Wilson, I. A. (2002) Crystal structure of Thy1, a thymidylate synthase complementing protein from *Thermotoga maritima* at 2.25 Å resolution, *Proteins* 49, 142-145.
255. Tanaka, Y., Tsumoto, K., Yasutake, Y., Umetsu, M., Yao, M., Fukada, H., Tanaka, I., and Kumaga, I. (2004) How oligomerization contributes to the thermostability of an archaeon protein, *J. Biol. Chem.* 279, 32957-32967.
256. Gerk, L. P., Levon, O., and Muller-Hill, B. (2000) Strengthening the dimerisation interface of Lac repressor increases its thermostability by 40 °C, *J. Mol. Biol.* 299, 805-812.
257. Goihberg, E., Peretz, M., Tel-Or, S., Dym, O., Shimon, L., Frolow, F., and Burstein, Y. (2010) Biochemical and structural properties of chimeras constructed by exchange of cofactor-binding domains in alcohol dehydrogenases from thermophilic and mesophilic microorganisms, *Biochemistry* 49, 1943-1953.
258. Thoma, R., Hennig, M., Sterner, R., and Kirschner, K. (2000) Structure and function of mutationally generated monomers of dimeric phosphoribosylanthranilate isomerase from *Thermotoga maritima*, *Struct. Fold. Des.* 8, 265-276.